Development of a Portable Solar Calorimeter System Used to Characterize Fenestration Systems

By

Kun Xie

M.S, University of Dayton, Dayton, Ohio, 2014
B. Eng., Zhengzhou University, China, 2010

Submitted to the graduate degree program in the Department of Civil, Environmental, and Architectural Engineering and the Graduate Faculty of the University of Kansas in partial fulfillment of the requirements for the degree of Doctor of Philosophy in Civil Engineering.

_____
Mario A. Medina, Ph.D., P.E., Chairperson

_____
Brian Lines, Ph.D., P.E., Graduate Representative

_____
C. Bryan Young, Ph.D., PE., Member

_____
Jae D. Chang, Ph.D., Member

_____
Hugo A. Sheward, Ph.D., Member

Date Defended: 14 January 2022

The Dissertation Committee for Kun Xie
Certifies that this is the approved version of the following dissertation:

Development of a Portable Solar Calorimeter System Used to Characterize Fenestration Systems

_____

Mario A. Medina, Ph.D., P.E., Chairperson

Date Defended: 14 January 2022

ABSTRACT

In architecture, a fenestration system is the arrangement and proportioning of transparent surfaces in a building, most notably windows, curtain walls, glass doors, and skylights. In terms of heat transfer from the outdoors to the indoors, and vice-versa, through building envelopes, fenestration systems embody elements with more complex heat transfer mechanisms relative to other components (e.g., opaque walls, roofs, etc.). Understanding and improving the energy performance of fenestration systems would result in higher building energy efficiency and management, which would also result in significant reductions in space cooling and heating energy consumption in buildings. Furthermore, reductions in energy use are linked to reduction in CO_2 emissions and thus reduce global warming.

The main objective of this dissertation was to design, construct, and validate a solar calorimeter to measure SHGCs of different single-sheet glasses. With modification, the solar calorimeter described here could be used to estimate the SHGCs of several other types of architectural glazing. For this dissertation, a portable solar calorimeter ("calorimeter") was designed, constructed, and calibrated to be used to determine the solar heat gain coefficient (SHGC)[1] of architectural glass[2] sheets

[1] The solar heat gain coefficient (SHGC) is the fraction of solar radiation admitted through a fenestration system, either transmitted directly and/or absorbed, and subsequently released as heat to the inside of a building.

[2] Although in architecture they have specific meanings, in this dissertation terms such as glass, window, and fenestration are often used interchangeably to represent a solid, relatively thin, transparent surface.

used in fenestration systems. The calorimeter was designed to be portable, with a fast response, and with the capability to be used in both indoor and outdoor environments. For the calorimeter to be used in indoor environments, a solar simulator was also designed and built. For the calorimeter to be used outdoors, a customized solar tracking system was designed, built, and installed on the calorimeter stand to keep the test specimens in a position perpendicular (normal) to the direct beam of solar radiation during testing. The SHGC was determined through the solution of energy balance calculations around the calorimeter box. The produced SHGCs compared very favorably with values found in the literature. The average SHGC obtained for a 6 mm (1/4 in) clear glass was 0.791. With the combined uncertainty calculated for the SHGC, the average SHGC was 0.791 ± 0.03. The maximum difference between the obtained SHGC and others found in the open literature was -3.16% (-0.025 in absolute terms). The solar calorimeter will support further student research and five courses in the Architectural Engineering curriculum at the University of Kansas. The courses are Building Materials Science (ARCE 350), Building Material Science, Honors (ARCE 351), Building Thermal Science (ARCE 660), Building Thermal Science, Honors (ARCE 670), and Energy Management (ARCE 663).

ACKNOWLEDGEMENTS

I would like to express my sincere gratitude to my advisor, Professor Mario A. Medina. Prof. Medina has been completely supportive throughout my entire Ph.D. program and research studies with his immense knowledge and plentiful experience. I deeply appreciate his professionalism, patience, and generosity in guiding me. During some of my most difficult times studying in KU, Prof. Medina gave me the moral support and the freedom I needed to move on, without which I would not be able to make my way to graduation, especially for me having two kids to support and care for. His kindness and consideration made my life a lot easier in Lawrence.

Also, I would like to thank Mr. Kent Dye for providing technical support during the construction of the solar calorimeter. Mr. Dye helped out by sharing his rich experience, creative ideas, and by his positive disposition and very diligent work.

I thank Prof. Brian Lines, Prof. C. Bryan Young, Prof. Jae D. Chang, and Prof. Hugo A. Sheward for accepting to be members of my Ph.D. committee.

I am grateful to the faculty and staff at the Department of Civil, Environmental & Architectural Engineering at University of Kansas for their support over the years.

In particular, I thank Ms. Susan Scott for taking time from her busy schedule to talk to me, both academically and non-academically, whenever I stopped by her office.

Thanks are due to my friends, Can Rong for all the good time we have spent together in Lawrence.

I thank my parents, who supported me financially in the first 2 years of study. I also thank my brother and sister for taking care of my parents in China.

Finally, to my wife, Yanhao, who has been with me throughout my whole graduate studies; to my son, Nolan and my daughter, Nora, who are the best gifts for us. Thanks for loving and supporting me unconditionally during the best and the difficult moments.

TABLE OF CONTENT

LIST OF FIGURES

LIST OF TABLES

NOMENCLATURE

α_{plate}	Solar absorptance of solar-air heat transfer coefficient meter (0-1)
A_p	Percentage of absorbed solar radiation by the window (0-1)
A	Area, m^2 (ft^2)
c_p	Heat capacity of water, kJ/kg°C (Btu/lb·°F)
e	Euler's number (≈ 2.7182818)
E_S	Solar irradiation incident on specimen, W/m^2 ($Btu/hr \cdot ft^2$)
$h_{h\text{-}sun}$	Measured weather side surface heat transfer coefficient, W/m^2K ($Btu/hr \cdot ft^2 \cdot {}^oF$)
k	Thermal Conductivity, W/m·K (Btu/hr·ft·°F)
L	Wall thickness, cm (in)
N	Inward flow fraction of absorbed heat
ρ	Water density, kg/m^3 (lb/ft^3)
Q_{solar}	Total solar heat gain on the surface of the glass, W (Btu/hr)
$Q_{solar\text{-}in}$	Net solar heat gain through the glass, W (Btu/hr)
Q_{water}	Heat extracted by the water in the absorber plate, W (Btu/hr)
Q_{wall}	Heat losses through all insulated walls, W (Btu/hr)
$Q_{heat\ flow}$	Heat gain due to the difference of internal and external air Temperature, W (Btu/hr)
Q_{fan}	Heat generated by internal fan, W (Btu/hr)

SHGC	Solar heat gain coefficient
T_p	Percentage of solar radiation directly transmitted through window
T	Temperature, ºC (K) (ºF (ºR))
T_c	Air temperature outside solar calorimeter, ºC (K) (ºF (ºR))
T_{plate}	Temperature of solar-air heat transfer coefficient meter, ºC (K) (ºF (ºR))
t	Time in minutes
τ	Time constant
μ	Uncertainty
U	Heat transfer coefficient, W/m^{2}K (Btu/hr·ft²·°F)
U_m	Modified thermal transmittance of test specimen, W/m^{2}K (Btu/hr·ft^2·ºF)
U_{glass}	Thermal transmittance of test specimen, W/m^{2}K (Btu/hr·ft^2·ºF)
$\dot{v}$	Volume flow rate, m^3/s (ft^3/s)

CHAPTER I

INTRODUCTION

1.1 Background

Fenestration systems, such as windows and skylights, provide basic functions in modern buildings such as the admission of daylight and a view contact to the outside. For the purpose of architectural appearance in large buildings, curtain walls and large windows are preferred by designers, thus windows become an essential design element, not only architecturally, but also in the calculation of space cooling and heating loads. In terms of heat that enters and leaves the building, fenestration systems are points of relatively high heat transfer because of their use of elements with relatively high thermal conductivities (glass and frame). A significantly large amount of heat is transferred from the indoors to the outdoors during the winter through fenestration. Similarly, a significant amount of heat, which includes conduction, convection, and solar and thermal radiation, enters the building through the fenestration systems in the summertime. Winkelmann [1] reported that, for commercial buildings, the heat transfer through fenestration systems represents 31% of the space cooling load and 17% of the space heating load. For residential buildings, these values are 31% and 23%, respectively. These heat loses and gains through fenestration systems substantially increase space heating and cooling loads,

which leads to the selection of larger space conditioning equipment and increases the energy consumption during the operation over the life of the building. According to U.S. Energy Information Administration (EIA) [2], in the U.S., about 40% of total U.S. energy consumption is used in residential and commercial buildings, where space heating and cooling account for 60% of this energy consumption [3]. In addition, commercial and residential buildings account for 39% of carbon dioxide (CO_2) emissions per year [4]. CO_2 emissions from buildings are significant contributors to global warming [2]. Therefore, having a better understanding of fenestration system heat transfer is necessary for achieving overall higher building energy efficiency and lower space heating and cooling energy consumption in both commercial and residential buildings.

1.2 Heat Transfer through Windows

A schematic of the heat transfer through a window is shown in Figure 1.1. It includes directly transmitted solar radiation, conduction, convection, thermal radiation, and transfer of heat absorbed by the glass. The industry uses three major factors, namely the U-factor, the Solar Heat Gain Coefficient (SHGC), and Air Leakage (AL) to evaluate and rate window energy performance [6]. These are shown in a National Fenestration Rating Council (NFRC) label in Figure 1.2.

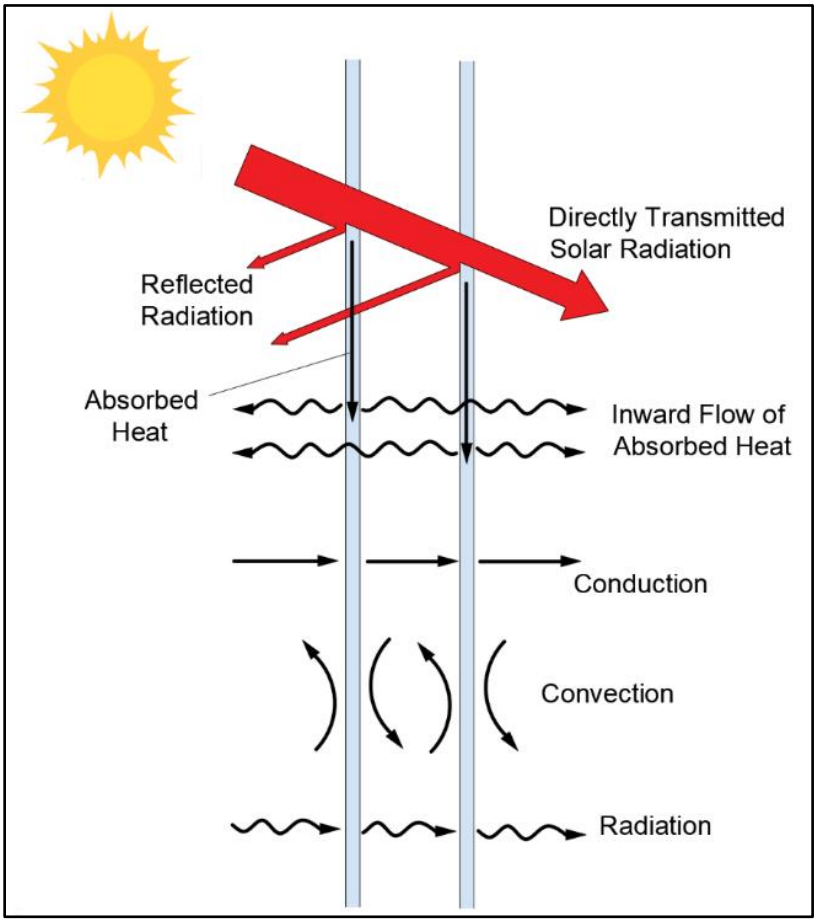

Figure 1.1 Heat Transfer through a Double-Pane Window [5]

1.2.1 U-factor

The window U-factor is related to the insulating ability of the system [5]. For most windows, the range of U-factor values is generally between 1.42 and 7.1 W/m^2K (0.25 and 1.25 $Btu/hr \cdot ft^2 \cdot °F$) [6]. A low value of U-factor indicates lower heat transfer rate through the window, especially via conduction heat transfer. A low U-factor could be achieved, for example, by increasing the number of glass sheets (i.e., double pane and triple pane windows), and/or by filling odorless, colorless, non-

toxic gases the volume between glass sheets in multi-pane assemblies. Common gasses used for this purpose include argon and krypton.

Figure 1.2 National Fenestration Rating Council Certified Window Energy Performance Ratings [6]

In cold climate regions that require more space heating, windows with a low U-factor should be selected to prevent heat losses. In warm to hot climates, low U-factor windows are preferred as well, but in this case to minimize heat gains in the summer.

1.2.2 Solar Hear Gain Coefficient (SHGC)

The solar heat gain coefficient (SHGC), which is also known as the *Solar Factor*, is the fraction of the solar irradiance transmitted through a window. This includes both directly transmitted and absorbed solar radiation which is transferred to the

conditioned space. That is, the SHGC measures how much solar energy passes through a window and is released into the conditioned space. Figure 1.3 shows the various components when solar radiation is transferred from the outside into a room through a window.

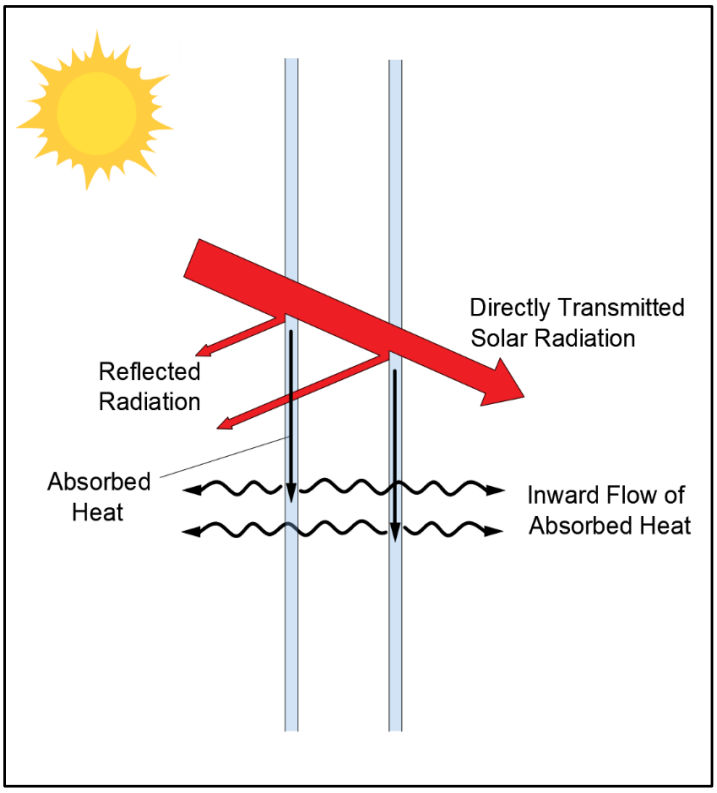

Figure 1.3 Solar Radiation through a Window [5]

The SHGC is expressed as [7]:

$$SHGC = T_p + NA_p \tag{1-1}$$

where:

SHGC = Solar heat gain coefficient, 0-1.

T_p = Fraction of directly transmitted solar radiation through the window, 0-1.

A_p = Fraction of absorbed solar radiation by the window, 0-1.

N= Fraction of inward heat flow of heat previously absorbed by the window, 0-1.

The solar radiation that reaches the earth consists of 3% ultraviolet rays (UV), 55% infrared radiation (IR), and 42% visible light [8]. Solar transmittance is expressed as the fraction of the combined ultraviolet and infrared radiation that is transmitted through the window. Solar energy is transformed into heat when it is absorbed by the window material, which is usually glass, thus raising its temperature. This absorbed heat is then transferred to the interior space via infrared radiation and convection heat transfer.

SHGC is expressed as a value between 0 and 1. A value closer to 1 translates into a higher transfer of solar energy through the fenestration system. For most areas in the United States, a low SHGC is preferred to reduce solar energy transfer into conditioned spaces through the fenestration system during the summertime. There are some areas in the northern part of the country, however, that would require higher space heating demand during the wintertime, thus in these cases fenestration with a higher SHGC would be preferred to introduce more passive solar heat into the building. In both cases the aim is to design energy efficient buildings that would

lessen the use of space conditioning systems to reduce energy consumption. Therefore, selecting the fenestration systems with the appropriate SHGC and finding a balance between preventing unwanted heat gains to enter the building in summer and allowing more heat to enter the building in winter adds to the complexity of designing energy efficient buildings for the various climates found in the United States.

1.2.3 Air Leakage

The Air Leakage (AL) rating measures the degree of air infiltration/exfiltration through a window assembly. It is defined as the volume of air going across and through a window outer area in terms of volume air flow rate per unit surface area of window ($m^3/s \cdot m^2$; $ft^3/min \cdot ft^2$). As an example, if a window assembly is of low quality, which would be the case with inexpensive, ready-to-install, commercially-available systems, and/or the window frame were not properly assembled, and/or maintained, and/or had deteriorated with age and exposure to the elements, it would be very likely that the air leakage of the system would be high, which would result in significant heat gains or losses and create indoor humidity problems. The reason for this is that infiltrated air enters a conditioned space at the temperature and humidity levels of the outside environment. On the other hand, air that exfiltrates from the building is air that had already been conditioned to satisfactory

temperature and humidity levels. This exfiltrated air would have to be made up and re-conditioned, which comes at an extra use of energy, and therefore, cost.

In the experiments carried out as part of this dissertation, multiple approaches were used to minimize the impact of AL to avoid experimental errors and inaccuracies resulting from air infiltration. For example, a tight seal and proper specimen installation were observed. This is presented in Chapter 3.

1.3 SHGC Measurements

There are several methodologies and calculation techniques to determine the SHGC. Calculation techniques are usually based on tables and charts and/or rely on building simulation software libraries of commercially-available windows. Measurement methodologies are mostly experiment-based and are conducted either under real-time weather conditions (outdoor), or under laboratory conditions, in which case, a solar simulator would be needed in addition to the solar calorimeter.

In comparing indoor with outdoor experiments, each has its own advantages and disadvantages, and different operation processes and requirements. Real-time outdoor weather conditions normally introduce errors and make the experimental process a complex one. For example, to minimize the variations of the solar angle of incidence (Figure 1.4) and diffuse radiation from the ground, outdoor experiments make use of solar trackers, which are set up to rotate the calorimeter

along the solar path. This is necessary to maintain the solar angle of incidence near zero so that the surface of a specimen being tested is positioned perpendicular to the solar beam radiation at all times during solar activity. Furthermore, under outdoor weather conditions, variables such as wind speed and direction, and air temperatures, require the use of a *solar-air-heat transfer coefficient* meter to obtain the heat transfer coefficient at the surface of a test specimen. As part of this dissertation, a solar-air-heat transfer coefficient meter was fabricated, following National Fenestration Rating Council guidelines [20].

Experiments in indoor environments are easier to control than those under outdoor conditions. However, a major challenge of indoor experiments is the requirement of providing an acceptable artificial direct-beam solar radiation. Laboratory-made solar simulators are fabricated using electric lamps, filters, and reflectors with the understanding that artificial lighting sources would introduce unwanted experimental errors.

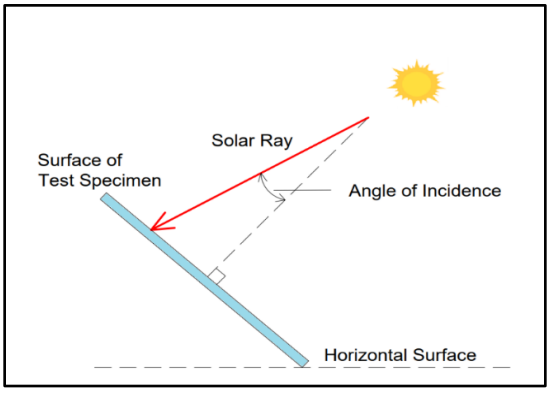

Figure 1.4 Solar Angle of Incidence [14]

1.3.1 Solar Calorimeter

A calorimetric box, or a calorimeter system ("calorimeter"), is an insulated enclosure used to measure the change in heat in a control volume. A solar calorimeter has an aperture where a specimen, usually a sheet of glass, is mounted to admit solar radiant heat. The solar calorimeter developed for this research has a chilled water circulation system was used to remove and quantify the solar heat that enters the box. A low-speed fan was installed to enhance the heat exchange between the internal air and the absorber plate. Figure 1.5 shows a cross section of the solar calorimeter built as part of this dissertation.

The absorber plate was the main heat extraction component within the calorimetric box. It was made of a copper plate and copper coils and was painted matte black for maximum solar heat absorptivity. A chilled water circulation system was designed, fabricated, and installed to remove the solar energy that had entered the calorimetric box and had been absorbed by the absorber plate.

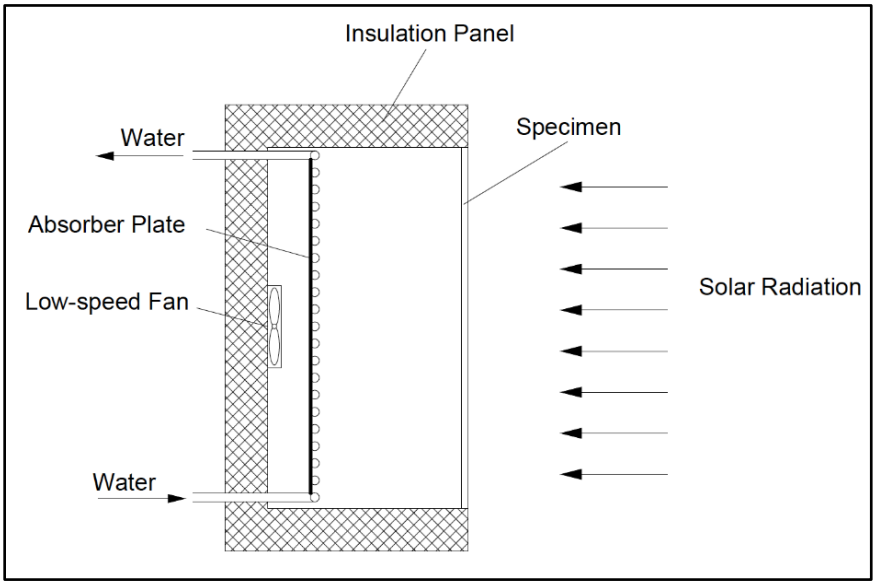

Figure 1.5 Cross Section of the Solar Calorimeter

1.3.2 Heat Exchange in the Solar Calorimeter

The heat transfer processes in a solar calorimeter include solar radiation that enters the box, conductive and convective heat transfer through and at the specimen surface, heat absorbed by and removed from the absorber plate, and heat losses/gains through the insulated side walls. These heat flows are shown in Figure 1.6. The net solar heat gain through the glass was be calculated by:

$$Q_{solar-in} = Q_{water} + Q_{wall} - Q_{heat\ flow} - Q_{fan} \qquad (1\text{-}2)$$

where:

$Q_{solar\text{-}in}$ = Net solar heat gain through the glass, W (Btu/hr).

Q_{water} = Heat extracted by the water in the absorber plate, W (Btu/hr).

Q_{wall} = Heat losses through all insulated walls, W (Btu/hr).

$Q_{heat\ flow}$ = Heat gains as a result of the difference between internal and external air temperatures, W (Btu/hr).

Q_{fan} = Heat generated by internal the low-speed fan, W (Btu/hr).

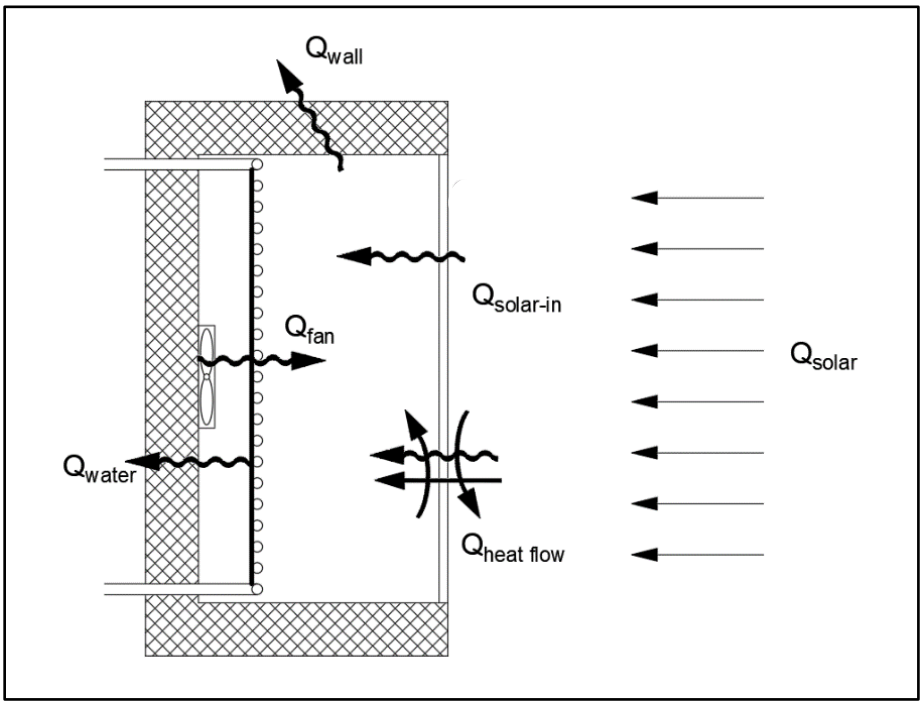

Figure 1.6 Calorimeter Heat Flows

Thus, combining the definition of SHGC with Eq. 1-2, the SHGC was expressed by:

$$SHGC = \frac{Q_{solar-in}}{Q_{solar}} = \frac{Q_{water} + Q_{wall} - Q_{heat\ flow} - Q_{fan}}{Q_{solar}} \qquad (1\text{-}3)$$

where:

Q_{solar} = Total solar heat irradiance measured on the surface of the glass, W (Btu/hr).

The heat flow through the insulated walls, Q_{wall}, is a function of measured surface temperature on both sides of walls, the wall thermal conductivity, and the surface area of the wall.

$Q_{heat\ flow}$ is a function of specimen heat transfer coefficient (U-factor), the air temperature difference of both inside and outside surface of test specimen, and the surface area of the solar calorimeter opening. The procedure to estimate $Q_{heat\ flow}$ differs for indoor and outdoor experiments. For indoor tests, the air speed over the specimen is close to zero; and therefore, the surface convective heat transfer coefficient can be assumed to be constant. For outdoor tests, the $Q_{heat\ flow}$ is determined in a way that accounts for the variation of the surface heat transfer coefficient, which results from changes in wind speed and direction.

Circulating chilled water is used to remove the heat that enters the calorimeter and is absorbed by the absorber plate. The heat extracted by the water from the absorber plate, Q_{water}, is a function of water volume flow rate and temperature difference between both inlet and outlet of the cooling coil. The heat extracted by water was calculated by:

$$Q_{water} = \rho \times \dot{v} \times c_p \times (T_o - T_i) \quad (1\text{-}3)$$

where:

ρ = Water density, kg/m^3 (lb/ft^3).

$\dot{v}$ = Volume flow rate, m^3/s (ft^3/s).

c_p = Specific heat capacity of water, kJ/kg°C (Btu/lb·°F).

T_o = Outlet water temperature, °C (°F).

T_i = Intlet water temperature, °C (°F).

1.3.3 Solar Simulator

The solar simulator plays a critical role in the indoor measurements of SHGCs. It is a device that provides a very similar electromagnetic spectrum to that of natural sunlight. Ideally, a solar simulator should produce a uniform spectral radiation distribution spatially and temporally and should match the solar radiation as closely as possible in the laboratory environment [10]. This section provides the think-through process that was used to arrive at the laboratory-made solar simulator that was built as part of this project.

Commercially-available solar simulators, which are highly specialized devices, for a very narrow market, that come at a steep price, do exist. However, their price is

often outside that of university sponsored academic research budgets. A solution to this scenario is a laboratory-made solar simulator that can provide acceptable solar radiation in the appropriate spectrum for conducting indoor solar calorimeter tests. There are two common standards used to classify solar simulators: IEC 60904-9 Edition 2 [31] and ASTM927-10 [32]. These standards are made for photovoltaic and solar thermal testing. According to ASTM standards [32], there are three methods to evaluate the performance of a solar simulator. These are spectral match, spatial uniformity, and temporal stability. Based on these three methods, each method is organized three classes: A, B, or C. These are listed in Table 1.1.

Table 1.1 Classification of Small Area Solar Simulator (ASTM) [32]

	Spectral Match, Each Interval	Irradiance Spatial Non-Uniformity	Temporal Instability
Class A	0.75 - 1.25	2%	2%
Class B	0.6 - 1.4	5%	5%
Class C	0.4 - 2.0	10%	10%

Xenon arc lamps are one of the most common type of lamps used to make solar simulators. They match the solar spectrum relatively well and has nearly identical color temperature[3] to that of the sun. These xenon arc lamps are the best option for

[3] Color temperature of a light source is the temperature of an ideal black-body radiator that emits energy in the form of light of a color comparable to that of the light source.

use in solar simulators. However, the xenon arc lamps have the potential to be dangerous because they function with pressurized gas, their spectral irradiance may change with aging, are expensive, a fragile filter must accompany them when used in solar simulators and have a relatively short life [13].

Compared to xenon arc lamp, LEDs have less maintenance and much longer lifetime with a relatively similar spectral match. LEDs have a life expectancy of 50,000-100,000 hours. In comparison, the xenon light bulbs are expected to be replaced after about 1000 hours of operation. The use of LED lights also reduces the maintenance cost of a solar simulator as well as to alleviate the aging problems inherent with the xenon bulbs [13]. The LEDs also have better energy efficiency and consume much less energy than xenon arc lamps. However, with relatively low thermal stability and low light intensity, the LEDs cannot become an ideal option when making a solar simulator especially for solar thermal experiments.

Halogen lamps offer a spectrum which is closely matched to that of a black body radiation, although typically with a lower color temperature than that of the solar radiation. Compared to xenon arc lamp and LEDs, a higher cost efficiency and better light intensity makes halogen lamp a better candidate for laboratory-made solar simulators for calorimetric measurements. When using halogen lamps, an assembly of a group of lamps is preferred since such assembly can cover a larger

area and provide better uniformity when it comes to incident solar radiation. With certain arrangement of a group of halogen lamps, this type of solar simulator can provide temporal stability, sufficient power, and good enough uniformity over a larger area for indoor SHGCs measurements.

1.3.4 Solar Tracker

Solar trackers are widely used in the solar industry. Trackers point solar panels or modules toward the sun to obtain maximum solar energy harvesting, and thus, produce higher electrical and/or thermal energy outputs. In SHGC tests, the results would be affected if the specimen were positioned at different solar angles of incidence during the testing periods. Therefore, to minimize angle variations a solar tracker was needed to ensure that the calorimeter would follow the sun's path throughout the day to achieve consistent measurements.

Single-axis solar trackers rotate on one axis and are often used for larger projects or utility-scale applications. Dual-axis trackers allow solar panel to rotate along two axes and are used more in smaller projects and applications. Single-axis trackers normally harvest less solar energy per unit area when compared to dual-axis trackers, but they require less space to install and have easier operations and maintenance.

Figure 1.7 shows solar azimuth and elevation angles, which are two angles that define the position of the sun in the sky relative to an observer on earth. In SHGC tests, a dual-axis tracker would rotate the solar calorimeter on two axes to better follow the sun's path throughout the day. One axis would rotate the calorimeter around a vertical axis along the solar azimuth angle and the other axis would rotate it along the solar elevation angles.

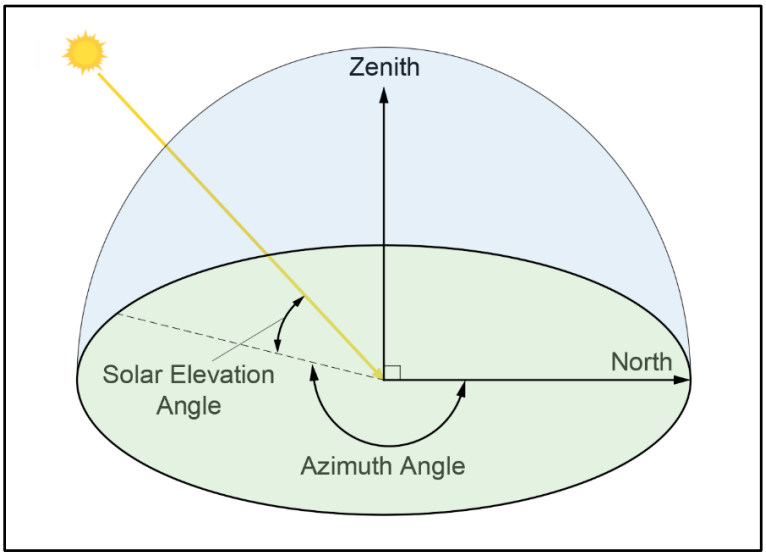

Figure 1.7 Solar Azimuth and Elevation Angles [14]

As stated above, this chapter presented the think-through processes used to arrive at the various components, materials, coatings, etc. that were selected during the design and fabrication of the solar calorimeter and solar simulator presented as part of this dissertation.

CHAPTER II

LITERATURE REVIEW

Fenestration systems represent areas of high heat transfer that significantly affect the use of energy and its management in buildings. A better understanding of the properties of the various components that make up fenestration systems is important for improving their performance, especially in terms of heat transfer. This is crucial for the ongoing efforts to reduce building energy consumption. Solar heat gain coefficient, as one of the most critical properties of windows, has drawn significant attention over the past three decades [33]. As stated in the previous chapter, there are several approaches that can be used to measure the SHGC of architectural glass. In every case, standard experimental methods and procedures are used to satisfy specific requirements and to accommodate environmental conditions. Many studies dealing with the measurement of architectural glass ("window") properties appear in the technical literature. The most relevant ones are summarized below.

Marinoski et al. [11] studied how to improve the measurements of solar heat gain through fenestration systems. They carried out two variations of the experiments, which had an effect on the accuracy of the measurements. One variation used calibrated heat flux meters. In this approach they applied a coating layer with high solar absorptivity to the heat flux meters surfaces to increase sensor solar radiation

sensitivity and based on this a second set of heat flux meters was calibrated. They found that by coating the sensor surfaces the average difference between experimental and published data ("error") was reduced from an average of 19% to an average of 5.4%. A second variation used water circulation instead of air circulation as a cooling system for part of the experimental setup. With water circulation, they realized that the temperature difference between the absorber plate's temperature and the surrounding air temperature could be better controlled and reduced in value, which in turn reduced the average experimental error from 2.2% to 0.94%.

Alvarez et al. [15] presented a test method to evaluate the thermal performance of architectural window glass. Four glass samples were tested by using a calorimeter. This calorimeter was an insulated box with dimensions of 0.5 m x 0.5 m x 0.5m (20 in x 20 in x 20 in), and the glass sample was installed over the opening of the box. An absorber system made up of a copper plate with copper tubes was placed toward the back wall of the calorimeter. Chilled water forced in and out of the absorber plate was used to absorb the heat gained through the glass. For their solar simulator halogen-tungsten lamps of 1000 W each were used to simulate the solar radiation. They calculated the shading coefficient (SC), which is the ratio of solar heat gain (due to direct sunlight) passing through a glass unit to the solar energy which passes

through 3 mm (1/8 in) clear float glass[4]. The results of 3 mm (1/8 in) clear glass, 6 mm (1/4 in) clear glass, 6 mm (1/4 in) filtrasol (colored) glass, and 6 mm (1/4 in) reflectasol (reflective) glass showed that the 6 mm (1/4 in) reflectasol glass had the lowest SC value which was 0.36 $\pm$ 0.045 compared with others.

Marinoski et al. [16] developed a calorimeter with two chambers to determine the SHGC of windows. Each chamber had a heat absorber plate. A water circulation system was used in both chambers to remove the heat gained through the window. In the larger chamber, which had dimensions of 1500 mm x 1200 mm x 30 mm (59 in x 47.2 in x 1.1 in), the heat gained through the window was calculated based on the temperature difference between the inlet and outlet of the water circulation in the absorber plate. In the smaller chamber, which had the dimensions of 500 mm x 500 mm x 18 mm (19.6 in x 19.6 in x 0.7 in), heat flux meters were installed on the absorber plate to measure the heat flux through the absorber plate. They tested 3-mm (1/8 in) thick clear glasses. All tests were conducted under outdoor conditions. The results of solar factor showed a good agreement with theoretical values.

Wright et al. [17] studied the solar heat gain through windows when different types of shading devices were installed. They compared computer simulated results to

[4] 3-mm clear float glass, also known as just clear glass, is the standard glass used by the industry for which a shading coefficient (SC) of 1.0 is assigned. All other SCs (e.g., tinted) are rated based on this glass.

experimental measurements. In their study, solar heat gain through various shading devices attached to a conventional double-glazed window were measured using the Government of Canada's National Solar Test Facility's (NSTF) solar simulator and solar calorimeter. The NSFT a research center for testing and rating solar technologies under controlled sunlight, temperature, and wind. The calorimeter consisted of inner and outer cells, where the outer cell was designed to provide a stable temperature for the inner cell. The chilled water heat exchanger connected to the absorber plate was used to quantify the amount of heat entering or leaving the inner cell. A new developed software ASHWAT (ASHRAE Window Attachment) was used for the analysis of fenestration with shading devices and to produce the computer simulated results. The conclusions from this research confirmed that ASHWAT software produced results with a high degree of accuracy when compared to measured values.

Chen et al. [9] measured the SHGCs of fenestration outfitted with semi-transparent photovoltaic modules (STPV) using a solar calorimeter. The calorimeter was designed for indoor measurements, and a chilled water heat exchanger was attached to the absorber plate to extract the entered solar heat. They mounted a turning system at the bottom of the calorimeter to measure SHGC at different angles. Both thermal transmittance and SHGCs were measured. The solar simulator was a single

hydrargyrum medium-arc iodide (HMI)[5] lamp system located 10 m (3.3 ft) away from the calorimeter specimen. They tested five STPV modules at four angles, namely 0°, 45°, 60°, and 70°. In general, double-glazed STPV showed significantly lower SHGC values compared to laminated STPV modules. Also, the SHGC showed a significant reduction in value as the solar angle of incidence increased. For example, the reduction was more than 20% when the angle was changed from 45° to 70° compared to only 5% when the angle was changed from 0° to 45° [9].

Moria [10] presented the development of a solar simulator for education and research purposes. The development started with the evaluation of three different lamp types: 500 W halogen, 1000 W halogen, and 150 W LED. To determine which lamp could produce the most adequate radiation distribution for solar simulator with rage of 800 - 1000 W/m^2 (250 - 315 Btu/hr·ft^2), the radiation of a single lamp was tested first. A pyranometer and data logger were used to measure the total radiation distribution of the lamp at four different heights of 10, 20, 30, and 40 cm (3.9, 7.9, 11.9, and 25.7 in) and four horizontal distances of 10, 15, 20, and 25 cm (3.9, 5.9, 7.9, and 9.8 in) from the sensor. They found that the LED lamps were insufficient for producing heat at 400 W/m^2 (127 Btu/hr·ft^2). The most acceptable results were obtained when a 500 W halogen lamp was installed at 15

[5] HMI is a brand name metal halide gas discharge lamp, which is used mainly in the film and entertainment industries.

cm (5.9 in) distance at 40 cm (25.7 in) in height. The second stage of the development was to determine the optimum arrangement and distance of four lamps. Four 500 W halogen lamps were installed perpendicularly to cancel out uneven distribution. They tested four different heights of 10, 20, 30, and 40 cm (3.9, 7.9, 11.9, and 25.7 in) with four distances of 10, 15, 20, and 25 cm (3.9, 5.9, 7.9, and 9.8 in) between the lamps. The results showed that the optimum irradiances were produced at an inter-lamp distance of 10 cm (3.9 in). Heat fluxes from the halogen lamps varied with height from 200 W/m^2 (63 $Btu/hr{\cdot}ft^2$) to 1200 W/m^2 (380 $Btu/hr{\cdot}ft^2$).

Harrison and Collins [18] presented a process to design, calibrate, and use a solar calorimeter at the Solar Calorimetry Laboratory of Queen's University in Canada. This calorimeter was designed to measure window U-factor and SHGC under both indoor and outdoor conditions. A thermal guard was installed in the calorimeter walls to reduce heat losses that included an active heater to prevent the heat loss from the calorimeter to the outside. The thermal guard would only operate when the internal temperature was higher than the external temperature. An absorber plate outfitted with a conditioned fluid circulating loop was installed to extract the heat via an air-to-fluid heat exchanger. The solar calorimeter was mounted on a dual-axle sun tracking frame, which operated based on the solar azimuth and

altitude angles. A calibration was performed using a monitored heat lamp installed on the calorimeter.

Macias-Melo et al. [19] presented the design, construction, and instrumentation of a calorimeter with solar tracking to determine the thermal and optical properties of monolithic glass samples. The calorimeter box was 50 cm x 50 cm x 21 cm (19.7 in x 19.7 in x 8.3 in) and the specimens were 15 cm x 15 cm (6 in x 6 in) with a maximum thickness of 6 mm (1/4 in). All the tests were conducted under outdoor conditions where the solar tracker operated based on the solar elevation and azimuth angles. To determine the convective heat transfer coefficient on the surface of the specimen, a heat transfer coefficient meter was fabricated following National Fenestration Rating Council guidelines [20]. The device contained an insulated black metal plate that was exposed to the same sunlight, ambient air flow and temperature as the face of the solar calorimeter. The exterior surface heat transfer coefficient on the specimen's surface was estimated by measuring the surface temperature of the plate and was calculated using the following equation [20]:

$$h_{h-sun} = \frac{E_S \cdot \alpha_{plate}}{T_{plate} - T_c} \quad (2\text{-}1)$$

Where:

$h_{h\text{-}sun}$ = measured weather-side surface heat transfer coefficient, W/m^2K ($Btu/hr \cdot ft^2 \cdot {}^oF$)

α_{plate} = solar absorptance of the plate (0 – 1)

T_c = air temperature outside solar calorimeter, K or ºC (ºR or ºF)

T_{plate} = temperature of the plate, K or ºC (ºR or ºF)

E_S = solar irradiance incident on the plate, W/m^2 (Btu/hr·ft^2)

The average U-factor and SHGC values for a 3 mm (1/8 in) glass sample were 6.95 $\pm$ 0.9 W/m^2·K (1.22 $\pm$ 0.16 Btu/hr·ft²·°F) and 0.803 $\pm$ 0.03, respectively. These values were in good agreement with those in the open literature.

CHAPTER III

EXPERIMENTAL SET-UPS

3.1 Outdoor Experimental Set-up

The outdoor experiments were conducted at the University of Kansas Engineering Complex on the roof of LEEP2 Building located in Lawrence, KS. The set-up consisted of a solar calorimeter box, a solar tracker, a chilled water system, and a data acquisition system. This experimental set-up is shown in Figure 3.1.

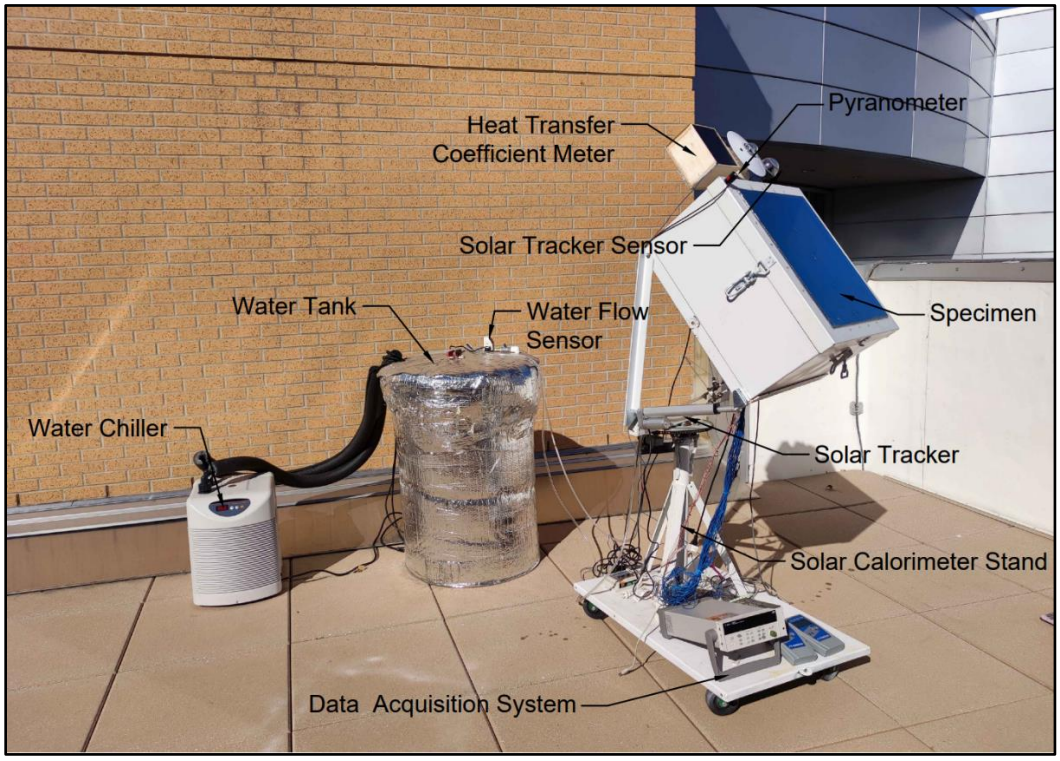

Figure 3.1 Outdoor Experimental Set-up

3.1.1 Solar Calorimeter

The calorimeter box was made of three sections: a casing, an absorber plate, and a and cover designed to support the testing specimens. The casing (Figure 3.2) was made of aluminum and thermal insulation with dimension of 60 cm x 60 cm x 30 cm (24 in x 24 in x 12 in). The aluminum sheet was 2 mm (0.08 in) thick and was painted white to increase solar reflection and reduce the absorption of solar energy. The thermal insulation consisted of one layer of polyisocyanurate board of 5.08 cm (2 in) in thickness a U-factor of 0.0288 $W/m^2 \cdot K$ (0.00507 $Btu/hr \cdot ft^2 \cdot °F$).

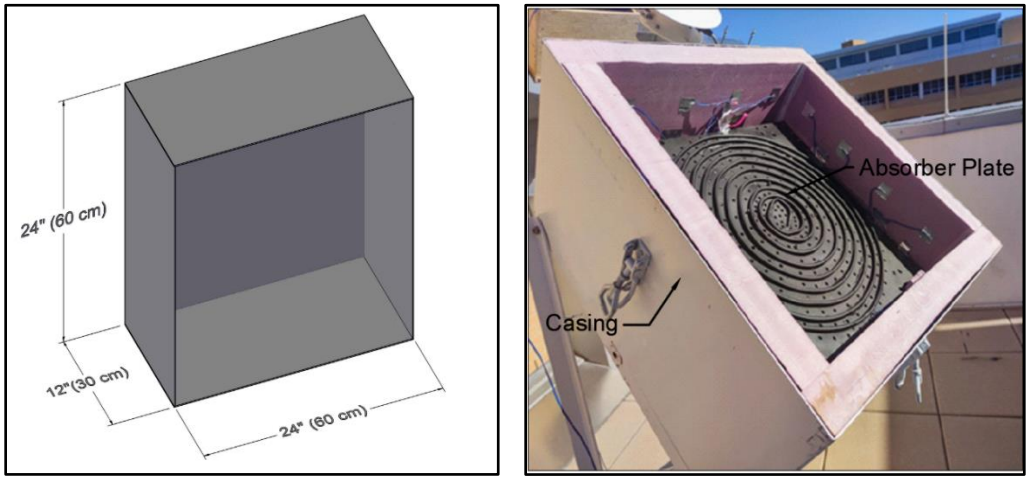

Figure 3.2 Calorimeter Box Casing

The absorber plate (Figure 3.3) was made of a copper and was outfitted with swirling copper tubing. The plate was 0.813 mm (0.032 in) thick, and the tubing had an outside dimeter of 6.35 mm (0.25 in). It was painted matte black with an absorption coefficient, $\alpha = 0.94$, to maximize its absorptance. Holes were drilled

on the plate to increase air circulation and heat exchange between the air and the plate.

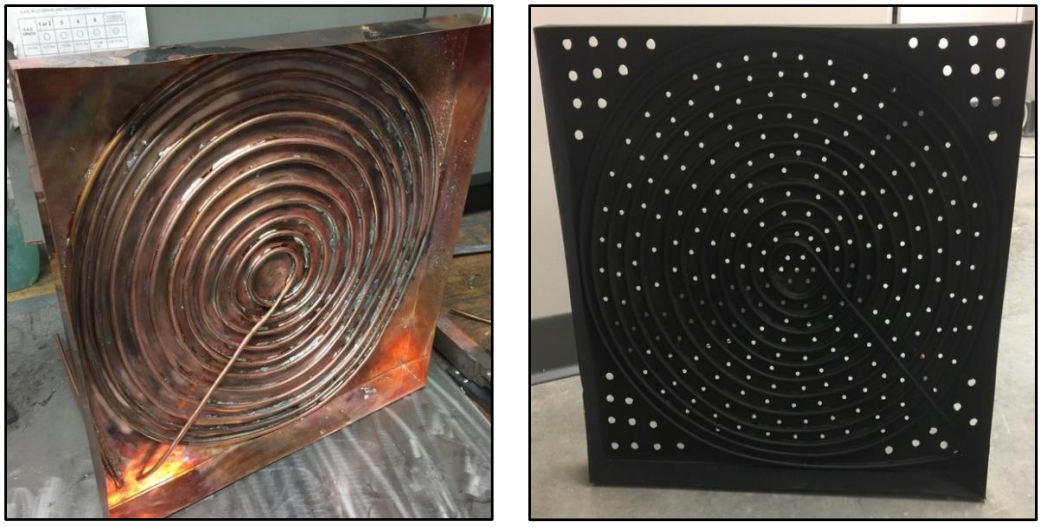

Figure 3.3 Unpainted and Painted Absorber Plate

Within the cover of the calorimeter (Figure 3.4) was an aperture of 49.5 cm x 49.5 cm (19.5 in x 19.5 in). The cover was attached to the casing using four adjustable draw latches. To minimize air infiltration, high density foam seal tape was applied between the casing and the cover.

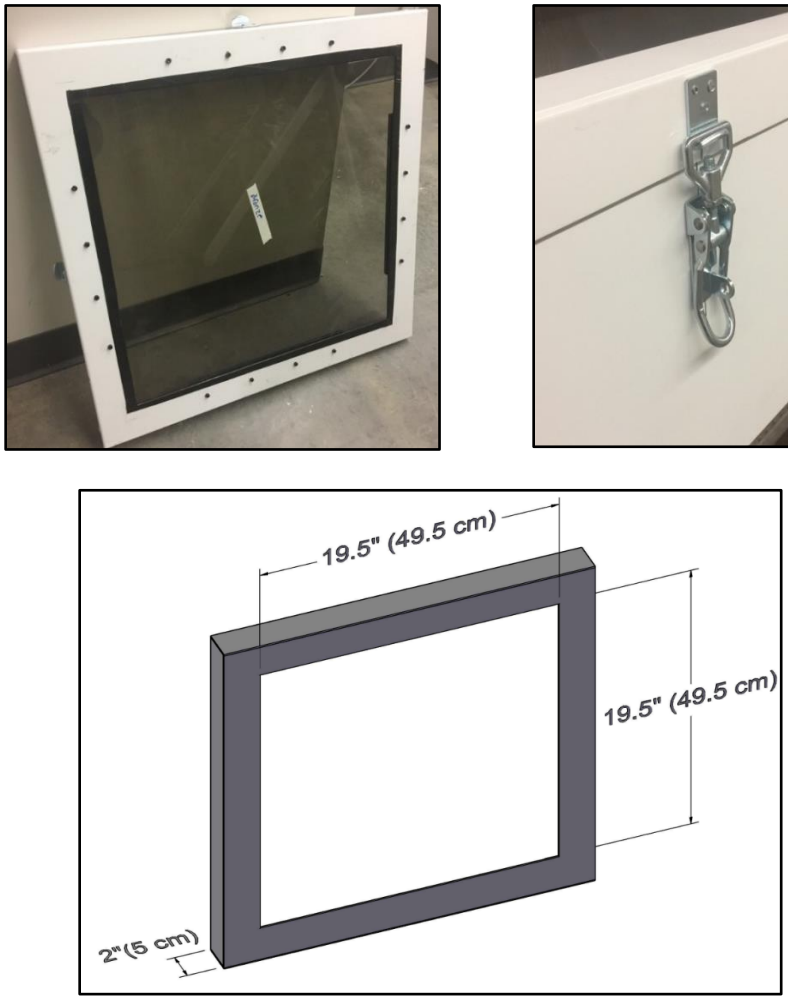

Figure 3.4 Calorimeter Box Cover with Specimen and Adjustable Draw Latch

3.1.2 Chilled Water System

Chilled water was used to remove the heat from the absorber plate. As shown in Figure 3.5, a 0.37 kW (0.5 hp) water chiller and a 208 L (55 gal) insulated water tank were integrated to maintain a stable water temperature at around 5.6 ºC (41 ºF). Two water pumps of the same size were set up. One pump circulated water

between the chiller and the water tank at a rate of 50 l/min (800 gph). The second pump circulated chilled between the water tank and the absorber plate at variable rates.

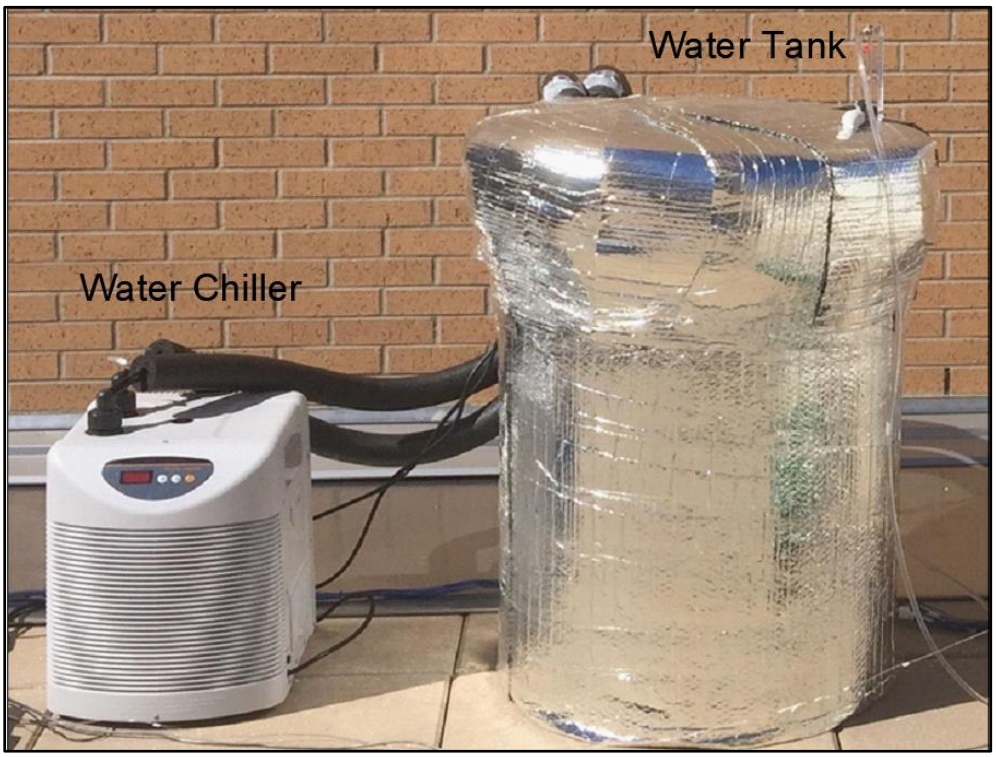

Figure 3.5 Chilled Water System

3.1.3 Data Acquisition System

Figure 3.6 shows two data loggers, one was an Agilent 34972A Data Acquisition Unit (DAU) and the other an OMEGA OM-DAQPRO-5300 portable data logger. They collected data from thermocouples, heat flux meters, water flow meter, and a pyranometer. All the data were collected every 10 seconds and were transferred to a computer for storage, calculation, and analysis. For indoor experiments, only the

Agilent DAU was needed. The use of the portable data logger became necessary for outdoor experiments.

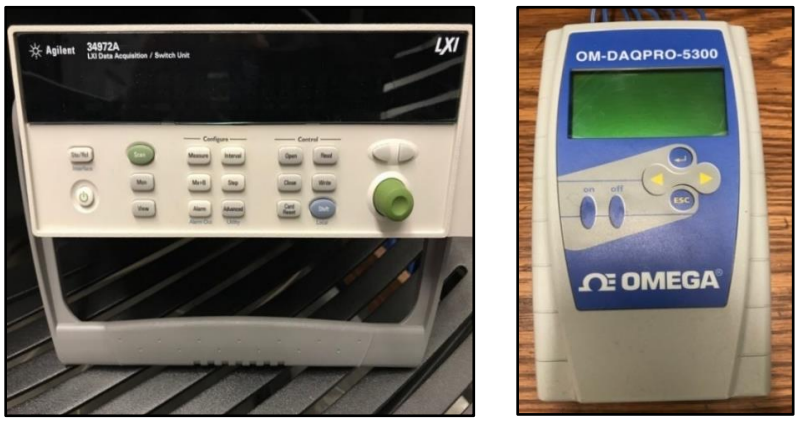

Figure 3.6 Agilent 34972A and OMEGA OM-DAQPRO-5300

3.1.3.1 Temperature Measurements

Type T thermocouples (T/C) with an error of ± 0.6 °C (± 1.1 °F) were used to measure temperatures. All T/Cs were connected in parallel and installed in grids to measure average interior and exterior surface temperatures of the polyisocyanurate board. The T/C are shown in Figure 3.7. Each side was instrumented with eight T/Cs on both the interior and exterior surfaces, and 16 T/Cs were installed on the interior and exterior surfaces of the rear side of the box behind the absorber plate.

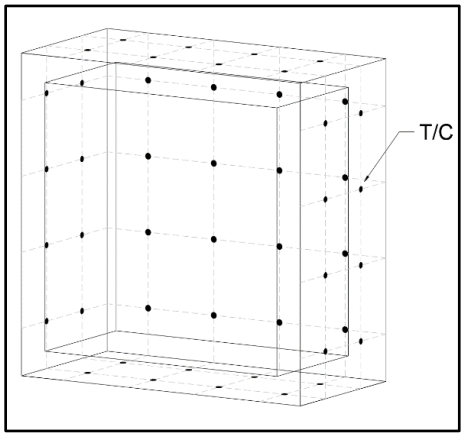

Figure 3.7 Thermocouple Grids on Interior and Exterior Surface of the Insulation

As shown in Figure 3.8, when measuring temperatures, the T/C sensor were covered with aluminum tape to minimize radiation effects.

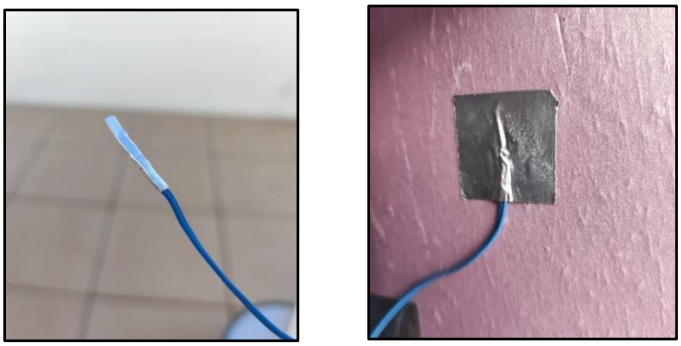

Figure 3.8 Thermocouples Covered with Aluminum Tape

A smaller size type T T/C was used to measure inlet and outlet water temperature in the absorber plate. The T/Cs were installed within the temperature probe, and the probe was installed in an inline flow-through fitting as shown in Figure 3.9.

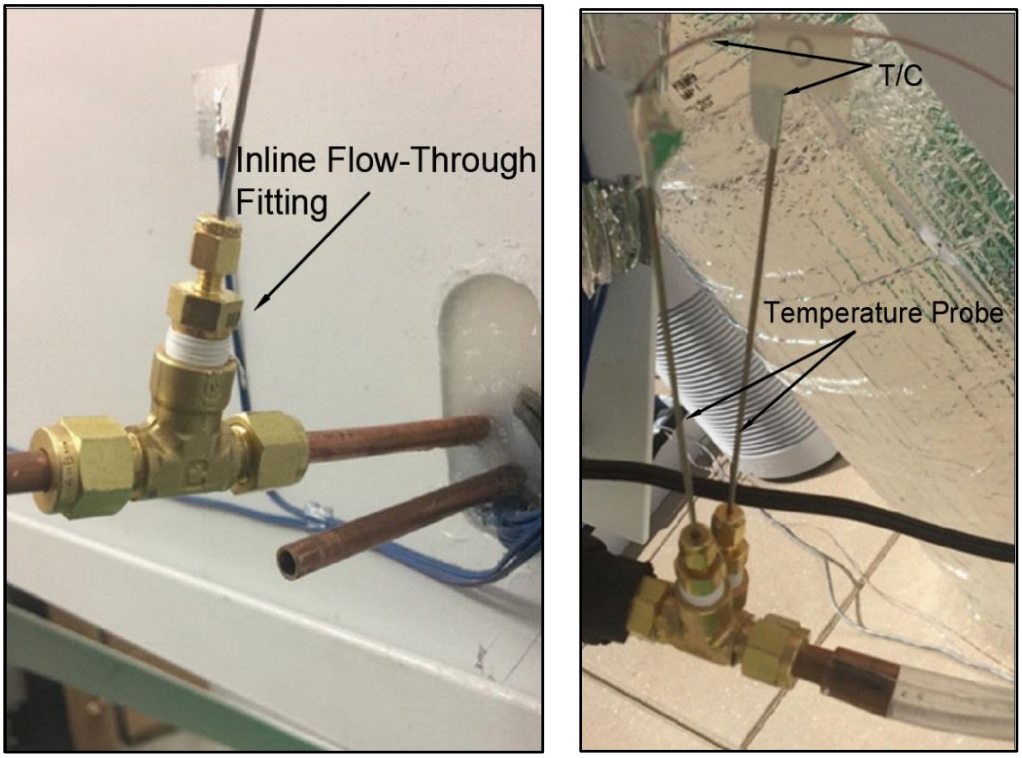

Figure 3.9 Inline Flow-Through Fitting and Temperature Probe

3.1.3.2 Heat Flux Measurements

Four Heat flux meters (HFMs) with dimension of 5.08 cm × 5.08 cm × 0.48 cm (2 in × 2 in × 3/16 in) were installed on the rear interior wall. Two thin film heat flux meters with dimension 3.51 cm × 2.85 cm × 0.018 cm (1.38 in × 1.12 in × 0.007 in) were installed on each side wall. The heat flux sensors had an error of ± 2%.

3.1.3.3 Solar Radiation Measurements

A LI-COR pyranometer was installed on the surface of the solar calorimeter cover to measure the solar global radiation (Figure 3.10).

Figure 3.10 LI-COR Pyranometer

3.1.3.4 Water Flow Rate Measurements

Water flow rates were measured using a water flow sensor. This sensor was installed at the top of water tank (Figure 3.11). Output signals of 0 - 5 V DC were linearly proportional to a flow range of 100 - 1000 ml/min (3.38 - 33.8 fl oz/min) with an error of ± 1%. The senor was connected to a control valve which served to adjust the water flow rates.

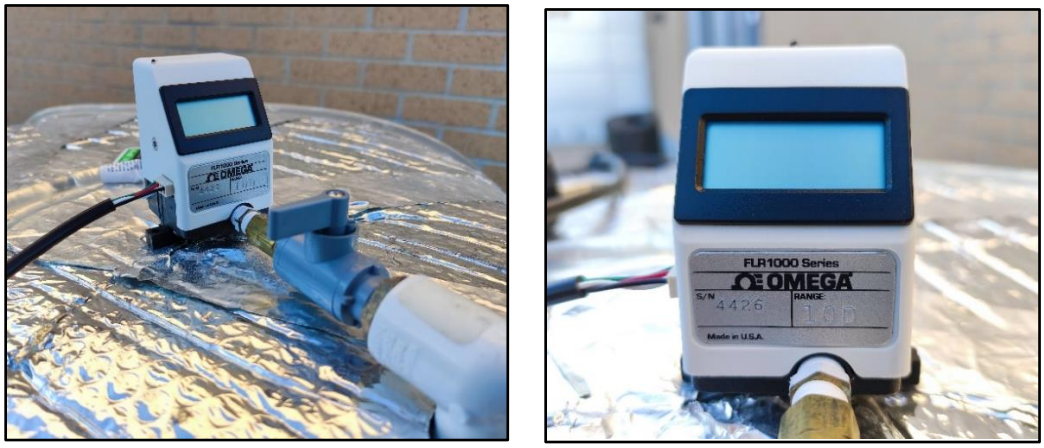

Figure 3.11 Water Flow Sensor

3.1.4 Solar Tracker System

A dual-axis solar tracker allows the rotation of a solar calorimeter along two axes following the path of the sun, which ensures that specimens be directly perpendicular to the direct beam of solar radiation during testing. The solar tracker used in this dissertation consisted of four parts: a four-quadrant-structure light sensor, a controller, and 2 motorized actuators (Figure 3.12).

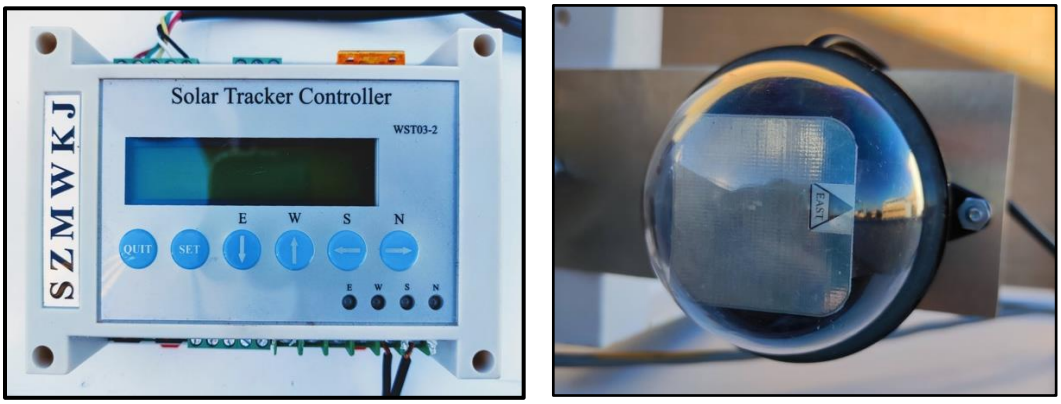

Figure 3.12 Solar Tracker Controller and Light Sensor

Figure 3.13 shows the two motorized actuators, which turned the solar calorimeter in two directions. One linear actuator was installed directly on the side of the solar calorimeter casing. The other actuator was made with a gear box, a car wheel hub, a chain, and a sprocket, and was installed on the solar calorimeter stand. With the analysis of light sensor's signal, the controller can control motor's positive rotation or negative rotation of each corresponding orientation, which maintains the solar calorimeter testing surface normal to the sun's direct beam radiation.

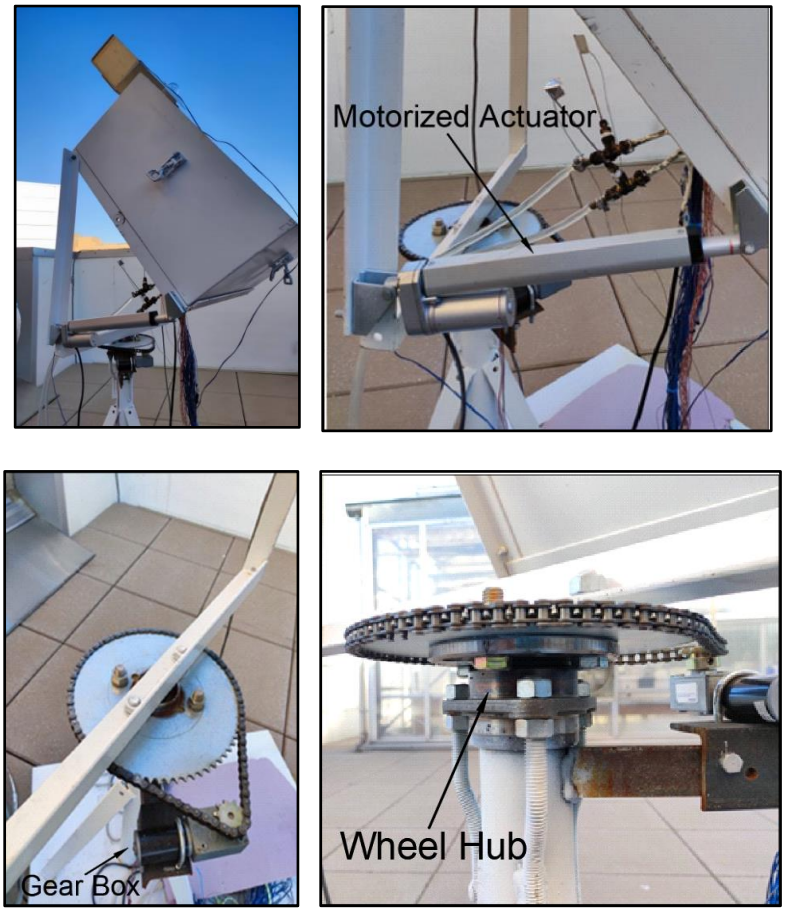

Figure 3.13 Motorized Actuators

The light sensor was installed on the frame of solar calorimeter at the same surface of the specimen. The light sensor was factory calibrated. To calibrate the solar calorimeter testing surface relative to the sun's position, solar elevation angle and azimuth angle were measured and compared with calculated angles using NOAA Solar Calculator from the Global Monitoring Laboratory [34].

3.1.5 Solar-Air Heat Transfer Coefficient Meter

For outdoor experiments, the heat transfer coefficient on the test specimen was measured using a laboratory-made solar-air heat transfer coefficient meter [20]. This coefficient meter has dimensions of 15 cm × 15 cm × 10.5 cm (6 in × 6 in × 4 in). A 1.25 mm (0.05 in) thick copper plate with a dimension of 15 cm × 15 cm (6 in × 6 in), painted matte black, was attached at the front of the meter. A type T thermocouple was soldered to the center of the back side of the copper plate. Foam insulation was attached to the plate in a manner by which the thermocouple was located between the plate and the foam. The foam had the same dimensions as the plate and had a thickness of 10.16 cm (4 in). The exposed edges of insulation foam were covered with a thin-wall five-sided box made from 5 mm (0.2 in) thick plywood. The coefficient meter is shown in Figure 3.14.

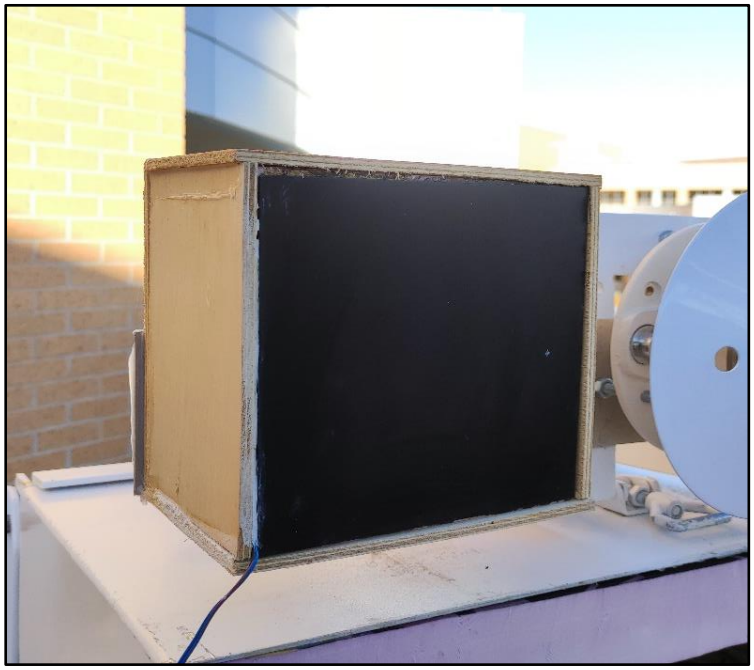

Figure 3.14 Solar-Air Heat Transfer Coefficient Meter

3.2 Indoor Experimental Set-up

3.2.1 Solar Simulator

The solar simulator, as shown in Figure 3.15, consisted of three parts: nine 500 W halogen lamps, a frame, and a stand. The frame was made using an aluminum sheet. Its dimensions are shown in the Figure 3.16. Nine lamps were installed in a special arrangement, in which all lamps were turned 90^{o} from each other. This arrangement of cancelled out any uneven radiation distribution along the two axes with respect to lamp centerline [10]. The fame and the stand were painted matte black to minimize the reflection effects within the laboratory.

Figure 3.15 Solar Simulator

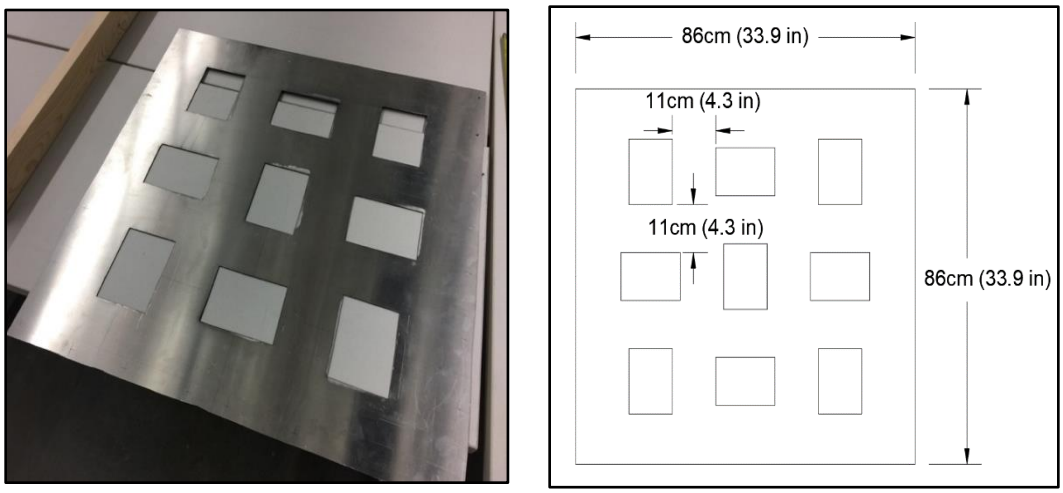

Figure 3.16 Solar Simulator Frame and Dimensions

3.2.2 Radiation Measurements

A LI-200R pyranometer was used to measure the radiation from the solar simulator. The radiation was measured at 196 points on a 14 x14 grids on the specimen. To accurately measure the radiation on each point, a similar number of holes was cut on a foam board, which secured the pyranometer and kept the consistency at each measure point (Figure 3.17). The total radiation was calculated by using an interpolation method in MATLAB.

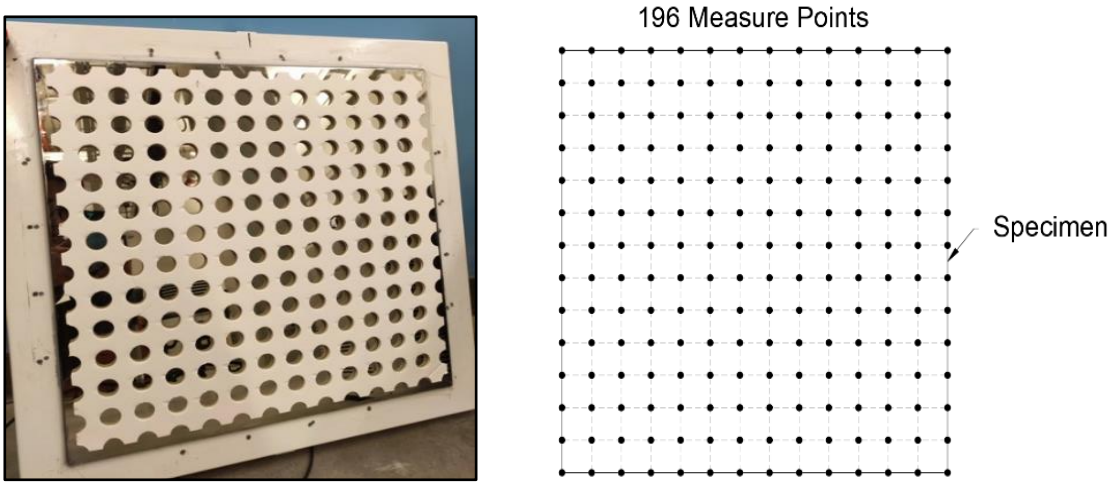

Figure 3.17 Foam Board with 196 Measuring Points

3.3 Solar Calorimeter System Portability

The calorimeter system was designed as a user-friendly system for student use for educational purposes. One of the goals was to easily move the system and set it up for use under indoor and outdoor conditions. For that reason, the system was designed of smaller size compared to other solar calorimeter systems found in the

open literature. Secondly, a platform, outfitted with heavy duty swivel casters was designed and built to support the calorimeter box and solar tracker and to accommodate the data acquisition system, all for easy transportability. The chilled water system could be easily moved by first draining the water from the water tank. Once the tank is filled up with water, a 24-hour period is required to reach desired water temperatures. It is recommended that the chilled water system be set up on a folding handle platform truck.

CHAPTER IV

EXPERIMENTAL RESULTS AND DISCUSSION

4.1 Indoor Experiments

4.1.1 Solar Calorimeter Calibration

The solar calorimeter was calibrated by using a 6 mm (1/4 in) thickness single-layer glass. The glass specimen, which was provided by a local architectural glass company, had a known U-factor of 5.81 W/m^2K (1.02 $Btu/hr \cdot ft^2 \cdot °F$). The calculated SHGC was compared with referenced values from other research and industry resources. All the indoor experiments were conducted in the Building Materials and Thermal Sciences Laboratory, located in the Engineering Complex's LEEP2 building at University of Kansas. The room indoor air temperature was kept around 21 ºC (69.8 ºF). All data were collected at 10 seconds intervals. To increase the accuracy of calculations, these 10-second values were averaged on a minute basis.

4.1.2 Solar Simulator Adjustment

The process of discovering the best uniformity in spatial, temporal, and spectral radiation and testing distance from simulator to the specimen was essential to the indoor experiments.

First, to determine the optimum testing distance, with all the nine halogen lamps turned on, the irradiance was tested at the 196 testing points on the surface of specimen. During the test, the distance from the surface of specimen to the surface of solar simulator was measured from the top, bottom, left, and right sides to ensure the solar simulator was completely aligned with the solar calorimeter. Figure 4.1 shows a picture of this the testing process.

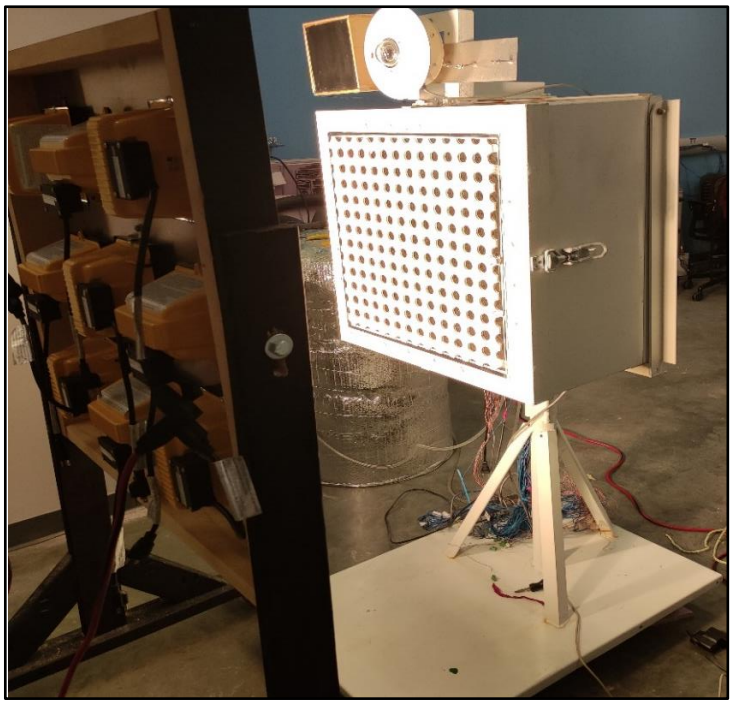

Figure 4.1 Testing Process to Determine Optimum Distance from Solar Simulator to Calorimeter

The light irradiance was tested at a distance of 25.4 cm (10 in), 38.1 cm (15 in), 50.8 cm (20 inch), 63.5 cm (25 in), and 76.2 cm (30 in). Table 4.1, Table 4.2, Table 4.3, Table 4.4, and Table 4.5 show the tested irradiance results on the 196 testing points with these five testing distances. The average irradiance produced with 25.4 cm (10 in), 38.1 cm (15 in), 50.8 cm (20 inch), 63.5 cm (25 in), and 76.2 cm (30 in) testing distance were respectively 2623.25 W/m^2 (831.57 $Btu/hr \cdot ft^2$), 2219.48 W/m^2 (703.57 $Btu/hr \cdot ft^2$), 1821.58 W/m^2 (577.44 $Btu/hr \cdot ft^2$), 1487.82 W/m^2 (471.43 $Btu/hr \cdot ft^2$), 1214.32 W/m^2 (384.93 $Btu/hr \cdot ft^2$). The average irradiance of all the five tests was high when comparing it with the maximum solar irradiance on

earth. Typically, the peak value of normal surface solar irradiance on earth on a clear day is around 1000 W/m^2 (317 $Btu/hr \cdot ft^2$) [21]. Figure 4.2, Figure 4.3, Figure 4.4, Figure 4.5, and Figure 4.6 show the irradiance distribution chart generated using the 196 testing points at these five testing distances. Figures 4.2 and 4.3 show that the irradiance distribution at the 25.4 cm (10 in) and 38.1 cm (15 in) distances were not uniform. As the testing distance increased, the 50.8 cm (20 inch) and 63.5 cm (25 in) distance distribution chart show a relatively more evenly irradiance distribution. However, as the testing distance increased to 76.2 cm (30 in), the irradiance distribution had a non-uniform curve and a large irradiance drop at the four corners.

Table 4.1 Irradiance at 25.4 cm (10 in) Testing Distance at 196 Test Points with 9 Lamps Turned On

25.4 cm (10 in) (W/m^2)	1	2	3	4	5	6	7
A	2102.63	2154.56	2364.04	2483.40	2610.54	2409.22	2447.12
B	2171.84	2239.35	2460.40	2611.88	2770.25	2540.74	2525.83
C	2303.59	2388.97	2574.05	2769.96	2990.79	2932.41	3188.48
D	2235.19	2344.83	2428.73	2542.74	2634.73	2598.15	2929.81
E	2333.41	2465.15	2508.62	2625.60	2654.98	2642.96	3070.76
F	2387.78	2493.93	2528.72	2600.08	2602.83	2556.84	2930.85
G	2541.04	2636.13	2645.93	2706.68	2641.62	2579.24	2862.38
H	2703.86	2802.67	2811.79	2830.12	2725.74	2674.34	2852.37
I	2914.31	3060.96	3025.43	2963.79	2773.44	2701.41	2854.37
J	2625.16	2777.30	2775.00	2776.33	2671.82	2691.70	2858.45
K	2481.77	2658.98	2626.12	2598.01	2550.61	2574.34	2669.22
L	2595.56	2683.31	2615.59	2565.22	2538.96	2575.16	2631.54
M	2424.05	2560.55	2512.70	2444.90	2379.47	2365.97	2456.62
N	2317.23	2507.95	2415.23	2357.44	2381.10	2325.17	2416.64

25.4 cm (10 in) (W/m^2)	8	9	10	11	12	13	14
A	2333.18	2381.10	2490.82	2527.54	2484.21	2398.09	2395.87
B	2519.97	2458.62	2530.58	2577.76	2595.19	2523.01	2482.95
C	3170.08	2944.35	2915.72	2854.59	2769.66	2634.58	2557.36
D	2890.79	2683.68	2726.86	2775.22	2751.26	2601.86	2563.29
E	2800.59	2496.23	2508.62	2574.27	2627.08	2527.16	2378.06
F	2970.54	2525.61	2559.80	2650.67	2623.89	2577.61	2377.32
G	3018.01	2463.15	2489.70	2534.51	2502.68	2460.70	2321.02
H	3101.99	2489.70	2537.92	2587.32	2514.92	2502.98	2320.20
I	3192.41	2548.60	2670.33	2624.12	2589.70	2648.00	2525.46
J	3306.50	2736.20	2844.73	2895.10	2794.36	2904.67	2748.15
K	3103.99	2675.90	2778.12	2808.53	2754.30	2879.82	2688.06
L	2900.51	2624.93	2687.24	2660.32	2600.16	2731.98	2631.02
M	2679.90	2584.13	2700.00	2615.66	2583.39	2724.56	2564.18
N	2565.00	2446.01	2579.09	2522.34	2489.33	2596.97	2522.27

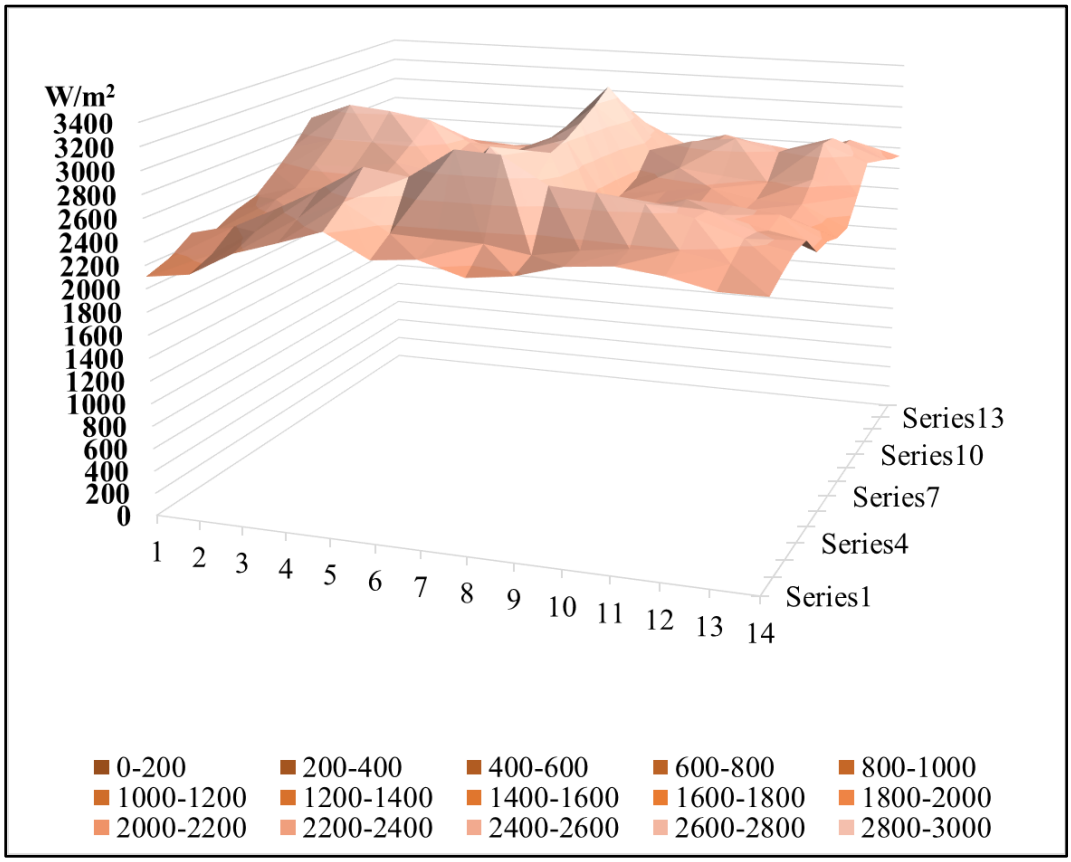

Figure 4.2 Irradiance Distribution for the 25.4 cm (10 in) Testing Distance

Table 4.2 Irradiance at 38.1 cm (15 in) Testing Distance at 196 Test Points with 9 Lamps Turned On

38.1 cm (15 in) (W/m^2)	1	2	3	4	5	6	7
A	1660.82	1730.17	1739.97	1824.38	1888.18	2079.86	2076.08
B	1719.34	1833.88	1813.18	1902.35	1993.66	2176.07	2159.75
C	1981.42	2083.42	2079.34	2129.71	2237.94	2413.67	2401.28
D	2078.67	2178.15	2235.64	2345.94	2423.61	2688.80	2685.76
E	2063.69	2151.52	2179.63	2283.11	2371.16	2591.48	2578.35
F	2091.06	2237.71	2273.99	2312.12	2383.03	2567.00	2552.39
G	2090.24	2268.57	2338.90	2392.53	2468.56	2626.34	2611.80
H	2224.14	2386.74	2464.48	2476.87	2574.12	2608.54	2599.93
I	2218.80	2423.83	2510.92	2493.78	2538.59	2594.37	2578.35
J	2234.52	2413.15	2537.10	2482.06	2543.93	2572.34	2577.61
K	2079.49	2230.59	2399.13	2334.89	2359.89	2428.73	2478.13
L	1905.61	2034.76	2234.60	2154.56	2210.49	2242.83	2308.63
M	1720.83	1904.27	2103.30	2070.22	2036.09	2075.11	2131.49
N	1640.19	1794.34	1963.25	1927.86	1959.24	1964.95	2069.84

38.1 cm (15 in) (W/m^2)	8	9	10	11	12	13	14
A	1964.95	2004.49	1932.02	1880.09	1880.17	1657.55	1586.64
B	2139.57	2078.67	2056.49	1948.63	1939.51	1724.61	1657.55
C	2406.62	2300.25	2234.23	2171.25	2108.79	1918.74	1783.06
D	2729.08	2612.03	2481.99	2386.22	2239.87	2046.40	1890.33
E	2646.07	2520.12	2426.50	2360.70	2249.73	2044.77	1880.31
F	2635.24	2549.12	2405.58	2370.87	2275.92	2103.15	1995.44
G	2714.32	2562.62	2417.01	2393.27	2290.98	2121.77	1952.79
H	2703.42	2524.64	2394.75	2405.21	2351.14	2145.95	1986.84
I	2681.98	2551.72	2342.01	2332.15	2301.43	2045.66	1923.78
J	2679.08	2545.78	2360.41	2346.61	2378.80	2083.49	1974.15
K	2688.36	2512.33	2390.23	2397.87	2450.68	2085.79	1950.12
L	2552.39	2417.01	2304.10	2350.47	2483.25	2066.88	1907.61
M	2266.57	2155.82	2041.66	2059.31	2190.31	1793.23	1761.55
N	2175.92	2079.49	1957.54	2077.26	2031.72	1668.23	1655.03

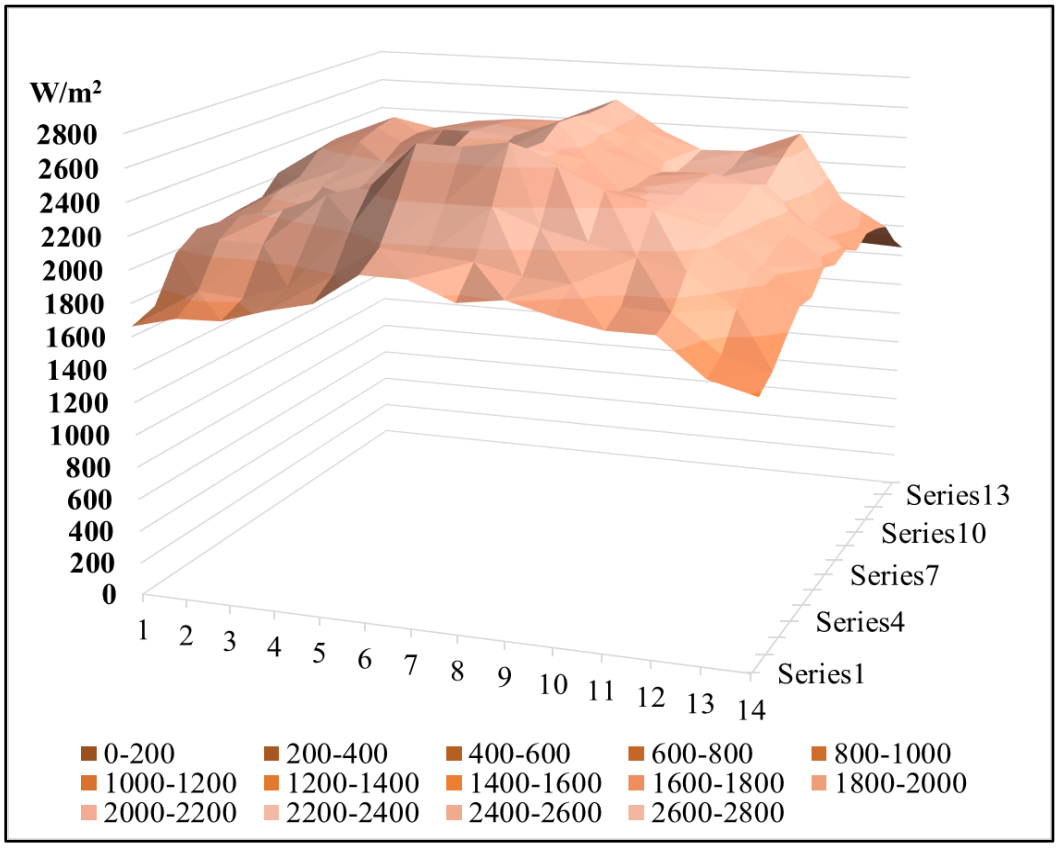

Figure 4.3 Irradiance Distribution for the 38.1 cm (15 in) Testing Distance

Table 4.3 Irradiance at 50.8 cm (20 in) Testing Distance at 196 Test Points with 9 Lamps Turned On

50.8 cm (20 in) (W/m^2)	1	2	3	4	5	6	7
A	1360.83	1377.30	1336.87	1415.21	1474.85	1500.07	1611.78
B	1385.16	1467.95	1482.86	1574.25	1546.50	1612.15	1643.16
C	1426.63	1432.71	1553.48	1634.63	1718.53	1841.74	1868.52
D	1553.85	1665.34	1719.64	1821.04	1927.49	1997.37	2016.14
E	1608.07	1805.10	1862.66	2004.20	2116.87	2189.87	2202.85
F	1594.05	1734.63	1853.02	1974.60	2086.61	2121.03	2132.30
G	1690.49	1706.66	1835.14	1976.90	2112.35	2146.70	2169.69
H	1601.47	1747.16	1886.10	2039.88	2149.96	2164.05	2182.67
I	1559.49	1741.30	1879.13	2028.67	2113.76	2113.83	2132.45
J	1509.41	1739.08	1838.85	1998.78	2061.61	2053.90	2074.59
K	1485.16	1658.29	1797.16	1970.44	2033.20	2016.14	2048.55
L	1471.29	1538.57	1697.98	1902.49	1936.84	1919.56	1963.10
M	1349.33	1397.55	1579.51	1786.92	1782.62	1765.93	1792.71
N	1303.12	1330.34	1497.62	1749.02	1727.21	1710.29	1772.16

50.8 cm (20 in) (W/m^2)	8	9	10	11	12	13	14
A	1656.88	1673.20	1589.60	1537.16	1426.41	1438.35	1404.90
B	1713.41	1715.78	1655.25	1560.75	1516.02	1621.87	1438.28
C	1950.86	1982.31	1907.76	1796.64	1733.44	1656.88	1552.81
D	2090.84	2119.47	2038.32	1923.78	1853.39	1707.33	1692.71
E	2282.59	2296.84	2207.97	2063.61	1964.14	1811.18	1752.35
F	2192.69	2233.63	2169.39	2050.04	1968.74	1793.75	1731.44
G	2221.69	2264.20	2194.10	2079.56	2009.83	1905.61	1743.16
H	2212.57	2258.11	2221.62	2088.24	1996.78	1809.55	1747.75
I	2156.04	2188.53	2179.19	2057.31	1953.98	1746.35	1696.94
J	2087.35	2115.54	2093.58	2009.76	1916.51	1718.90	1682.25
K	2070.96	2078.00	2028.67	1985.21	1901.38	1671.94	1629.96
L	1986.84	2014.80	1942.48	1937.14	1877.87	1652.29	1616.31
M	1799.90	1841.22	1824.75	1759.10	1726.17	1515.72	1426.70
N	1761.63	1764.37	1707.85	1702.28	1694.57	1430.04	1364.10

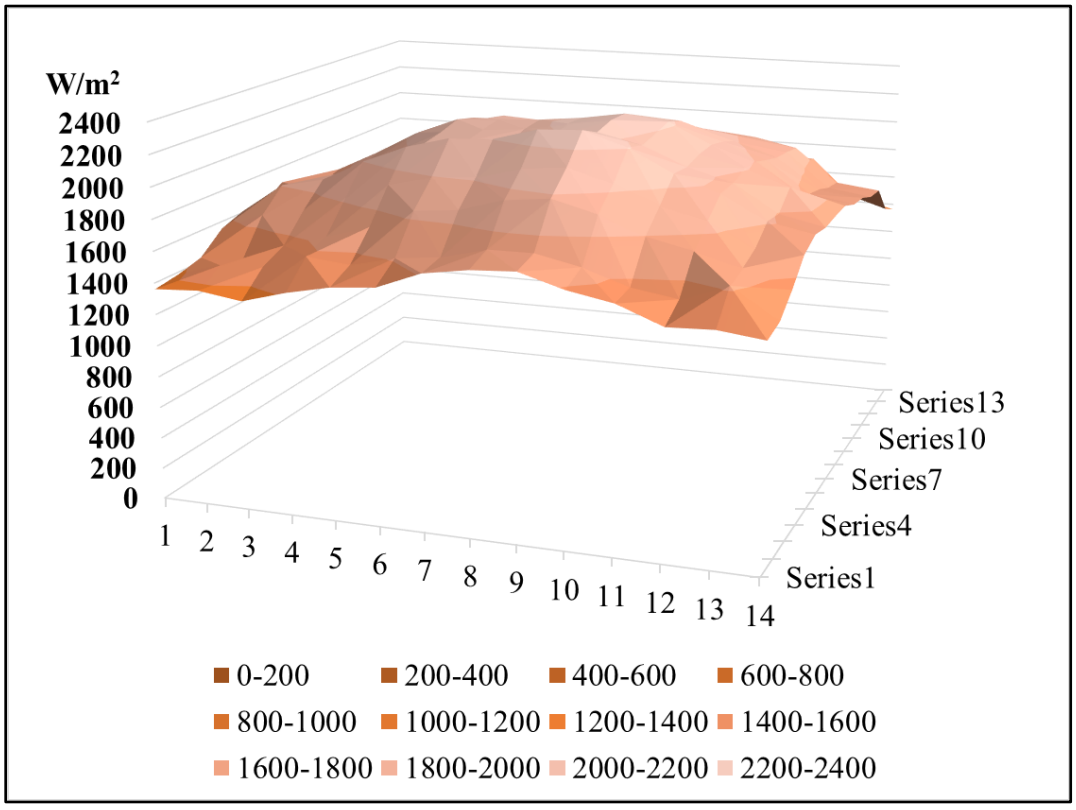

Figure 4.4 Irradiance Distribution for the 50.8 cm (20 in) Testing Distance

Table 4.4 Irradiance at 63.5 cm (25 in) Testing Distance at 196 Test Points with 9 Lamps Turned On

63.5 cm (25 in) (W/m^2)	1	2	3	4	5	6	7
A	1114.26	1130.87	1189.40	1212.40	1278.79	1352.97	1383.38
B	1114.33	1170.04	1230.42	1304.60	1394.51	1410.98	1435.16
C	1129.98	1218.78	1307.42	1397.03	1478.11	1494.58	1499.25
D	1212.77	1299.41	1381.38	1412.76	1571.87	1579.14	1602.51
E	1309.13	1383.83	1475.59	1575.51	1658.37	1678.69	1682.18
F	1329.45	1446.51	1555.11	1670.61	1792.71	1804.21	1829.95
G	1335.39	1423.07	1547.17	1660.89	1785.36	1788.92	1803.69
H	1263.58	1397.03	1516.31	1633.37	1746.94	1751.17	1777.43
I	1274.26	1375.52	1482.34	1584.11	1695.09	1707.92	1718.53
J	1276.64	1353.64	1448.74	1543.39	1662.67	1665.34	1682.55
K	1204.02	1331.16	1436.79	1539.83	1663.93	1645.39	1661.19
L	1216.48	1272.85	1378.19	1491.83	1603.10	1593.83	1605.92
M	1116.04	1189.70	1276.71	1407.94	1495.77	1499.99	1521.14
N	1114.48	1139.11	1230.57	1338.58	1411.94	1425.07	1476.11

63.5 cm (25 in) (W/m^2)	8	9	10	11	12	13	14
A	1441.91	1456.82	1386.35	1367.73	1294.00	1262.69	1191.26
B	1498.44	1520.69	1481.97	1462.98	1316.47	1262.91	1204.16
C	1546.50	1588.27	1566.09	1526.55	1363.06	1313.80	1253.57
D	1649.69	1666.60	1638.41	1601.84	1445.40	1360.98	1279.09
E	1727.65	1716.08	1691.45	1663.71	1497.99	1395.40	1284.95
F	1872.60	1872.75	1844.78	1800.13	1620.31	1516.02	1401.26
G	1839.81	1853.46	1856.80	1829.80	1655.40	1534.64	1411.05
H	1801.91	1803.24	1810.14	1799.46	1592.13	1464.09	1378.93
I	1734.55	1736.63	1757.32	1757.25	1547.25	1417.58	1338.58
J	1688.78	1686.48	1721.27	1731.06	1527.81	1393.92	1279.01
K	1667.49	1647.09	1677.58	1687.15	1478.63	1353.71	1296.52
L	1589.75	1589.38	1635.52	1625.43	1406.16	1321.81	1229.83
M	1507.49	1494.73	1540.35	1500.36	1333.24	1244.52	1116.04
N	1449.33	1434.05	1405.56	1386.28	1212.47	1177.90	1114.33

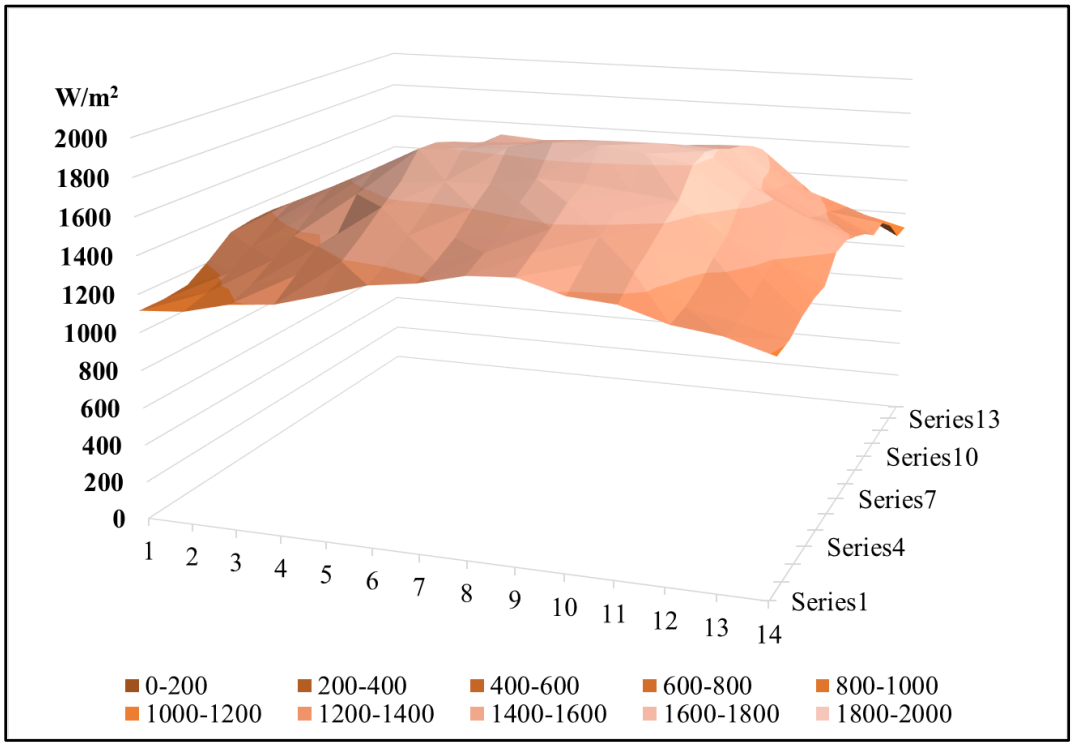

Figure 4.5 Irradiance Distribution for the 63.5 cm (25 in) Testing Distance

Table 4.5 Irradiance at 76.2 cm (30 in) Testing Distance at 196 Test Points with 9 Lamps Turned On

76.2 cm (30in) (W/m^2)	1	2	3	4	5	6	7
A	866.20	882.67	959.37	1017.82	1082.95	1113.74	1146.75
B	874.51	954.55	1013.00	1092.23	1136.88	1154.76	1175.09
C	940.16	1005.58	1070.27	1142.67	1205.80	1221.89	1245.56
D	984.15	1071.83	1143.04	1241.03	1296.00	1313.36	1327.60
E	1066.56	1132.06	1192.15	1304.46	1343.18	1368.84	1384.79
F	1114.33	1157.58	1232.43	1341.84	1393.40	1425.52	1440.35
G	1154.46	1182.28	1268.48	1391.62	1447.99	1480.11	1499.77
H	1101.50	1139.26	1228.64	1347.78	1385.76	1428.11	1439.54
I	1086.51	1115.89	1210.40	1304.38	1354.60	1395.40	1405.19
J	1022.87	1100.68	1192.81	1295.92	1345.77	1400.37	1398.22
K	1012.48	1073.31	1161.44	1253.20	1299.78	1353.86	1349.56
L	980.59	1049.65	1133.10	1224.79	1273.00	1372.92	1310.24
M	914.19	987.71	1063.96	1158.10	1210.10	1271.59	1244.44
N	832.60	915.83	980.81	1074.87	1166.85	1207.50	1211.58

76.2 cm (30in) (W/m^2)	8	9	10	11	12	13	14
A	1138.66	1159.43	1178.94	1114.41	1016.19	926.43	891.05
B	1180.72	1193.26	1204.91	1196.38	1094.90	1020.72	933.93
C	1254.90	1257.94	1276.12	1251.71	1157.58	1065.22	1013.97
D	1332.64	1340.66	1346.00	1307.79	1191.78	1103.95	1055.66
E	1387.09	1384.27	1392.73	1349.85	1241.18	1143.86	1108.55
F	1446.44	1439.76	1460.23	1418.47	1284.80	1196.23	1137.92
G	1504.52	1508.97	1539.01	1488.87	1369.73	1251.71	1195.04
H	1440.06	1452.59	1477.59	1427.07	1309.87	1199.19	1155.58
I	1404.82	1410.68	1441.09	1376.56	1269.74	1160.77	1121.01
J	1396.29	1403.34	1429.15	1348.74	1232.95	1124.87	1107.51
K	1344.44	1345.70	1378.34	1319.14	1199.42	1105.36	1067.45
L	1311.80	1293.48	1330.64	1271.00	1156.76	1073.38	1015.45
M	1251.42	1254.16	1280.27	1207.72	1094.38	1012.48	979.92
N	1214.10	1187.70	1228.20	1181.69	1062.26	965.16	942.01

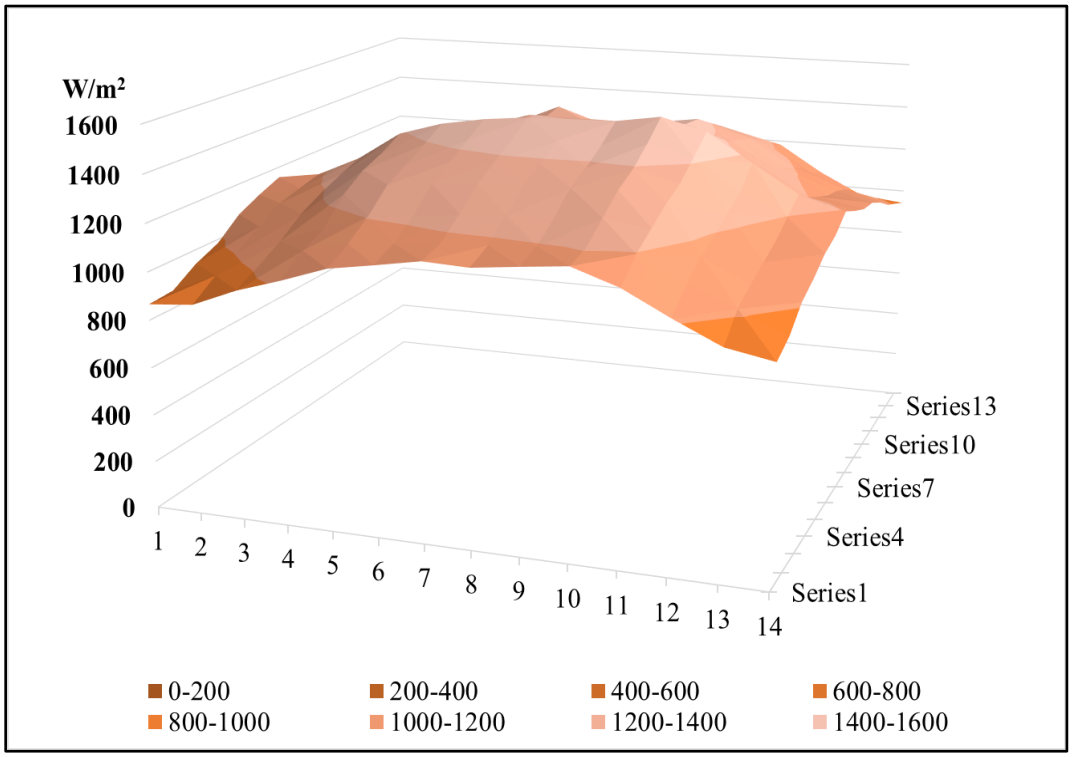

Figure 4.6 Irradiance Distribution for the 76.2 cm (30 in) Testing Distance

To achieve a lower average irradiance, three other arrangements where some lamps were not turned on were tried. These arrangements are shown in Figure 4.7. Figure 4.7 (a) shows the results when the four lamps at the corners are turned on. Figure 4.7 (b) shows the results when four side lamps were turned on. Figure 4.7 (c) shows the results when four-corner and the center lamps were turned on. These tests were carried out at a testing distance of 63.5 cm (25 in). Table 4.7, Table 4.8, and Table 4.9 show the irradiance results at the 196 testing points for arrangement (a), (b), and (c), respectively. The comparison of irradiance distribution for arrangements (a), (b), and (c) is shown in Table 4.6. It was found that the average irradiance was less than 1000 W/m^2 (317 $Btu/hr \cdot ft^2$). However, the maximum irradiance for arrangement (b) and (c) were higher than 1000 W/m^2 (317 $Btu/hr \cdot ft^2$). Moreover, with the corner lamps turned on, the difference between maximum and minimum irradiance provided the lowest value among all three arrangements. Figure 4.8, Figure 4.9, and Figure 4.10 show the irradiance distribution generated with arrangements (a), (b), and (c), respectively. Combining this with the results from Table 4.6, it was observed that that the arrangement with the 4-corner lamps turned on provided the most uniform irradiance distribution among all three arrangements.

Thus, the arrangement where the 4 corner lamps were turned on was chosen for the solar calorimeter calibration. Two more tests at distances of 38.1 cm (15 in) and 50.8 cm (20 in) were carried out and the results were compared with the results

from the test at 63.5 cm (25 in). All these irradiances are shown in Tables 4.10 and 4.11. The irradiance distribution is shown in Figures 4.11 and 4.12. Comparing all three irradiance distributions, it was found that best suitable irradiances were generated at a testing distance of 50.8 cm (20 in). Therefore, the arrangement using 4 corner lamps at a distance between solar simulator and calorimeter of 50.8 cm (20 in) was used for all indoor experiments.

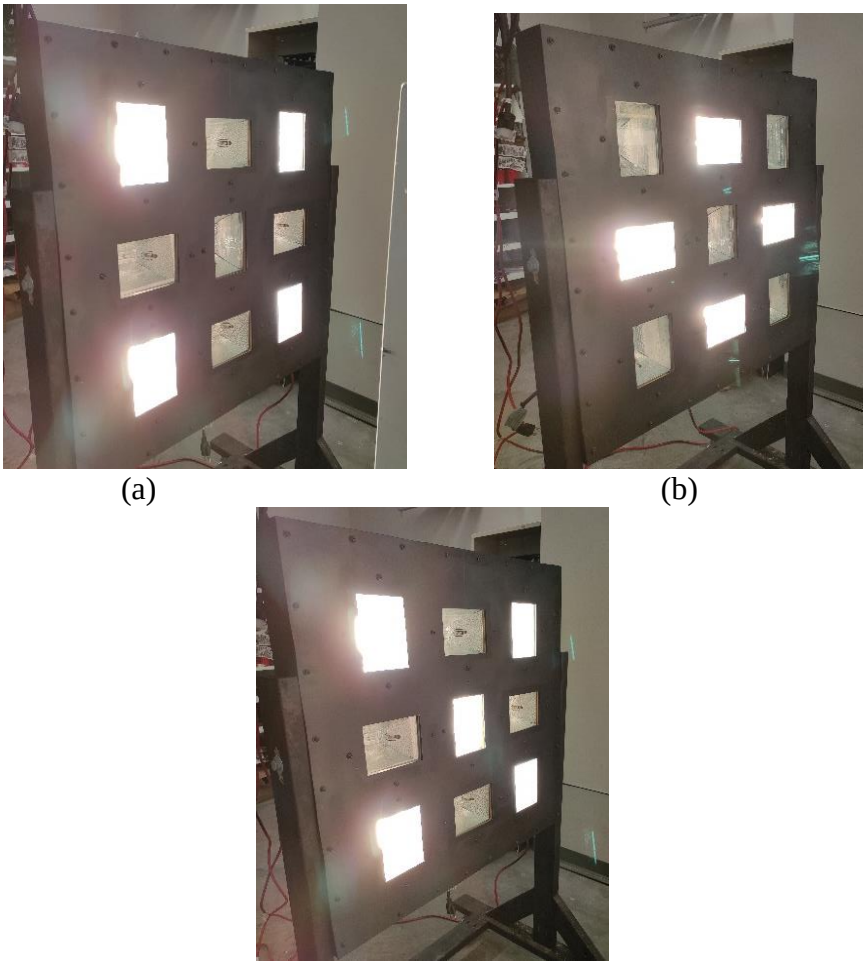

(a) (b)

(c)

Figure 4.7 Solar Simulator Lamp Arrangements

Table 4.6 Comparison of Irradiance for Arrangement (a), (b), and (c)

Lamp Arrangement	Average Iraddiance W/m^2 ($Btu/h \cdot ft^2$)	Maximum Irradiance W/m^2 ($Btu/h \cdot ft^2$)	Minimum Irradiance W/m^2 ($Btu/h \cdot ft^2$)	Difference between Maximum and Minimum Irradiance W/m^2 ($Btu/h \cdot ft^2$)
4 Corner Lamps	577.97 (183.21)	683.67 (216.72)	428.13 (135.72)	255.54 (81.01)
4 Side Lamps	834.30 (264.47)	1083.38 (343.43)	570.98 (180.99)	512.40 (162.43)
4 Corner and Center Lamps	844.49 (267.70)	1051.47 (333.31)	612.19 (194.06)	439.28 (139.25)

Table 4.7 Irradiance at a Testing Distance of 63.5 cm (25 in) at 196 Test Points with 4 Corner Lamps Turned On

4 Corner Lamps 63.5 cm (25 in) (W/m^2)	1	2	3	4	5	6	7
A	443.87	521.91	522.13	589.78	582.13	616.78	637.11
B	447.26	555.46	564.10	616.78	607.38	640.28	653.29
C	473.92	548.58	558.20	626.84	626.40	646.84	663.34
D	475.02	562.57	594.15	645.20	642.57	662.47	674.16
E	494.15	578.74	620.17	664.00	653.61	676.89	680.17
F	481.36	574.92	623.45	654.27	659.08	671.43	669.68
G	472.83	570.55	619.95	655.91	660.61	661.16	665.64
H	471.63	567.16	620.06	662.90	667.93	661.37	667.39
I	472.07	568.58	624.32	676.24	674.60	667.17	667.71
J	468.35	562.68	616.78	670.23	683.67	662.58	672.20
K	464.42	534.80	595.25	658.31	648.59	636.13	635.14
L	444.52	521.14	584.65	642.14	647.49	616.45	610.99
M	441.13	507.70	561.04	616.23	616.45	596.34	587.05
N	433.92	473.16	530.98	562.57	562.35	563.77	549.45

4 Corner Lamps 63.5 cm (25 in) (W/m^2)	8	9	10	11	12	13	14
A	640.06	631.64	616.34	581.15	534.04	496.11	450.97
B	660.28	645.53	623.01	590.66	541.25	519.39	476.88
C	665.86	651.76	623.12	587.38	550.87	517.97	457.31
D	664.87	660.61	635.03	591.42	558.52	521.91	470.54
E	678.21	661.92	637.33	596.12	560.82	534.15	491.63
F	666.18	651.32	623.01	583.55	557.65	530.00	486.06
G	654.27	640.72	613.72	573.39	554.81	523.11	478.30
H	652.30	636.24	610.99	575.46	556.66	526.61	497.86
I	653.61	633.61	606.18	575.03	555.35	522.78	497.64
J	647.82	621.59	603.23	573.61	546.39	516.01	485.18
K	612.95	592.41	562.57	549.89	528.03	493.60	484.42
L	586.50	569.78	546.39	537.76	511.96	480.26	474.69
M	562.68	540.93	518.19	521.58	504.75	471.19	448.79
N	528.79	508.90	492.07	489.77	473.05	452.50	428.13

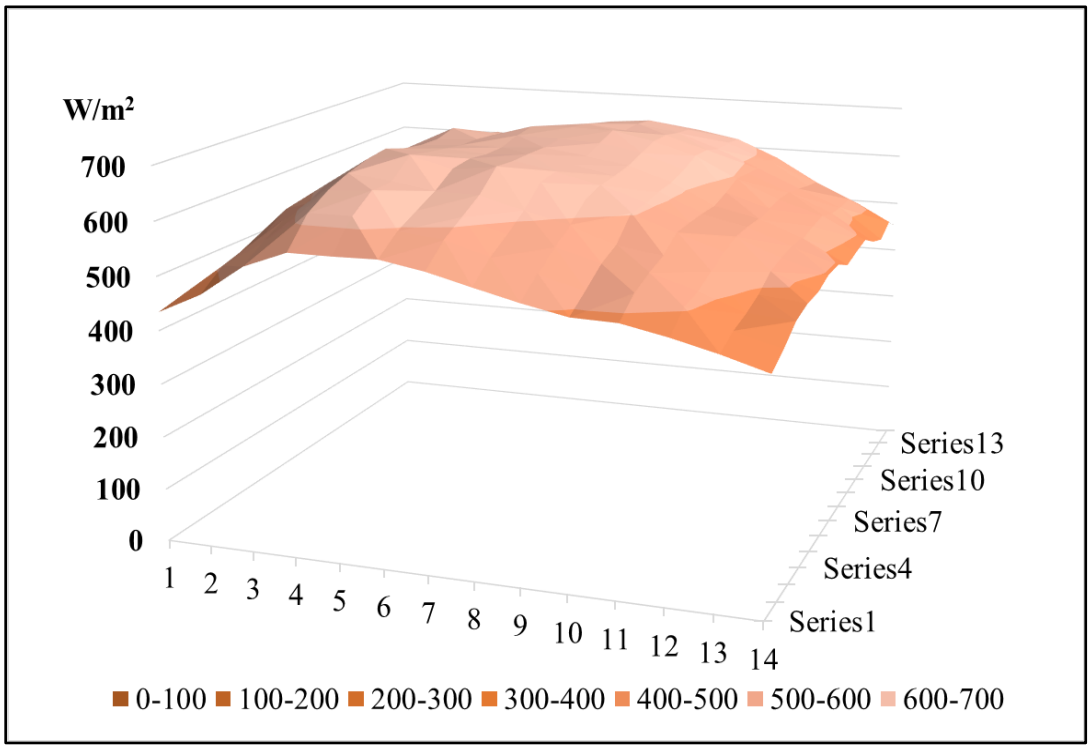

Figure 4.8 Irradiance Distribution for a Testing Distance of 63.5 cm (25 in) with 4 Corner Lamps Turned on

Table 4.8 Irradiance at a Testing Distance of 63.5 cm (25 in) at 196 Test Points with 4 Side Lamps Turned On

4 Side Lamps 63.5 cm (25 in) (W/m^2)	1	2	3	4	5	6	7
A	570.98	623.34	656.78	689.46	717.77	747.07	756.90
B	623.34	698.65	737.34	769.58	792.21	810.46	821.39
C	718.54	791.44	828.49	854.07	885.33	896.59	892.00
D	881.40	946.98	993.54	1013.87	1026.22	1031.57	1029.93
E	924.13	995.50	1034.20	1058.90	1077.04	1083.38	1080.10
F	818.55	913.09	949.27	980.86	1002.50	1018.46	1028.62
G	776.80	846.31	881.18	902.60	920.42	934.08	927.08
H	724.99	792.64	831.34	855.27	875.27	887.95	899.54
I	730.23	797.12	840.30	866.20	882.05	904.02	910.47
J	789.26	842.48	879.97	906.64	927.74	945.45	954.52
K	816.25	869.59	914.40	937.68	960.09	974.08	981.51
L	838.66	886.42	921.73	941.84	937.47	930.14	922.93
M	665.96	719.19	768.82	782.81	801.17	820.84	814.61
N	574.92	624.10	662.14	692.85	707.61	726.08	748.16

4 Side Lamps 63.5 cm (25 in) (W/m^2)	8	9	10	11	12	13	14
A	761.27	743.02	725.31	699.63	668.92	628.04	588.03
B	814.83	806.85	788.05	757.12	724.44	675.58	636.34
C	881.72	865.55	849.59	826.64	779.31	728.38	685.53
D	1010.04	976.92	956.48	914.73	877.02	809.37	727.94
E	1054.09	1031.46	1010.92	980.42	925.66	876.70	818.55
F	1019.66	998.56	964.68	935.72	884.67	817.02	767.29
G	917.90	895.49	879.21	839.75	805.65	751.98	697.99
H	892.22	876.37	857.24	832.43	789.04	735.15	703.89
I	903.80	886.86	863.58	840.95	801.50	746.74	697.44
J	946.87	931.13	905.66	872.54	820.84	766.96	743.68
K	965.01	940.96	900.74	860.08	805.21	750.13	715.04
L	913.86	872.87	846.97	805.32	718.87	716.90	696.35
M	807.18	778.11	743.57	721.60	683.23	626.94	623.56
N	757.23	745.64	733.29	711.87	686.08	649.35	607.71

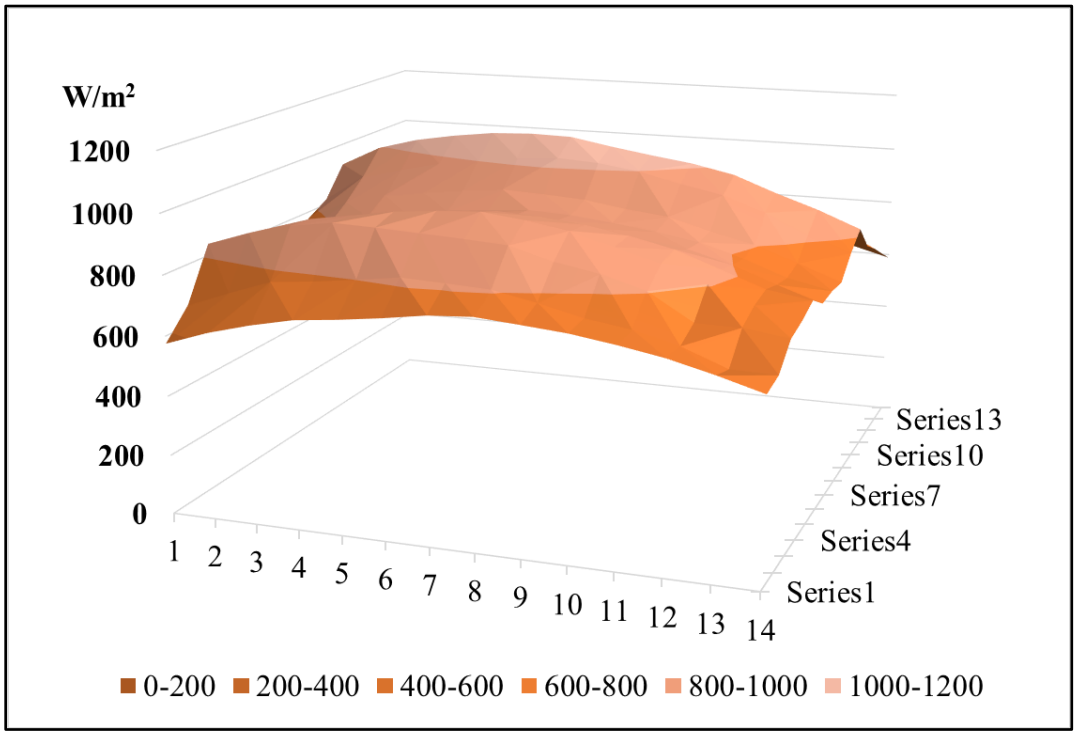

Figure 4.9 Irradiance Distribution for a Testing Distance of 63.5 cm (25 in) with 4 Side Lamps Turned on

Table 4.9 Irradiance at a Testing Distance of 63.5 cm (25 in) at 196 Test Points with 4 Corner and Center Lamps Turned On

4 Corner and Center Lamps 63.5 cm (25 in) (W/m^2)	1	2	3	4	5	6	7
A	634.49	710.67	735.37	809.37	799.31	844.78	872.98
B	665.42	761.82	802.37	859.54	865.44	906.86	935.39
C	697.55	794.06	833.41	915.06	912.44	945.45	975.07
D	725.21	811.01	862.05	939.11	929.38	968.73	999.11
E	745.32	847.29	904.46	972.44	964.68	1012.45	1028.62
F	750.89	866.20	934.84	1000.97	993.65	1031.68	1051.47
G	756.79	860.85	931.24	995.18	997.36	1037.48	1048.84
H	765.21	849.92	931.67	995.83	1000.64	1025.12	1038.68
I	749.80	840.30	912.87	994.41	1002.50	1010.15	1016.16
J	744.44	827.51	895.93	990.26	995.07	989.93	988.29
K	710.34	793.74	858.33	962.28	975.07	945.45	950.25
L	697.77	757.67	818.00	922.05	936.70	901.83	889.05
M	641.81	721.16	777.45	889.16	906.10	857.68	823.25
N	612.19	674.27	740.62	803.14	828.06	816.69	789.15

4 Corner and Center Lamps 63.5 cm (25 in) (W/m^2)	8	9	10	11	12	13	14
A	865.00	820.62	790.02	774.39	708.37	686.51	644.87
B	911.34	859.43	826.09	798.87	759.31	716.24	684.33
C	942.06	887.30	862.38	825.32	776.47	739.20	685.42
D	957.47	902.60	874.18	833.19	799.75	765.76	719.19
E	987.09	929.05	898.45	849.26	803.14	756.47	719.19
F	994.74	943.70	910.25	868.94	843.69	816.91	734.39
G	988.62	942.38	911.78	865.55	843.69	815.49	733.08
H	971.13	932.22	899.65	861.94	842.05	818.77	764.66
I	946.87	911.56	885.22	850.35	816.69	804.23	751.33
J	924.35	893.64	858.22	828.28	806.20	789.26	757.56
K	885.33	854.07	825.65	808.05	780.18	776.69	743.02
L	852.65	809.37	790.57	782.81	757.67	751.66	723.46
M	804.89	762.91	733.51	738.76	744.77	705.09	685.53
N	756.36	723.13	706.08	704.00	685.53	680.06	655.03

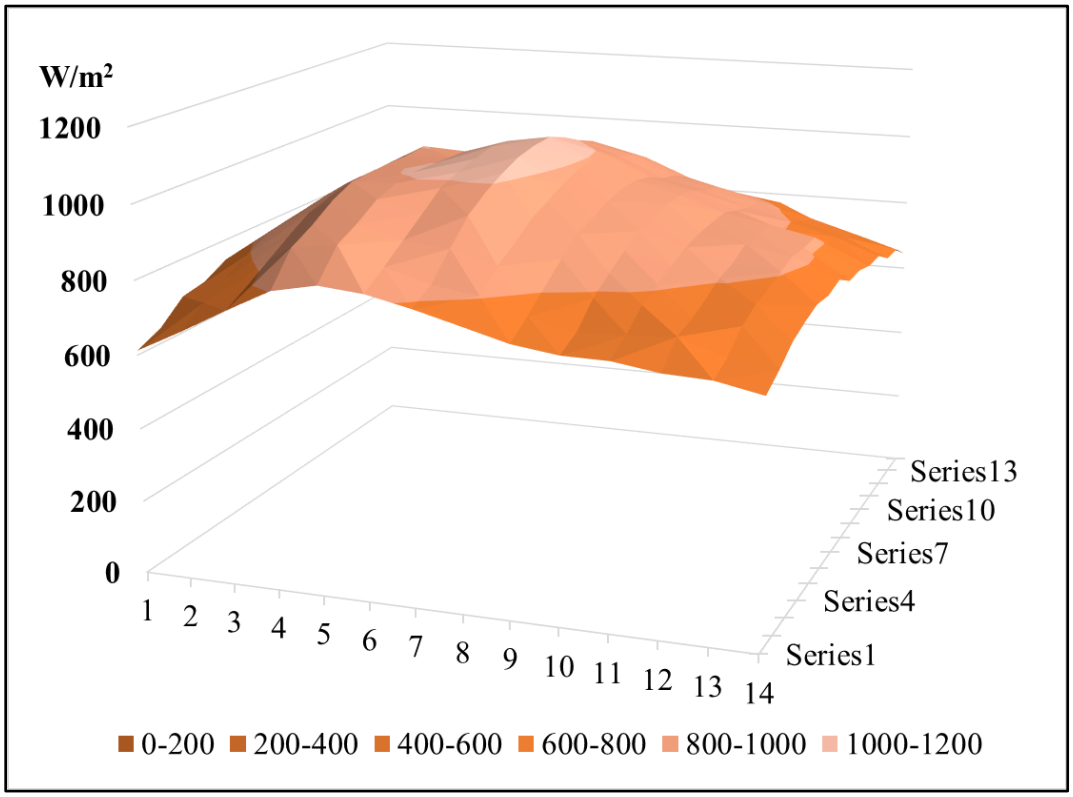

Figure 4.10 Irradiance Distribution for a Testing Distance of 63.5 cm (25 in) with 4 Corner and Center Lamps Turned On

Table 4.10 Irradiance at a Testing Distance of 50.8 cm (20 in) at 196 Test Points with 4 Corner Lamps Turned On

4 Corner Lamps 50.8 cm (20 in) (W/m^2)	1	2	3	4	5	6	7
A	549.89	562.57	624.10	621.26	621.26	646.73	608.36
B	566.83	597.98	657.33	650.77	653.61	669.57	642.25
C	576.01	609.13	676.02	668.92	668.59	681.05	657.66
D	591.64	631.64	694.82	695.15	690.45	692.96	679.85
E	600.17	646.07	699.08	721.49	717.88	714.71	713.18
F	595.79	668.48	703.78	738.10	722.36	717.77	722.04
G	584.76	668.59	708.48	746.30	706.95	697.12	703.56
H	585.63	661.92	711.76	705.64	689.57	689.57	697.88
I	592.95	655.03	724.66	741.93	708.37	701.16	718.98
J	586.29	655.69	733.29	728.48	693.40	692.85	707.94
K	579.18	639.95	669.24	690.99	668.26	656.57	676.02
L	571.31	611.75	655.58	669.24	638.75	631.32	658.86
M	568.69	610.66	640.06	659.30	639.62	626.18	651.54
N	553.60	573.61	612.08	633.94	623.56	610.33	621.70

4 Corner Lamps 50.8 cm (20 in) (W/m^2)	8	9	10	11	12	13	14
A	598.42	631.97	631.75	643.67	616.23	604.65	531.85
B	630.33	664.11	661.92	657.11	648.26	623.56	540.38
C	638.42	667.39	690.99	687.39	657.22	625.31	553.93
D	661.70	690.78	718.87	723.78	655.14	618.64	570.22
E	696.02	711.43	714.82	712.75	641.04	639.62	585.19
F	701.71	702.80	714.28	695.91	644.21	621.59	581.80
G	681.05	678.97	697.01	669.13	627.16	604.32	577.98
H	682.36	673.94	676.24	686.62	618.86	619.08	593.72
I	695.26	680.94	681.81	684.76	621.92	630.66	600.49
J	694.06	666.18	654.27	671.65	617.11	626.84	591.42
K	656.13	648.37	616.78	630.22	601.26	614.48	594.81
L	633.61	598.64	597.11	604.65	603.45	604.76	590.22
M	629.79	590.11	582.90	588.25	578.74	572.62	570.55
N	615.14	582.90	571.64	576.23	561.15	555.79	544.31

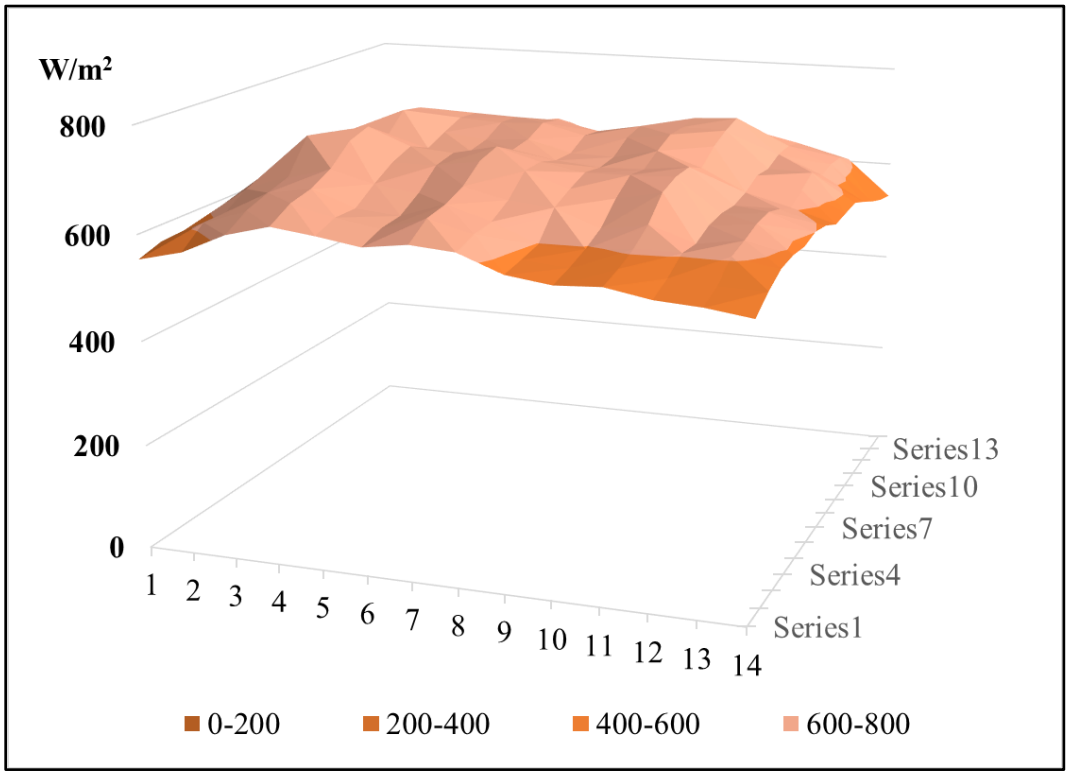

Figure 4.11 Irradiance Distribution for a Testing Distance of 50.8 cm (20 in) with 4 Corner Lamps Turned on

Table 4.11 Irradiance at a Testing Distance of 38.1 cm (15 in) at 196 Test Points with 4 Corner Lamps Turned On

4 Corner Lamps 38.1 cm (15 in) (W/m^2)	1	2	3	4	5	6	7
A	915.06	891.01	832.87	771.99	640.28	563.99	503.55
B	927.85	917.57	815.38	779.42	629.46	566.39	509.23
C	892.00	889.26	823.68	779.75	638.09	574.92	511.96
D	861.07	915.39	806.96	762.48	635.47	587.49	523.55
E	820.73	866.31	785.76	731.54	626.73	603.55	540.93
F	790.57	836.04	783.03	712.85	630.88	614.16	545.95
G	808.38	833.08	797.45	715.81	650.55	642.36	576.23
H	815.16	850.03	807.62	707.39	644.98	643.12	568.91
I	809.15	850.79	804.67	682.80	627.49	613.39	545.95
J	838.33	885.22	836.80	692.52	635.36	620.17	555.90
K	872.87	916.26	912.33	720.07	656.13	628.48	562.57
L	898.88	907.52	981.62	710.01	650.88	615.58	547.59
M	916.81	916.59	1037.91	733.95	670.88	617.11	546.94
N	917.68	911.23	1057.81	729.80	662.90	602.68	544.10

4 Corner Lamps 38.1 cm (15 in) (W/m^2)	8	9	10	11	12	13	14
A	544.86	620.82	705.64	911.78	940.31	1055.07	829.37
B	612.95	550.33	715.48	909.05	923.69	1011.57	839.53
C	557.98	528.47	691.54	880.52	891.23	955.72	823.03
D	578.09	597.54	696.35	848.50	848.82	890.25	804.67
E	582.13	625.63	670.56	777.89	792.86	817.78	779.75
F	580.71	629.57	640.28	719.52	735.37	778.33	775.70
G	610.77	654.71	646.07	721.93	731.00	778.76	811.22
H	611.31	650.77	627.93	682.58	697.77	770.67	815.92
I	570.76	620.06	580.93	642.25	669.68	742.47	805.98
J	591.20	632.19	584.32	644.43	671.10	772.53	820.41
K	597.43	619.40	601.37	661.70	700.83	821.83	840.30
L	581.26	623.01	595.58	658.53	706.08	862.49	840.19
M	587.05	645.64	599.84	666.18	717.34	901.07	845.44
N	554.04	634.38	580.93	648.37	704.55	874.51	813.63

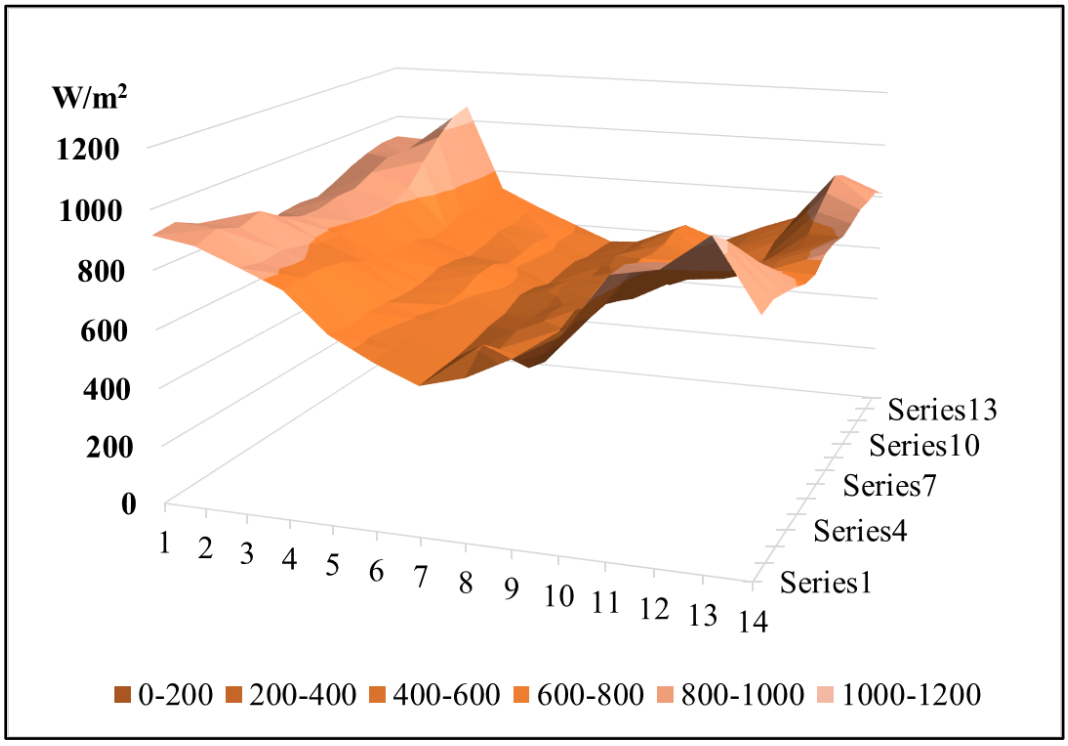

Figure 4.12 Irradiance Distribution for a Testing Distance of 38.1 cm (15 in) with 4 Corner Lamps Turned on

4.1.3 Experimental Time Determination

In this section, the process to determine the experimental time to conduct a solar calorimeter test is presented. It was determined by analyzing the speed response of solar calorimeter to changes during the experiments. It was important to determine the time required to establish steady-state conditions where the recorded solar irradiance, temperature, flow rate and wind speed would have relatively constant values. The steady state defined as the conditions that were achieved when these conditions had remained steady for a period of 5 continuous time constants of the calorimeter. Time constant is a measurement of the response time to changes in testing environments. It is the time required for the system to respond to within 37% of its final value of response [22]. Typically, in solar calorimeter test, the time constant is measured the energy flow response to a step change in forcing condition such as a sudden exposure to the solar irradiation.

The time constant varies as a result to different design of solar calorimeter. By designing a portable solar calorimeter which has relatively smaller size than the commercial one, we can expect that this solar calorimeter has a smaller time constant due to its lower thermal resistance and faster response time to changes in its test environment. During the operation of indoor solar calorimeter test, the flow rate and the solar irradiation were set to constant values for the entire testing process. So, the solar calorimeter time constant τ_{sc} will be determined by comparing the time

constant of calorimeter walls τ_{wall} and time constant of water flow τ_{water}. If the wall time constant is greater than water flow time constant, then the wall time constant will be controlling factor in determining solar calorimeter test constant, and vice versa.

To establish a good estimate of the minimum time constant for calorimeter walls and water flow, the clear glass with highest solar transmittance among all test specimens was used to produce the longest test time constant for the testing system.

With the clear glass installed on the solar calorimeter, the chilled water system and the data acquisition system turned on. Running the whole system until the steady state is achieved. Once the steady state is reached, the solar simulator was turned on, so the solar calorimeter was suddenly exposed to the irradiation. The test data was continuously monitored until steady state is reached again.

The universal time constant formula is showing below [22]:

$$\text{Change} = (\text{Final} - \text{Start}) \times \left(1 - \frac{1}{e^{t/\tau}}\right) \quad (4\text{-}1)$$

where:

Final = Value of calculated variable after infinite time (In this test, Final is

the final temperature when the final steady state is reached)

Start = Initial value of calculated variable (The temperature of the initial steady state)

e = Euler's number (≈ 2.7182818)

t = time in minute

τ = time constant

After one time constant's worth of time, the percentage of change from starting value to final value is:

$$\left(1 - \frac{1}{e^1}\right) \times 100\% = 63.2\% \quad (4\text{-}2)$$

After two-time constants' worth of time, the percentage of change from starting value to final value is:

$$\left(1 - \frac{1}{e^2}\right) \times 100\% = 86.5\% \quad (4\text{-}3)$$

Based on equation (4-2) and (4-3), the time constant was determined using the difference of the elapsed time from the time that the solar simulator was turned on to the temperature was 63.2% of the final value and to the temperature was 86.5% of the final value [22].

The wall time constant will be the maximum time constant of all five walls of solar calorimeter. Figure 4.13, Figure 4.14, Figure 4.15, Figure 4.16, and Figure 4.17 show the time versus interior wall temperature for center, top, bottom, left, and right walls respectively. So, the maximum wall time constant is 16 min. Figure 4.18 shows the water flow time constant is 11 min. Thus, the solar calorimeter time constant τ_{sc} is 16 min. The steady state is achieved when the test time have been met for a period of 5 continuous time constant of the solar calorimeter. So, the experimental time for this solar calorimeter to achieve steady state is about 80 min.

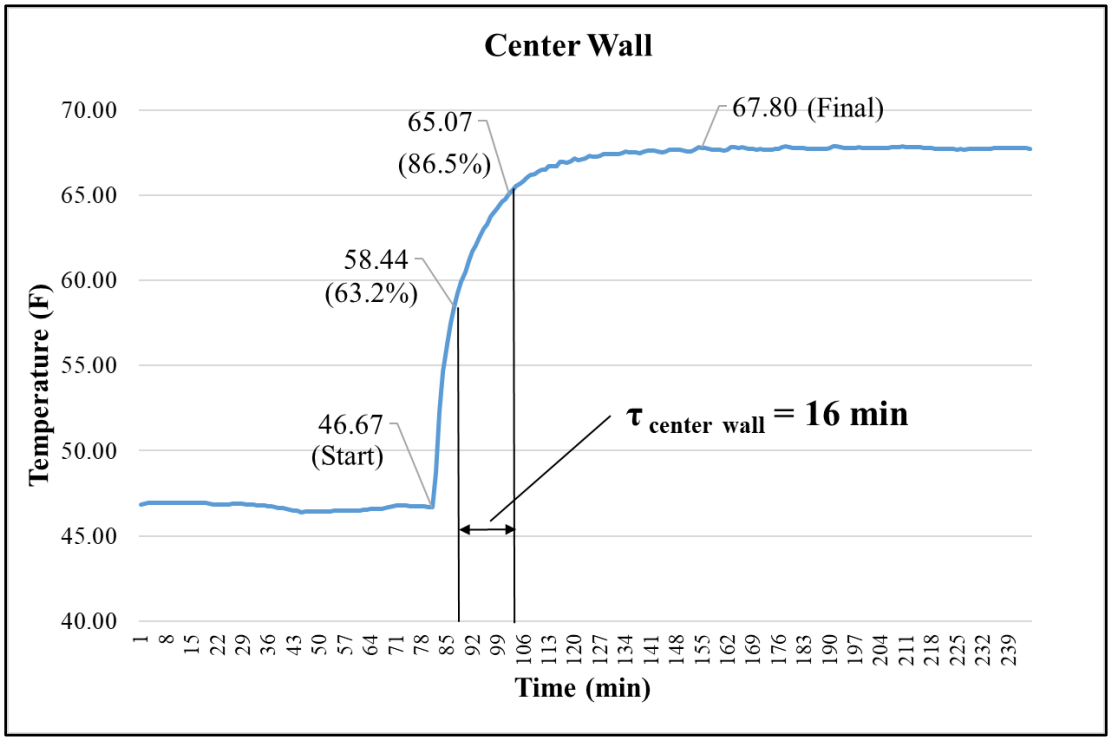

Figure 4.13 Center Wall Time Constant

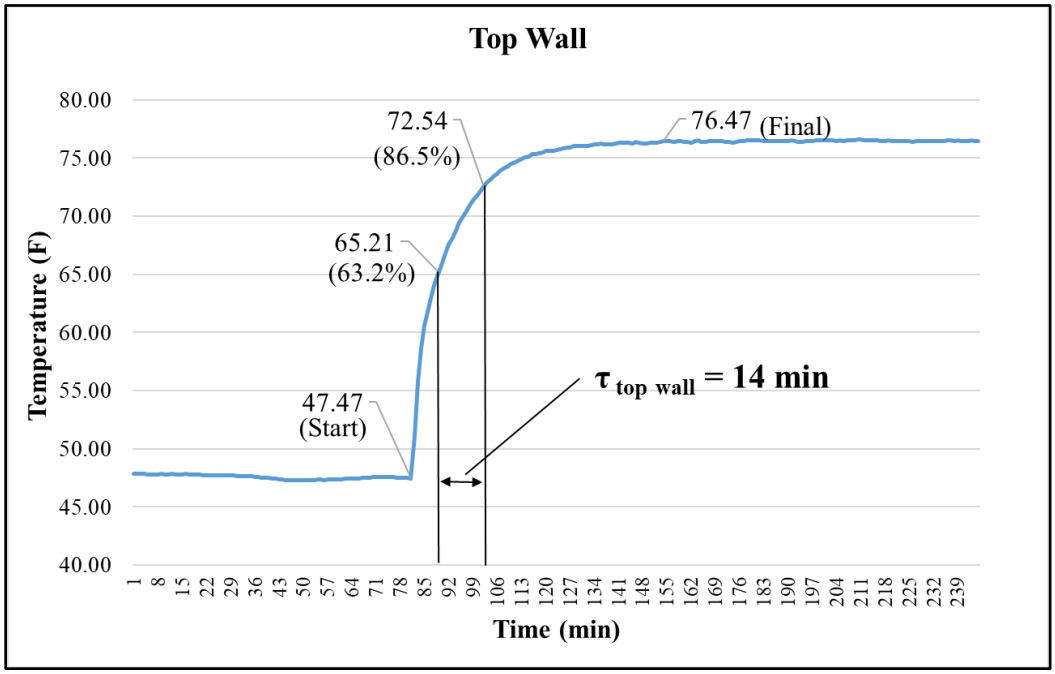

Figure 4.14 Top Wall Time Constant

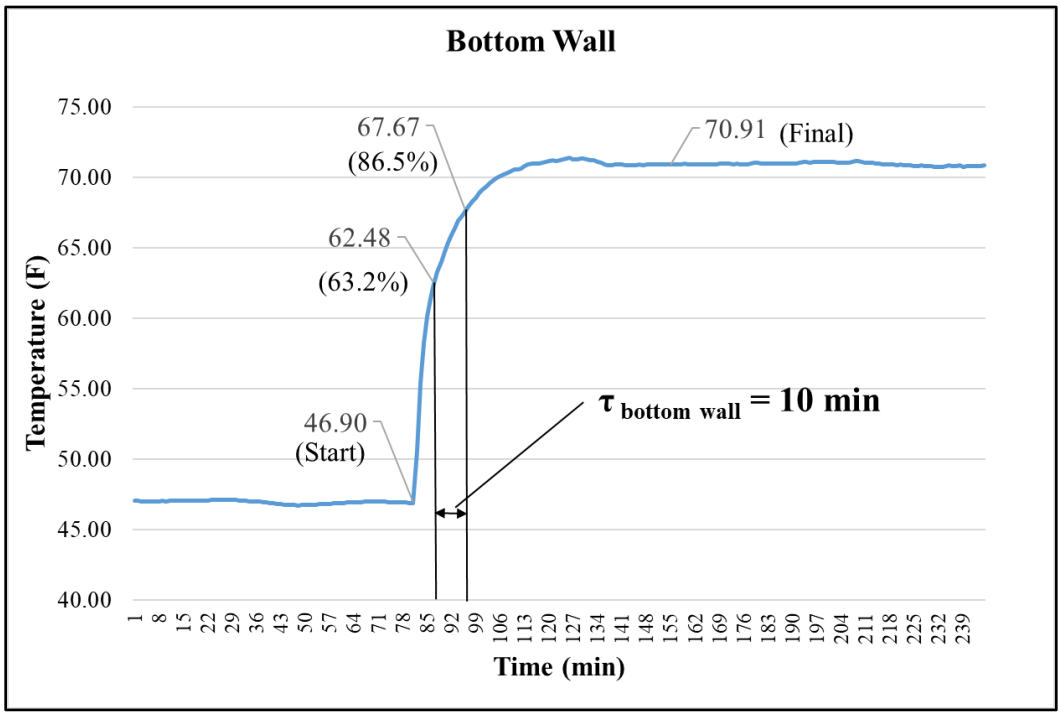

Figure 4.15 Bottom Wall Time Constant

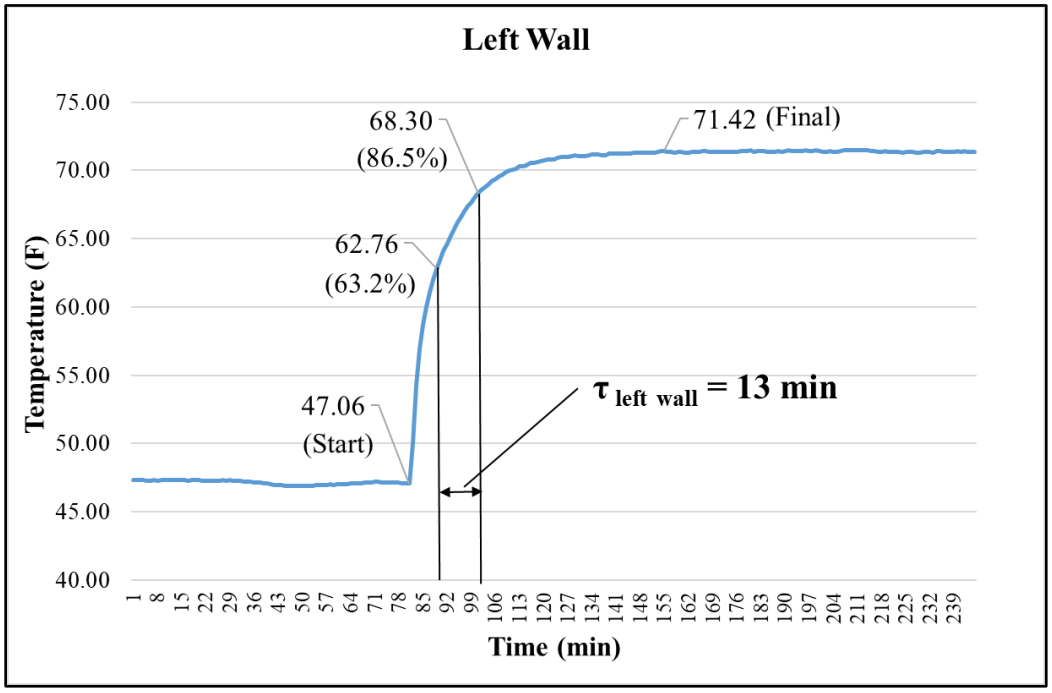

Figure 4.16 Left Wall Time Constant

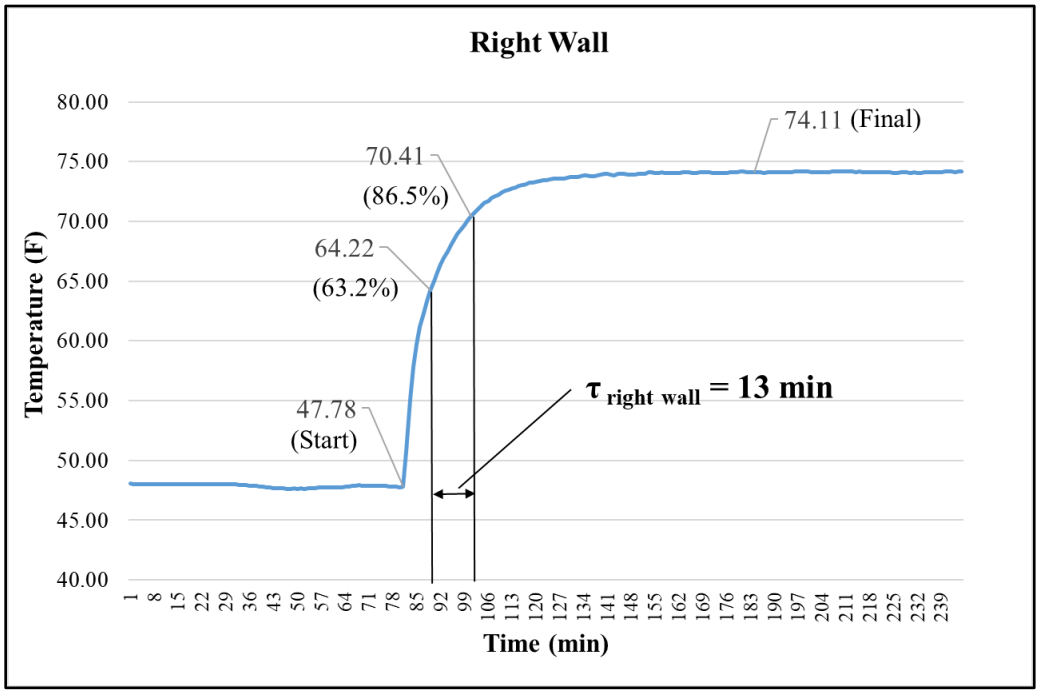

Figure 4.17 Right Wall Time Constant

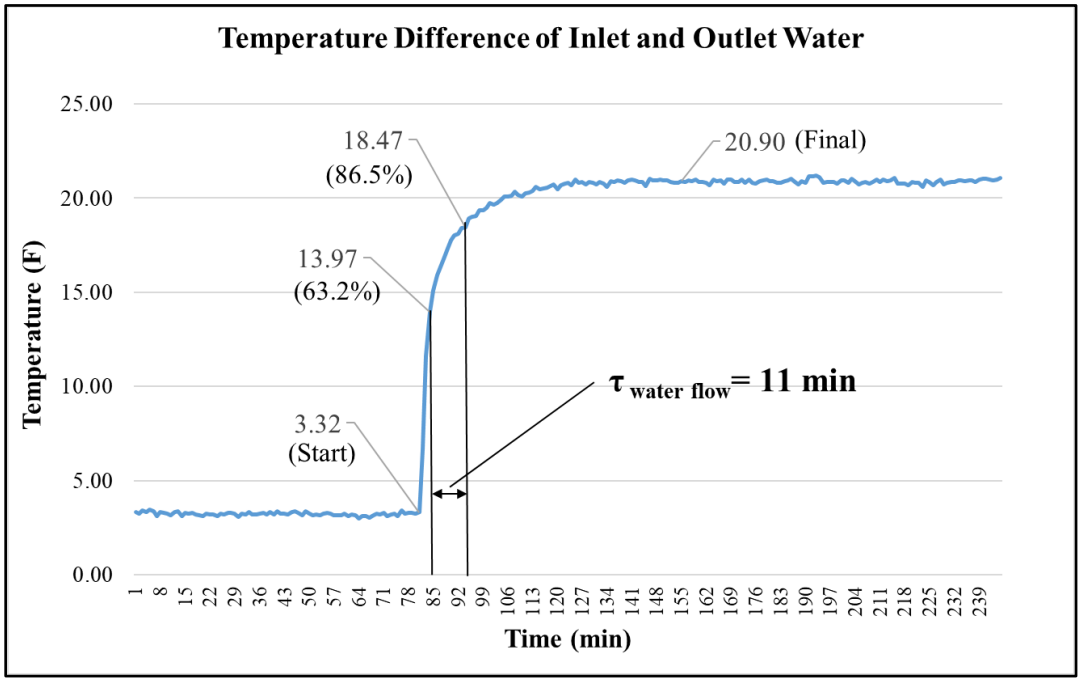

Figure 4.18 Water Flow Time Constant

4.1.4 Indoor Calibration

The solar calorimeter was calibrated using 6 mm (1/4 in) thick single-pane glass, with the 4-corner lamps of solar simulator turned on and at 20-inch (50.8 cm) testing distance. Based on the time constant of the solar calorimeter, steady state is achieved at around 80 minutes after the experiment started. Thus, four hours experimental time is adequate for the calculation of SHGC. To ensure the accuracy of calculation, the SHGC was calculated based on the last 2-hour data, and all the data were averaged on a minute basis. The heat balance and SHGC are calculated for each measurement time interval. If the measured SHGC does not vary over a period of the test, then those SHGC results may be averaged over the period.

Based on equation (1-3) in Chapter I, to calculate SHGC, the total solar heat gain on the surface of the glass Q_{solar} and the net solar heat gain through the glass $Q_{solar-in}$ need to be calculated. To estimate $Q_{solar-in}$, in equation (1-2), the heat extracted by the water in the absorber plate Q_{water}, the heat losses through all insulated walls Q_{wall}, the heat gain due to the difference of internal and external air $Q_{heat\ flow}$ and heat generated by the low-speed fan Q_{fan} need to be determined respectively. A sample averaged data for one minute test time interval and the sample calculation process are showing below.

Sample data:

Exterior surface temperature of center wall: 75.01 °F

Interior surface temperature of center wall: 64.87 °F

Exterior surface temperature of top wall: 84.35 °F

Interior surface temperature of top wall: 73.54 °F

Exterior surface temperature of left wall: 81.02 °F

Interior surface temperature of left wall: 68.54 °F

Exterior surface temperature of right wall: 80.50 °F

Interior surface temperature of right wall: 71.37 °F

Exterior surface temperature of bottom wall: 81.48 °F

Interior surface temperature of bottom wall: 69.09 °F

Inlet water temperature: 39.37 °F

Outlet water temperature: 55.86 °F

External air temperature: 81.91 °F

Internal air temperature: 69.48 °F

Water flow rate: 413.23 ml/min

4.1.4.1 Solar Calorimeter Walls, Q_{wall}

The heat flow through all insulated walls Q_{wall} is a function of measured surface temperature on both sides of wall insulations as described in Section 3.1.3.1. The temperature difference is multiplied by the insulation thermal conductivity and the surface area of the insulation, then divided by the thickness of insulation. The heat flow through the solar calorimeter wall is calculated by the following equation:

$$Q_{wall} = kA \frac{T_o - T_i}{L} \qquad (4\text{-}1)$$

where:

k= Thermal Conductivity, 0.0288 W/m^2·K (0.00507 Btu/hr·ft²·°F),

A = Heat transfer area, m^2 (ft^2).

T_o = External surface temperature, °C (°F).

T_i = Internal surface temperature, °C (°F).

L = Wall thickness, cm (in).

Center Wall:

$T_o = (75.01\ °F - 32) \times 5/9 + 273.15 = 297.04\ K$

$T_i = (64.87\ °F - 32) \times 5/9 + 273.15 = 291.41\ K$

$Q_{center\ wall} = 0.0288\ W/m^2 \cdot K \times 0.508\ m \times 0.508\ m \times (297.04 - 291.41)\ K \div 0.0508 m$

$= 0.82\ W$

Top Wall:

$T_o = (84.35\ °F - 32) \times 5/9 + 273.15 = 302.23\ K$

$T_i = (73.54\ °F - 32) \times 5/9 + 273.15 = 296.23\ K$

$Q_{top\ wall} = 0.0288\ W/m^2 \cdot K \times 0.508\ m \times 0.254\ m \times (302.23 - 296.23)\ K \div 0.0508\ m$

$= 0.44\ W$

Left Wall:

$T_o = (81.02\ °F - 32) \times 5/9 + 273.15 = 300.38\ K$

$T_i = (68.54\ °F - 32) \times 5/9 + 273.15 = 293.45\ K$

$Q_{left\ wall} = 0.0288\ W/m^2 \cdot K \times 0.508\ m \times 0.254\ m \times (300.38 - 293.45)\ K \div 0.0508\ m$

$= 0.51\ W$

Right Wall:

$T_o = (80.05\ °F - 32) \times 5/9 + 273.15 = 299.84K$

$T_i = (71.37\ °F - 32) \times 5/9 + 273.15 = 295.02\ K$

$Q_{right\ wall} = 0.0288\ W/m^2 \cdot K \times 0.508\ m \times 0.254\ m \times (299.84 - 295.02)\ K \div 0.0508 m$

$= 0.37\ W$

Bottom Wall:

$T_o = (81.48\ °F - 32) \times 5/9 + 273.15 = 300.64\ K$

$T_i = (69.09\ °F - 32) \times 5/9 + 273.15 = 293.76\ K$

$Q_{bottom\ wall} = 0.0288\ W/m^2 \cdot K \times 0.508\ m \times 0.254\ m \times (300.64 - 293.76)\ K \div 0.0508 m$

$= 0.50\ W$

So,

$Q_{wall} = Q_{center\ wall} + Q_{top\ wall} + Q_{left\ wall} + Q_{right\ wall} + Q_{bottom\ wall}$

$= 0.82\ W + 0.44\ W + 0.51\ W + 0.37\ W + 0.50\ W$

$= 2.65\ W$

4.1.4.2 Heat Extracted by Water in Absorber Plate, Q_{water}

The absorber plate in the solar calorimeter removes the heat absorbed by the solar calorimeter through a chilled water system. The heat extracted by the water in the absorber plate Q_{water} is a function of the property of water, the water volume flow rate, temperature difference of both inlet and outlet, and specific heat capacity. The heat extracted by water is calculated by equation (1-3) with an average specific heat capacity of water 4195 J/K·kg.

T_o = (49.36 °F − 32) × 5/9 + 273.15 = 282.79 K

T_i = (40.37 °F − 32) × 5/9 + 273.15 = 277.8 K

Q_{water} = 4195 J/K·kg × 413.23 ml/min × 1 min /60 s × 0.001 kg/ml × (282.79−277.8) K

= 144.36 W

4.1.4.3 Solar Irradiation on Surface of Specimen, Q_{solar}

As described in Section 4.1.2, solar irradiation is measured when the 4-corner lamp of solar simulator turned on at 20-inch (50.8 cm) testing distance. 196 solar irradiances were measured on a 14 × 14 grid lines on the surface of specimen. To obtain a good estimate of average solar irradiation, the solar irradiation is calculated in MATLAB by first using Trapezoid Rule to do the interpolation and then double integration. The MATLAB code in shown in Figure 4.19. The Solar Irradiation on the surface of specimen is,

$$Q_{solar} = 165.44 \text{ W}$$

```
clear all; clc;
filename = sprintf('SolarData.xlsx');
T        = readtable(filename);
A        = table2array(T);

indices    = find(isnan(A));          % there are NAN data, set them to be 0;
A(indices) = 0;                       % set NAN data to be 0 --- a better way: interpolation;

A_col1   = A(:,1);                    % the 1st column is number
solar_z    = A(:,2:length(A_col1)+1); % rthe NAN numbers are dropped
dx = 0.495/13; dy  = 0.495/13;
x1 = A_col1*dx; x2 = A_col1*dy;       % set the x1 and x2 grid here
[X1,X2] = meshgrid(x1,x2);

figure; surf(X1,X2,solar_z);
volume = trapz(x1,trapz(x2,solar_z,2),1);
fprintf('Volume by trapzoid rule (twice, one in x1, one in x2) = %2.4f', volume);
```

Figure 4.19 MATLAB Code to Estimate Solar Irradiation

4.1.4.4 Heat Generated by Low-Speed Fan, Q_{fan}

There is a low-speed fan installed on the absorber plate to enhance heat exchange of inside air and absorber plate. Even though this fan is operated on a very low power with a small 7 W motor, it could be a source of heat input. For more accuracy estimation of SHGC, we can assume that more than 85% of the energy is converted to the kinetic energy, and about 15% of energy is converted to heat. So, the Q_{fan} could be estimated as,

$$Q_{fan} \approx 7\ \text{W} \times 15\% = 1.05\ \text{W}$$

4.1.4.5 Heat Transfer through The Test Specimen, $Q_{heat\ flow}$

The heat transfer through the test specimen due to the air temperature difference across the test specimen is a function of specimen thermal transmittance, the air temperature difference of both inside and outside surface of test specimen and the surface area of the solar calorimeter opening. In the indoor test where the exterior wind speed is close to zero, the heat transfer coefficient can be held relatively constant at a value close to standard surface heat transfer coefficient 5.81 W/m^{2}K (1.02 Btu/h·ft²·°F). The heat transfer through the test specimen is determined by the following equation:

$$Q_{heat\ flow} = U \times A \times (T_o - T_i) \qquad (4\text{-}2)$$

where,

U = Overall heat transfer coefficient, W/m^{2}K (Btu/hr·ft²·°F)

A = Heat transfer area, m^2 (ft^2)

T_o = External air temperature, °C (°F)

T_i = Internal air temperature, °C (°F)

So,

T_o = (81.91 °F − 32) × 5/9 + 273.15 = 300.88 K

T_i = (69.48 °F − 32) × 5/9 + 273.15 = 293.97 K

$Q_{heat\ flow}$ = 5.81 W/m^{2}K × 0.495 m × 0.495 m × (300.88 – 293.97) K

= 9.83 W

4.1.4.6 Instant SHGC at 1-minute Time Intervals

The instant solar heat gain coefficient at 1-minute time interval is determined by equation (1-3) in Section 1.3.2

SHGC = (144.36 W – 2.65 W – 9.83 W – 1.05W) / 165.44 W

= 0.791

4.1.4.7 Indoor Calibration Results

All 120 instant SHGC in two hours of steady state is determined in same process. Figure 4.20 shows the heat flow through each wall, $Q_{center\ wall}$, $Q_{top\ wall}$, $Q_{left\ wall}$, $Q_{right\ wall}$, and $Q_{bottom\ wall,}$ and the total heat flow through all five walls of solar calorimeter Q_{wall} in the 2-hour steady state. All heat flow through walls is at a very constant level during the 2-hour test. The heat flow through top, bottom, left and right walls are at similar level. The heat flow through center wall is about twice of the heat flow of other walls since the heat transfer area is twice of that of other walls. Figure 4.21 shows the heat transfer through the test specimen, $Q_{heat\ flow}$. Even though the air temperature and wind speed and direction in the indoor environment are at more constant level than the outdoor environment, we can see there is still

some variations in the $Q_{heat\ flow}$ compared with Q_{wall} due to the small changes in air temperature and wind speed and direction. Figure 4.22 shows the heat extracted by water in the absorber plate. Even though there are some variations in the results due to the change in the temperature difference of inlet and outlet water, the average of Q_{water} is kept at a relatively constant level in the steady state. Figure 4.23 shows the 120 instant calculated SHGCs for 6 mm (1/4 in) clear glass in 2-hour steady state. The average SHGC for 6 mm (1/4 in) clear glass is 0.791.

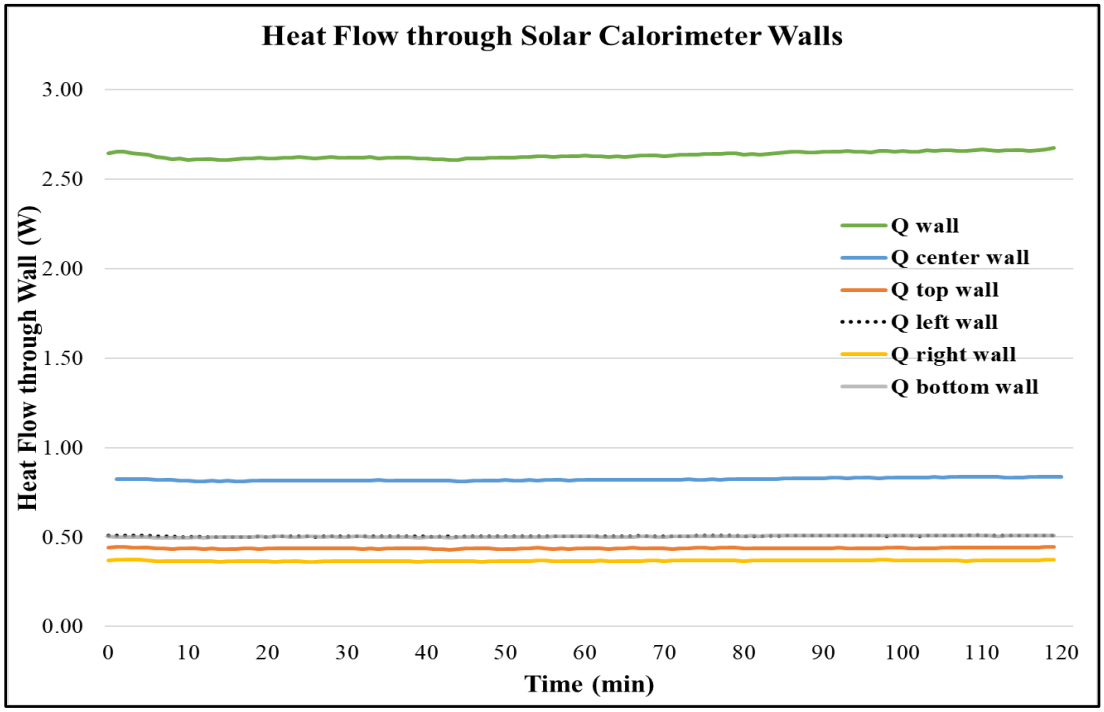

Figure 4.20 Heat Flow through Solar Calorimeter Walls

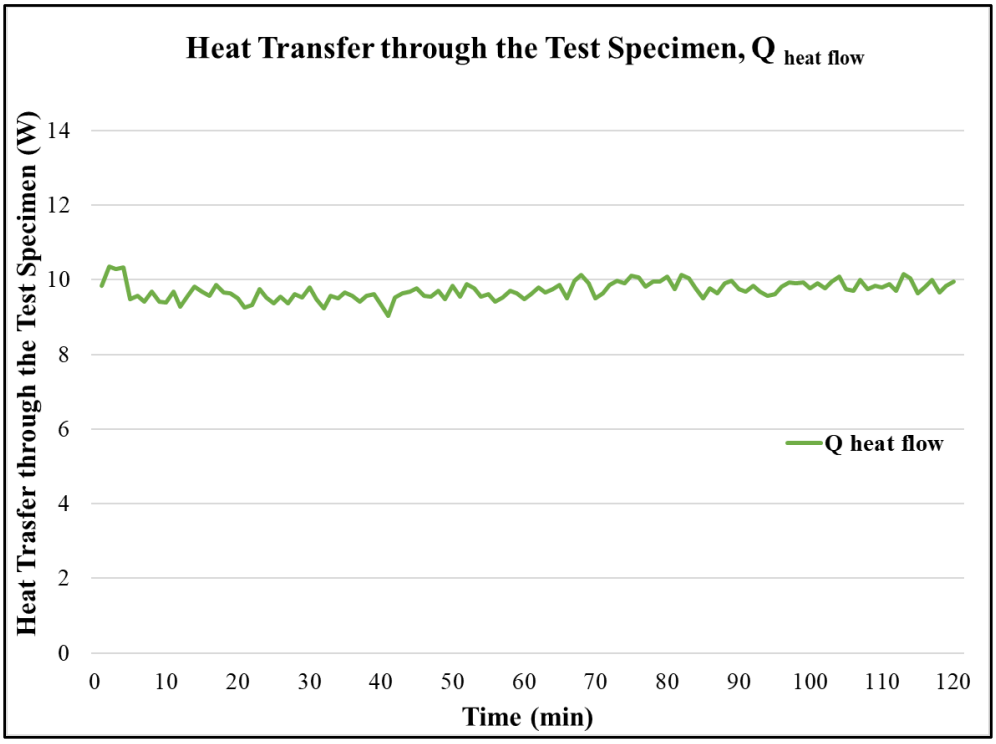

Figure 4.21 Heat Transfer through The Test Specimen

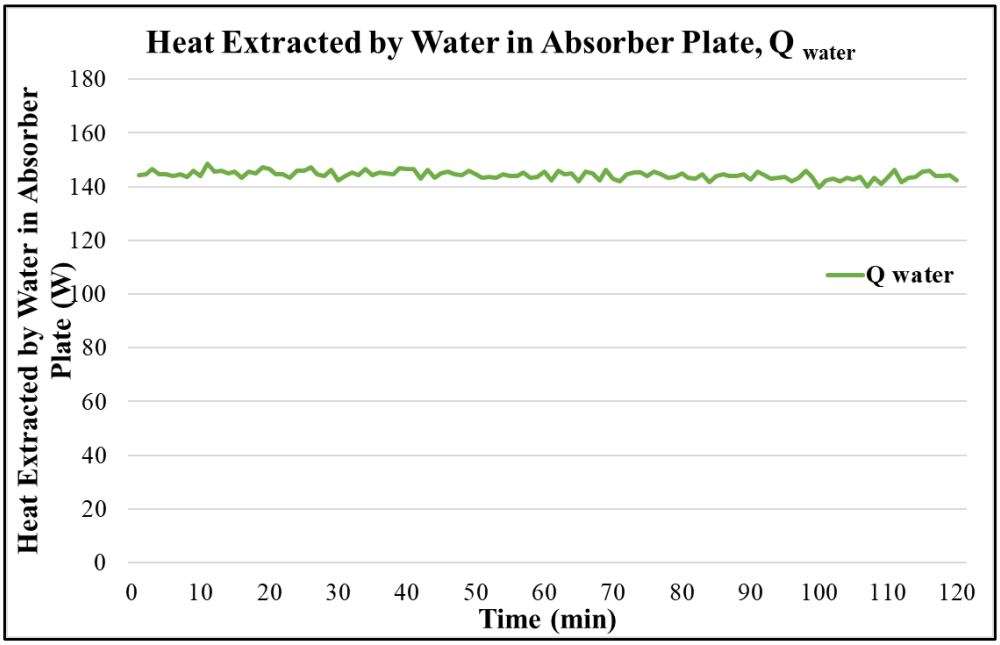

Figure 4.22 Heat Extracted by Water in Absorber Plate for Indoor Test

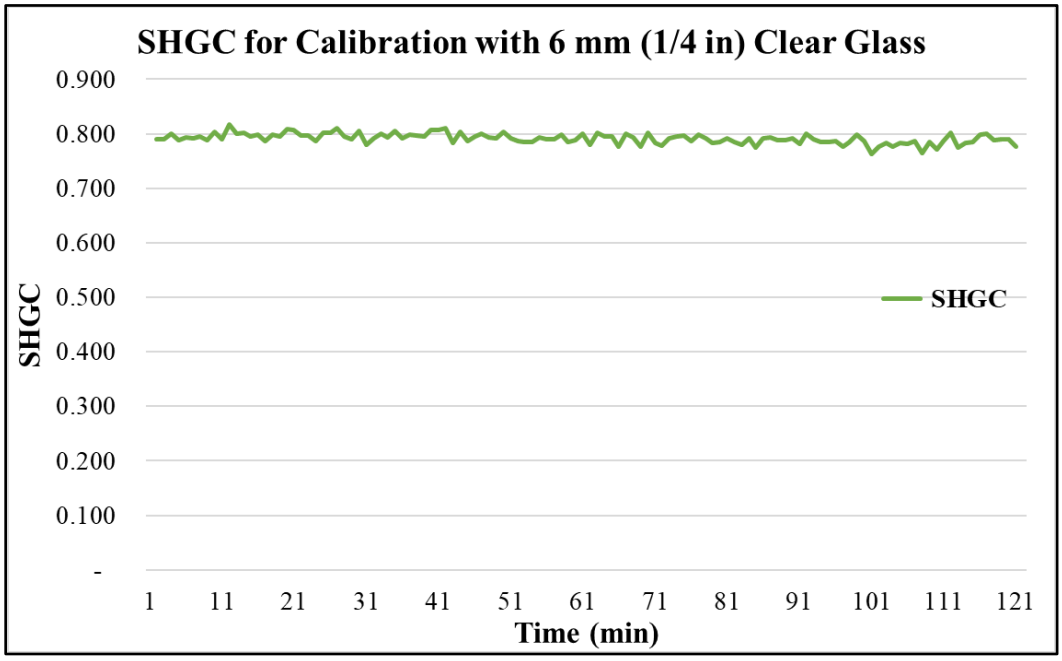

Figure 4.23 SHGC for Calibration with 6 mm (1/4 in) Clear Glass

4.1.5 Uncertainty Analysis

Since the SHGC is determined from other values instead of a directed measurement, the individual uncertainty of each component has its effects to the final results. Therefore, there is a little chance that random variations of each input will results in a combination of all extreme values are reached at the same time. It is necessary to estimate the combined uncertainty (μ) of the SHGC. The total uncertainty is determined by the error propagation method to determine the combined uncertainty.

In the process of determination of SHGC, not only the monitoring sensors such as thermocouple, water flow sensor and pyranometer are involved, but also some

theoretical values such as specific heat of water and thermal heat transfer coefficient. The combined uncertainty of the SHGC will be determined by the valued obtained from monitoring sensors. For the calculation of addition or subtraction (i.e., $Q = (x_1, x_2, x_3 \cdots)$), the uncertainty is determined by the following equation,

$$\mu(Q) = \sqrt{\mu(x_1)^2 + \mu(x_2)^2 + \mu(x_3)^2 + \cdots} \quad (4\text{-}3)$$

For the combined uncertainty associated with multiplications or divisions of various independent inputs (i.e., $G = f(y_1, y_2, y_3 \cdots)$), it shall be determined by the following equation,

$$\frac{\mu(G)}{G} = \sqrt{\left(\frac{\mu(y_1)}{y_1}\right)^2 + \left(\frac{\mu(y_2)}{y_2}\right)^2 + \left(\frac{\mu(y_3)}{y_3}\right)^2 + \cdots} \quad (4\text{-}4)$$

The uncertainties of the heat losses through all insulated walls Q_{wall} and the heat gain due to the difference of internal and external air $Q_{heat\ flow}$ are determined by the uncertainty of thermocouple, which means the uncertainty of ΔT the temperature difference needs to be determined. The uncertainty of the heat extracted by the water in the absorber plate Q_{water} is determined by equation (4-4) with uncertainty of ΔT and water flow sensor. The uncertainty of the net solar heat gain through the

glass $Q_{solar\text{-}in}$ is determined by equation (4-3). Finally, the uncertainty of SHGC is determined by equation (4-4). Table 4.12 shows the uncertainty of each monitoring sensors. Table 4.13 shows the calculated uncertainty of $Q_{center\ wall}$, $Q_{top\ wall}$, $Q_{left\ wall}$, $Q_{right\ wall}$, $Q_{bottom\ wall}$, Q_{wall}, $Q_{heat\ flow}$, Q_{water}, $Q_{solar\text{-}in}$, and Q_{solar}. The combined uncertainty of SHGC is 3.5%, so the average SHGC for calibration is 0.791 ± 0.03.

Table 4.12 Uncertainty of Monitoring Sensors

Monitoring Sensor	Uncertainty
LI-200R Pyranometer	3%
OMEGA Type T Thermocouple	0.75%
OMEGA FLR1000 Water Flow Sensor	3%

4.1.6 Results and Comparisons

A SHGC of 0.791 ± 0.03 for a 6 mm (1/4 in) clear glass was compared to the SHGC from other values found in the open literature. Table 4.14 shows the comparison of SHGC with those from other resources. The experimental SHGC obtained with the systems presented in this dissertation was in close agreement with values reported in the experimental work of Marinoski et al. [23] for a sample of 1.8 m^2 (19.38 ft^2) of surface area, which was 0.79. The difference between the result of this study and that obtained by Marinoski et al. was 0.13%. Moreover, the average SHGC in this study was compared to the NFRC [24] approved solar optical data for 6 mm (1/4 in) clear glass. The SHGC from NFRC was 0.816, yielding a difference of -3.16%. Comparison of average SHGC of this study with the value from National Glass of

Australia [25], which was 0.81, yielded a difference of -2.40%. Gregg D. Ander in the article Windows and Glazing [26] on the Whole Building Design Guide website reported the SHGC value for a 6 mm (1/4 in) single pane glass of 0.81, which was obtained using Lawrence Berkeley National Laboratory's (LBNL) WINDOW computer analysis program, a computer program for calculating total window thermal performance indices. The difference between the value obtained in this dissertation and the one from LBNL was also -2.40%.

Table 4.13 Uncertainty of Inputs

Inputs	Absolute Uncertainty (W)	Relative Uncertainty
$Q_{center\ wall}$	0.033	4.01%
$Q_{top\ wall}$	0.020	4.65%
$Q_{left\ wall}$	0.019	3.68%
$Q_{right\ wall}$	0.019	5.18%
$Q_{bottom\ wall}$	0.019	3.74%
Q_{wall}	0.051	1.92%
$Q_{heat\ flow}$	0.369	3.80%
Q_{water}	2.319	1.61%
$Q_{solar\text{-}in}$	2.348	1.79%
Q_{solar}	4.963	3.00%

Table 4.14 Comparison of Calculated SHGC with Other Sources

Measured SHGC	Source	SHGC of 6 mm (1/4 in) Clear Glass	Difference	
			Absolute	(%)
0.791 ± 0.03	Marinoski et al. [23]	0.79	0.001	0.13%
	National Fenestration Rating Council [24]	0.816	-0.025	-3.16%
	Glass Performance Data [25]	0.81	-0.019	-2.40%
	Windows And Glazing [26]	0.81	-0.019	-2.40%

4.1.7 SHGC of Gray, Bronze and Mirror Glasses and Comparisons

After the calibration of solar calorimeter with a 6 mm (1/4 in) clear glass. The result indicated a good agreement with the SHGCs from other resources, which means this solar calorimeter is adequate to obtain the characteristic parameters with similar optical properties of glazing sample of 56.5 cm x 56.5 cm x 0.6 cm (22.25 in x 22.25 in x 0.25 in). Three other glazing samples, bronze, gray, and mirror glasses with thickness of 6 mm (1/4 in) were tested. The testing procedure, calculation process and uncertainty analysis were the same as those presented above. Testing time for each type glass was about four hours, and the SHGC was calculated using the data collected during the final two hours of the testing.

Table 4.15 shows the calculated SHGC for 6 mm (1/4 in) bronze glass, 6 mm (1/4 in) gray glass, and 6 mm (1/4 in) mirror glass compared with SHGC from other resources. The measured SHGC values of bronze and gray glasses were compared to those from the glass manufacturer Vitro Architectural Glass [27]. The differences in values between those in this dissertation to those of source [27] differed by 7.07% and 8.81%, respectively. Moreover, the difference between the SHGC of bronze and gray glass in this study and those reported from Glass Performance Data were 4.13% and 4.09%, respectively. For mirror glass or reflective glass, it is difficult to find the reliable reference SHGC in other resource. Most reflective glass in the industry are low-E glasses which have lower SHGCs compared to SHGCs of mirror glass obtained in this study. Vitro Architectural Glass shows the SHGC of reflective glass is 0.26, which was 44.6% lower than the value obtained in this study.

Table 4.15 SHGC of Bronze, Gray and Mirror Glass and Comparison

Glass Type	Measured SHGC	Vitro Architectural Glass [27]			Glass Performance Data [25]		
		SHGC	Difference		SHGC	Difference	
			Absolute	(%)		Absolute	(%)
6 mm Bronze Glass	0.678 ± 0.02	0.63	0.048	7.07%	0.65	0.028	4.13%
6 mm Gray Glass	0.636 ± 0.02	0.58	0.056	8.81%	0.61	0.026	4.09%
6 mm Mirror Glass	0.469 ± 0.02	0.26	0.209	44.56%	-	-	-

4.2 Outdoor Experiments

The outdoor test is conducted on the roof of LEEP2 at The University of Kansas. It is conducted on a clear day without clouds when the level of solar radiation and wind speed are fairly constant in summer or early fall. Four same glass specimens were tested in outdoor condition. Both indoor and outdoor experiments share the same chilled water system, data acquisition system, solar calorimeter box and pyranometer. For outdoor test, a solar tracking system was used to keep the face of solar calorimeter pointed normal to the direct sunlight. Outdoor test also requires a Solar-Air Heat Transfer Coefficient Meter to estimate exterior surface heat transfer coefficient of the test specimen in order to estimate the heat transfer through the test specimen [20].

During the outdoor tests, to ensure that solar calorimeter reaches steady state, based on the time constant of solar calorimeter, the steady state is achieved at around 80 minutes after the experiment started. Around four hours experimental data was collected, and the calculation was performed based on the last two hours data. Again, all the data was collected every 10 seconds, and was averaged on a minute basis.

The following section shows a sample data and the calculation procedure to determine the heat losses through all insulated walls Q_{wall}, the heat extracted by the

water in the absorber plate Q_{water}, the heat gain due to the difference of internal and external air temperature $Q_{heat\ flow}$, the total solar heat gain on the surface of the glass Q_{solar} and the net solar heat gain through the glass $Q_{solar\text{-}in}$.

Sample data:

Exterior surface temperature of center wall: 83.86 °F

Interior surface temperature of center wall: 60.15 °F

Exterior surface temperature of top wall: 84.55 °F

Interior surface temperature of top wall: 62.61 °F

Exterior surface temperature of left wall: 83.07 °F

Interior surface temperature of left wall: 61.41 °F

Exterior surface temperature of right wall: 79.34 °F

Interior surface temperature of right wall: 61.77 °F

Exterior surface temperature of bottom wall: 81.31 °F

Interior surface temperature of bottom wall: 63.07 °F

Inlet water temperature: 45.68 °F

Outlet water temperature: 55.41 °F

External air temperature: 87.96 °F

Internal air temperature: 61.80 °F

Water flow rate: 620.83 ml/min

Copper plate temperature: 156.4 °F

Solar radiation: 1056.99 W/m^2

4.2.1 Solar Calorimeter Walls, Q_{wall}

The heat flow through all insulated walls Q_{wall} is calculated equation (4-1)

Center Wall:

$T_o = (83.86\ °F - 32) \times 5/9 + 273.15 = 301.96\ K$

$T_i = (60.15\ °F - 32) \times 5/9 + 273.15 = 288.79\ K$

$Q_{center\ wall} = 0.0288\ W/m^2 \cdot K \times 0.508\ m \times 0.508\ m \times (301.96 - 288.79)\ K \div 0.0508 m$

$= 1.93\ W$

Top Wall:

$T_o = (84.55\ °F - 32) \times 5/9 + 273.15 = 302.34\ K$

$T_i = (62.61\ °F - 32) \times 5/9 + 273.15 = 290.15\ K$

$Q_{top\ wall} = 0.0288\ W/m^2 \cdot K \times 0.508\ m \times 0.254\ m \times (302.34 - 290.15)\ K \div 0.0508\ m$

$= 0.89\ W$

Left Wall:

$T_o = (83.07\ °F - 32) \times 5/9 + 273.15 = 301.52\ K$

$T_i = (61.41\ °F - 32) \times 5/9 + 273.15 = 289.49\ K$

$Q_{left\ wall} = 0.0288\ W/m^2 \cdot K \times 0.508\ m \times 0.254\ m \times (301.52 - 289.49)\ K \div 0.0508\ m$

$= 0.88\ W$

Right Wall:

$T_o = (79.34\ °F - 32) \times 5/9 + 273.15 = 299.45K$

$T_i = (61.77\ °F - 32) \times 5/9 + 273.15 = 289.69\ K$

$Q_{right\ wall} = 0.0288\ W/m^2 \cdot K \times 0.508\ m \times 0.254\ m \times (299.45 - 289.69)\ K \div 0.0508m$

$= 0.71\ W$

Bottom Wall:

$T_o = (81.31\ °F - 32) \times 5/9 + 273.15 = 300.54\ K$

$T_i = (63.07\ °F - 32) \times 5/9 + 273.15 = 290.41\ K$

$Q_{bottom\ wall} = 0.0288\ W/m^2 \cdot K \times 0.508\ m \times 0.254\ m \times (300.54 - 290.41)\ K \div 0.0508m$

$= 0.74\ W$

Thus,

$Q_{wall} = Q_{center\ wall} + Q_{top\ wall} + Q_{left\ wall} + Q_{right\ wall} + Q_{bottom\ wall}$

$= 1.93\ W + 0.89\ W + 0.88\ W + 0.71\ W + 0.74\ W$

$= 5.15\ W$

4.2.2 Heat Extracted by Water in Absorber Plate, Q_{water}

The heat extracted by the water in the absorber plate Q_{water} is calculated by equation (1-3) with an average specific heat capacity of water 4192 J/K·kg.

$T_o = (45.68\ °F - 32) \times 5/9 + 273.15 = 280.75\ K$

T_i = (55.41 °F − 32) × 5/9 + 273.15 = 286.15 K

Q_{water} = 4192 J/K·kg × 620.83 ml/min × 1 min /60 s × 0.001 kg/ml × (286.15−280.75) K

= 234.33 W

4.2.3 Heat Transfer through the Test Specimen, $Q_{heat\ flow}$

The heat transfer through the test specimen due to the air temperature difference across the test specimen is determined by equation (4-2). In the outdoor test where the exterior wind speed and direction is changing during the test, so the heat transfer across the specimen should be determined when the thermal transmittance in equation (4-2) is modified by measured weather side exterior surface heat transfer coefficient h $_{h\text{-}sun}$ by equation (4-5). The measured weather side heat transfer coefficient is determined by equation (2-1).

$$U_m = \frac{1}{\frac{1}{U_{glass}} - \frac{1}{h_{h-sun}}} \quad (4\text{-}5)$$

Where:

U_m = modified overall heat transfer coefficient, W/m^{2}K (Btu/hr·ft^2·ºF)

U_{glass} = overall heat transfer coefficient of test specimen, W/m^{2}K (Btu/hr·ft^2·ºF)

h_{h-sun} = measured weather side surface heat transfer coefficient, W/m^{2}K (Btu/hr·ft2·ºF)

thus,

$T_o = (87.96\ °F - 32) \times 5/9 + 273.15 = 304.24\ K$

$T_{plate} = (156.40\ °F - 32) \times 5/9 + 273.15 = 342.26\ K$

$h_{h\text{-}sun} = 1056.99\ W/m^2 \times 0.95 \div (342.26 - 3.4.24)\ K$

$= 26.41\ W/m^2K$

$U_m = 1 \div (1 \div 5.81\ W/m^2K - 1 \div 26.41\ W/m^2K)$

$= 7.45\ W/m^2K$

$T_i = (61.8\ °F - 32) \times 5/9 + 273.15 = 289.71\ K$

$Q_{heat\ flow} = 7.45\ W/m^2K \times 0.495\ m \times 0.495\ m \times (304.24 - 289.71)\ K$

$= 26.52\ W$

4.2.4 Instant SHGC at 1-minute Time Intervals

The instant solar heat gain coefficient at 1-minute time interval is determined by equation (1-3) in Section 1.3.2.

$Q_{solar} = 1056.99\ W/m^2 \times 0.495\ m \times 0.495\ m = 258.99\ W$

$SHGC = (234.33\ W - 5.15\ W - 26.52\ W - 1.05W) / 258.99\ W$

$= 0.778$

4.2.5 Outdoor Test Results

All 120 instant SHGC in two hours of steady state were determined in same manner discussed previously. Figure 4.24 shows the heat flow through each wall, $Q_{center\ wall}$,

$Q_{top\ wall}$, $Q_{left\ wall}$, $Q_{right\ wall}$, and $Q_{bottom\ wall}$, and the total heat flow through all five walls of solar calorimeter Q_{wall} in the 2-hour steady state. All heat flow through walls are at a constant level during the 2-hour test. The heat flow through top, bottom, left and right walls are at similar level. The heat flow through center wall is about twice of the heat flow of other walls since the heat transfer area is twice of that of other walls.

Figure 4.25 shows the heat transfer through the test specimen, $Q_{heat\ flow}$. Due to the changing air temperature and wind speed and direction in the outdoor environment, we can see there are some variations in the $Q_{heat\ flow}$ compared to results in indoor tests shown in Figure 4.21. Figure 4.26 shows the heat extracted by water in the absorber plate. Even though there are some variations in the results due to the change in the temperature difference of inlet and outlet water, the average of Q_{water} is kept at a relatively constant level in the steady state.

Figure 4.27 shows the 120 instant calculated SHGCs for 6 mm (1/4 in) clear glass in 2-hour steady state for both outdoor and indoor tests. Due to the continuous changing temperature and wind speed and direction, the SHGC results from outdoor test shows more variations than indoor SHGC results. The average SHGC for 6 mm (0.25 in) clear glass for outdoor test is 0.800 which is very close to the indoor average SHGC 0.791.

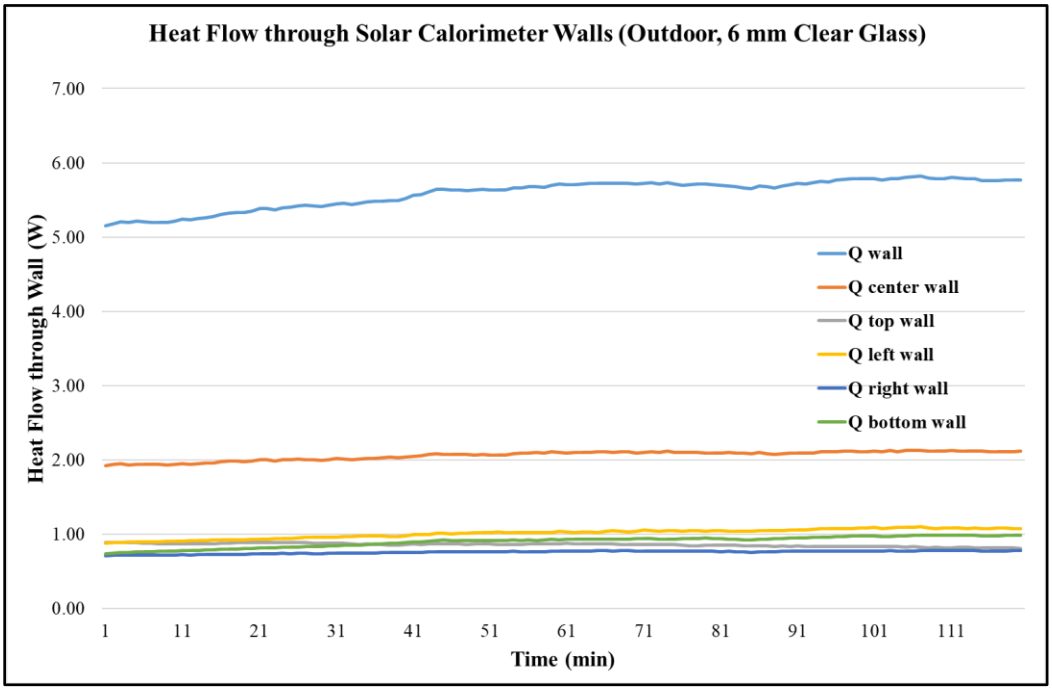

Figure 4.24 Heat Flow through Solar Calorimeter Walls

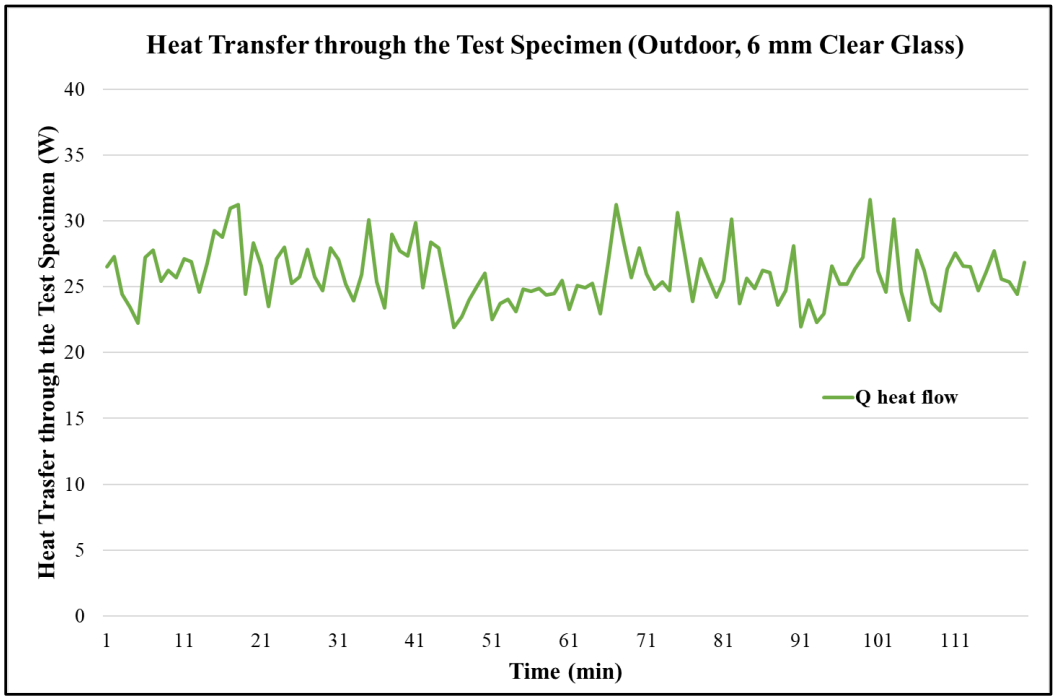

Figure 4.25 Heat Transfer through The Test Specimen

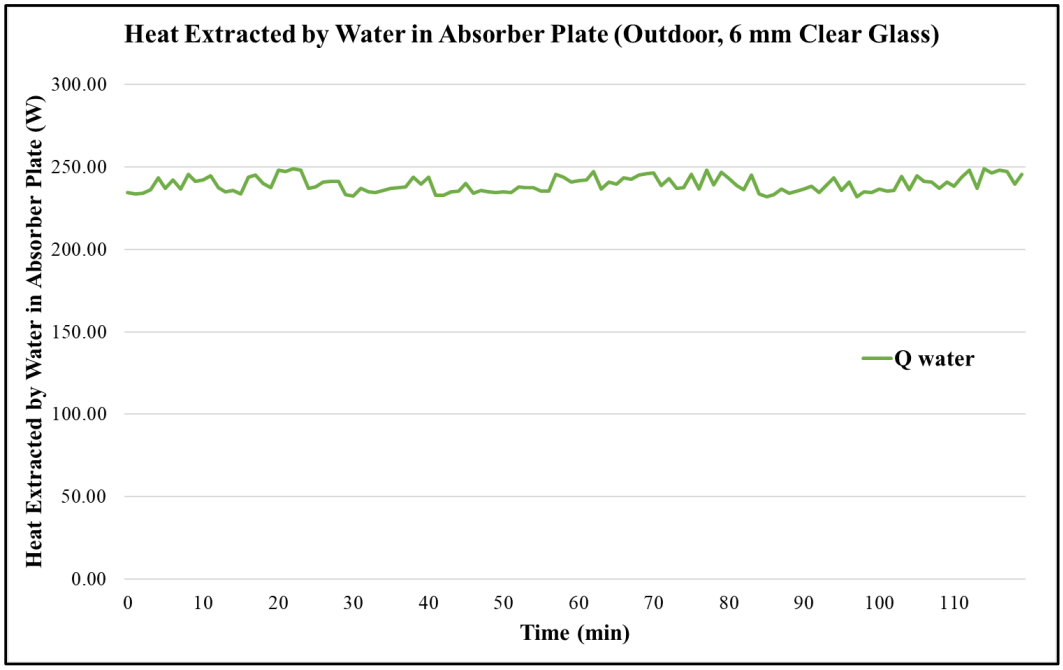

Figure 4.26 Heat Extracted by Water in Absorber Plate for Outdoor Test

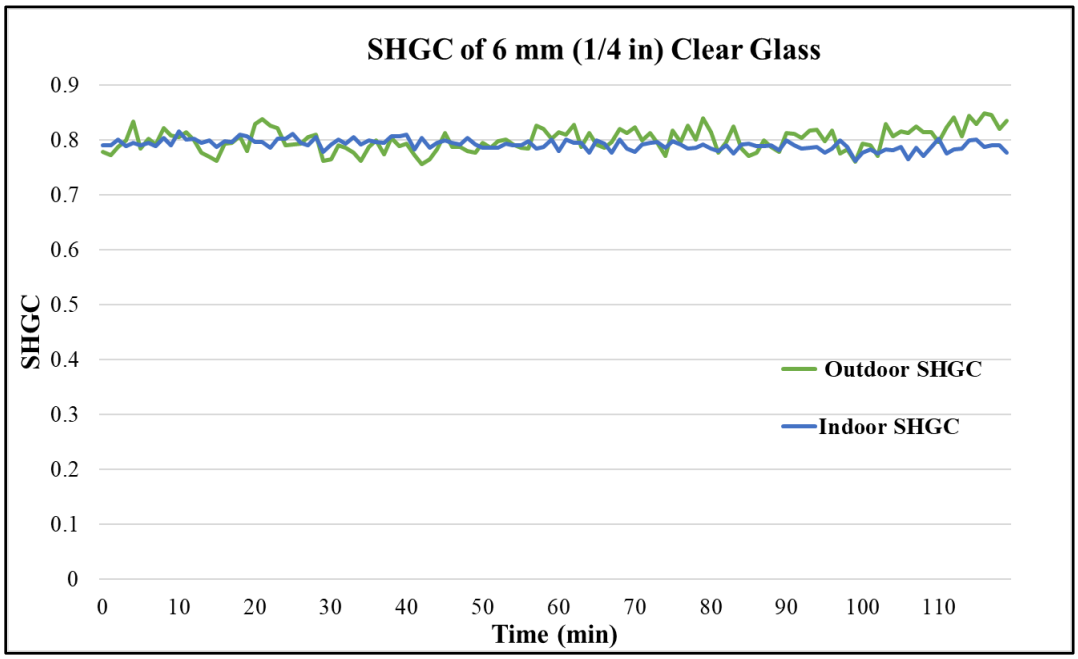

Figure 4.27 SHGC of 6 mm (1/4 in) Clear Glass for Outdoor and Indoor Tests

4.2.6 Uncertainty Analysis

The calculation of uncertainty of each inputs $Q_{center\ wall}$, $Q_{top\ wall}$, $Q_{left\ wall}$, $Q_{right\ wall}$, $Q_{bottom\ wall}$, Q_{wall}, $Q_{heat\ flow}$, Q_{water}, $Q_{solar\text{-}in}$, and Q_{solar} and the combined uncertainty of SHGC is determined in the same process as the indoor calculation in Section 4.1.5. Table 4.16 shows the calculated uncertainty of each inputs. The combined uncertainty of SHGC is determined using the uncertainty of $Q_{solar\text{-}in}$ and Q_{solar} in Table 4.18 by equation (4-4). The combined uncertainty is 3.91%, so the average SHGC of 6 mm clear glass in outdoor test is 0.800 ± 0.03.

Table 4.16 Uncertainty of Inputs

Inputs	Absolute Uncertainty (W)	Relative Uncertainty
$Q_{center\ wall}$	0.038	1.85%
$Q_{top\ wall}$	0.019	2.24%
$Q_{left\ wall}$	0.020	1.94%
$Q_{right\ wall}$	0.018	2.38%
$Q_{bottom\ wall}$	0.019	2.09%
Q_{wall}	0.054	0.96%
$Q_{heat\ flow}$	0.382	1.47%
Q_{water}	5.178	2.16%
$Q_{solar\text{-}in}$	5.192	2.51%
Q_{solar}	7.759	3.00%

4.2.7 Results Comparison

Both outdoor and indoor test results for a 6 mm (1/4 in) clear glass were compared to the SHGC from the open literature. Table 4.17 shows the weather data during all the outdoor tests. Table 4.18 shows the comparison of SHGC with those from other sources. It was observed that both obtained SHGC in indoor and outdoor were in good agreement to the values reported in the experimental work of Marinoski et al. [23] for a sample of 1.8 m^2 of surface area, obtaining an average SHGC of 0.79. The difference between the results of this study for outdoor and indoor tests and that obtained by Marinoski et al. were 1.25% and -0.13% respectively. Moreover, the average SHGC in this study was compared to the NFRC approved solar optical data for 6 mm clear glass [24]. It was noted the SHGC from outdoor test presented better agreement with the theoretical result from NFRC with a difference of -2%. Another comparison of the averaged SHGC of this study with that from industrial area, National Glass from Australia [25] was made. They listed SHGC for all the glass types they have on their website. The SHGC for a 6 mm (1/4 in) clear glass was 0.81, and the indoor test results indicated a better agreement with the value on the National Glass website. This was a difference of -1.25%. At last, Gregg D. Ander in the article Windows and Glazing on the Whole Building Design Guide website [26] reported the SHGC for a 6 mm (1/4 in) single pane glass is 0.81. This SHGC was obtained using Lawrence Berkeley National Laboratory WINDOW computer analysis program, a computer program for calculating total window

thermal performance indices. The difference between the results of this study for outdoor and indoor tests and that obtained by Gregg D. Ander [26] is -1.25% and -2.68 % respectively, which is also showing that the outdoor test results are closer to the theoretical value.

4.2.8 SHGC of Gray, Bronze and Mirror Glasses and Comparisons

The result of 6 mm (1/4 in) clear glass indicated a good agreement with the SHGCs from other resources. Three other glazing samples, bronze, gray, and mirror glasses with same thickness of 6 mm (1/4 in) were tested outdoor using this solar calorimeter. The testing procedure, calculation process and uncertainty analysis are the same as what we did for 6 mm (1/4 in) clear glass. Testing time for each type glass is about four hours, and the SHGC is calculated using the data collected in last two hours.

Table 4.19 shows the calculated SHGC for both outdoor and indoor test of 6 mm (1/4 in) gray glass, 6 mm (1/4 in) bronze glass, and 6 mm (1/4 in) mirror glass compared with SHGC from other resources. The measured SHGC of bronze and gray glass is compared to that on the glass vendor Vitro Architectural Glass [27] website, there is a difference of 7.07% and 8.81% respectively. Moreover, the difference between the SHGC of bronze and gray glass in this study and that reported from Glass Performance Data [25] is 4.13% and 4.09% respectively. For

mirror glass (reflective glass), it is very difficult to find the reliable reference SHGC in other resource. Most reflective glass in the industry are Low-e glasses which has a lower SHGC comparing with the SHGC of mirror glass obtained in this study. Vitro Architectural Glass [27] shows the SHGC of reflective glass is 0.26. It is 44.56% lower than the value obtained in this study.

Table 4.17 Weather Data during the Outdoor Tests

Outdoor Test	Time & Date	Weather Data during the Test				
		Average T_{air} °C (°F)	RH	Wind Speed m/s (mph)	Wind Direction	Average Solar Radiation W/m^2 ($Btu/hr \cdot ft^2$)
6 mm (1/4in) clear glass	11:00 am - 3:00 pm 10/06/2020	31.71 (89.08)	32%-55%	0-2.2 (0-5)	WSW - W	1055.55 (334.61)
6 mm (1/4in) bronze glass	11:00 am - 3:00 pm 10/08/2020	35.34 (95.61)	40%-58%	3.6-7.2 (8-16)	SSE - S	964.88 (305.86)
6 mm (1/4in) gray glass	11:00 am - 3:00 pm 10/07/2020	37.17 (98.90)	29%-54%	3.1-4.5 (7-10)	SSW- WSW	972.02 (308.13)
6 mm (1/4in) mirror glass	11:00 am - 3:00 pm 10/09/2020	33.28 (91.91)	51%-67%	7.6-8.9 (17-20)	S	975.86 (309.35)

Table 4.18 Comparison with SHGC from Other Sources for Clear Glass

Test	Measured SHGC	Marinoski et al. [23]			National Fenestration Rating Council [24]		
		SHGC	Difference		SHGC	Difference	
			Absolute	(%)		Absolute	(%)
Outdoor Test	0.800 ± 0.03	0.79	0.01	1.25%	0.816	-0.016	-2%
Inddor Test	0.791 ± 0.03		-0.001	-0.13%		-0.025	-3.16%

Test	Measured SHGC	Glass Performance Data [25]			Windows And Glazing [26]		
		SHGC	Difference		SHGC	Difference	
			Absolute	(%)		Absolute	(%)
Outdoor Test	0.800 ± 0.03	0.81	-0.01	-1.25%	0.81	-0.01	-1.25%
Inddor Test	0.791 ± 0.03		-0.019	-2.68%		-0.019	-2.68%

Table 4.19 Comparison with SHGC from Other Sources for Bronze, Gray and Mirror Glass

Glass Type	Measured SHGC (Outdoor)	Glass Performance Data [25]			Vitro Architectural Glass [27]		
		SHGC	Difference		SHGC	Difference	
			Absolute	(%)		Absolute	(%)
6 mm (1/4 in) Bronze Glass	0.667 ± 0.03	0.65	0.017	2.55%	0.63	0.037	5.55%
6 mm (1/4in) Gray Glass	0.623 ± 0.03	0.61	0.013	2.09%	0.58	0.043	6.90%
6 mm (1/4in) Mirror Glass	0.405 ± 0.02	-	-	-	0.26	0.145	35.80%

Glass Type	Measured SHGC (Indoor)	Glass Performance Data [25]			Vitro Architectural Glass [27]		
		SHGC	Difference		SHGC	Difference	
			Absolute	(%)		Absolute	(%)
6 mm (1/4 in) Bronze Glass	0.678 ± 0.02	0.65	0.028	4.13%	0.63	0.048	7.07%
6 mm (1/4in) Gray Glass	0.636 ± 0.02	0.61	0.026	4.09%	0.58	0.056	8.81%
6 mm (1/4in) Mirror Glass	0.469 ± 0.02	-	-	-	0.26	0.209	44.56%

CHAPTER VI

CONCLUSIONS, RECOMMENDATIONS, AND FUTURE STUDIES

5.1 Conclusions

This dissertation presented the design, construction, and validation of a portable solar calorimeter for the investigation of solar heat gain coefficient of single pane glass under indoor and outdoor conditions. For indoor experiments, a solar simulator was designed and constructed to simulate sun light and to allow for more repeatable testing under more controlled circumstances. For outdoor experiments, a customized solar tracking system was fabricated to track the solar path to keep the test specimen normal to the sun's direct beam radiation during the testing phase.

This calorimeter was designed to have a smaller size and faster response than most other similar devices described in the available literature. The time constant of the solar calorimeter, which is the time needed for it to achieve steady state, was determined before the calibration test. Based on calculation, the experimental time for this solar calorimeter to achieve steady state is around 80 minutes. The solar calorimeter was calibrated using a 6 mm (1/4 in) thick single pane glass under indoor condition with solar simulator. The SHGC was calculated based on data collected during the final 2-hours at steady state.

The average SHGC obtained for a 6 mm (1/4 in) clear glass was 0.791. With the combined uncertainty calculated for the SHGC, the average SHGC was 0.791 ± 0.03. The maximum difference between the obtained SHGC and others found in the available literature was -3.16% (-0.025 in absolute terms). Three other types of glasses, bronze, gray, and mirror glasses were also tested under indoor conditions. The average SHGCs were 0.678 ± 0.02, 0.636 ± 0.02, and 0.469 ± 0.02 respectively. The maximum differences between obtained between the SHGC and those from other resources were 7.07% (0.048), 8.81% (0.056), and 44.56% (0.209), respectively. The results showed larger differences for tinted glasses than the clear glasses. Since the coating level in the manufacturing process of tinted glasses may vary, it was difficult to obtain precise, scientific, values of SHGC for tinted glasses. The same four types of glasses were tested under outdoor conditions with a customized solar tracking system. The average SHGCs were 0.800 ± 0.03, 0.667 ± 0.03, 0.623 ± 0.03, and 0.405 ± 0.02. The maximum differences between obtained SHGC and those from other resources were -2% (-0.016), 5.55% (0.037), 6.90% (0.043), and 35.80% (0.145). Thus, the results of the outdoor tests were slightly more accurate when compared with the results of the indoor tests.

The produced SHGCs compared very favorably with values found in the literature showing that the device designed, fabricated, and calibrated as part of this dissertation fulfilled the expectation of a portable, accurate, fast response, and

multi-purpose test device. In addition, the solar calorimeter will support further student research and five courses in the Architectural Engineering curriculum at the University of Kansas.

5.2 Future Studies

This dissertation was developed for educational purposes and for future use by graduate and undergraduate research assistants. This device will offer the capabilities and opportunities to conduct further experiments related to fenestration systems. This section describes some ideas for future research using the solar calorimeter.

5.2.1 Window Blinds Integrated with PCMs

Phase change materials (PCMs) can store (during melting) and release (during solidification) large amounts of energy at an almost constant temperature. In passive application methods, PCM has been extensively studied by integrating it into the walls, windows, and roofs [28].

The use of PCMs is currently a promising solution to improve the energy performance of building elements considering their capacity to store and release energy. This capacity contributes to reducing buildings energy demand [29]. The

solar calorimeter has ability to test the thermal performance of window with blinds integrated with PCMs.

5.2.2 Aerogels

Aerogels are light and effective insulating materials. They are nanostructured solid materials with high porosity (> 90%) and low density (80 – 200 kg/m^3 (5 – 12.5 lb/ft^3)), which are defined as superinsulation materials, because of their very low thermal conductivity, comprised in the range of 0.012 – 0.023 W/m·K (0.0069 – 0.013 Btu/hr·ft·°F) depending on the granule size [30]. Aerogels also have high daylight transmittance which makes these very interesting materials for use in highly energy-efficient windows.

Aerogels can be integrated between two layers of glass when applied in fenestration systems. Aerogel windows have a solar energy transmittance equal to plain double glazing and at the same time a heat loss coefficient equal to the best triple-layered gas-filled window units [30]. The solar calorimeter presented in this dissertation could be used to investigate the thermal performance and SHGC of aerogel windows.

5.2.3 Photovoltaic Windows

Building Integrated Photovoltaic systems (BIPV) has become a promising way to generate electricity and reduce energy consumption through fenestration systems. Numerical studies indicate that BIPV can make a significant contribution to electricity generation in a building and can be used to reduce peak electricity demand. The solar calorimeter presented in this dissertation could be used to investigate the thermal performance and SHGC of BIPV systems.

5.3 Recommendations for Future Research

For indoor testing, a better solar simulator is recommended if budget allows. A solar simulator can be formed by one single lamp or by an array of lamps. In this dissertation, an array of lamps was used. One drawback of the simulator used in this study is that they produced a divergent angle of incident. One singe lamp with a long test distance would provide a more uniform distribution and smaller divergence angle.

Since the majority of the heat the enters solar calorimeter is absorbed by chilled water system in the absorbing plate, the estimation of the heat extracted by the chilled water Q_{water} has a significant compact on the accuracy of the SHGC calculations. Since the Q_{water} is a function of the inlet and outlet water temperature,

to increase the accuracy when determining the heat extracted by the chilled water system, a higher accuracy temperature sensor is recommended for the future study.

REFERENCES

[1] F.C. Winkelmann, Modeling windows in Energyplus, in: Proceedings of International IBPSA Conference, Building Simulation 2001, Rio de Janeiro, August 13-15, (2001), pages 457-464.

[2] U.S. Energy Information Administration (EIA), Monthly Energy Review, Tables 2.2 and 2.3, April 2021, preliminary data for 2020.

[3] U.S. Energy Information Administration, Annual Energy Outlook 2020.

[4] Global Alliance for Buildings and Construction, International Energy Agency and the United Nations Environment Programme (2019): 2019 global status report for buildings and construction: Towards a zero-emission, efficient and resilient buildings and construction sector.

[5] Anuranjan Sharda, Heat transfer through glazing systems with inter-pane shading devices: a review, Energy Technology & Policy (2014) 1, pages 23-34.

[6] Patrick Aniol, U-factor value on replacement windows explained, ROYALTY WINDOWS, 2019. Retrieved from https://www.royaltywindows.com/blog/u-factor-value-explained

[7] McCluney, Ross, Fenestration solar gains analysis, Florida Solar Energy Center/University of Central Florida, retrieved 8 November 2017, 1996.

[8] Matthias haldumann, Structural Use of Glass, Structural Engineering Document, 10th edition, 2008.

[9] Chen, Fangzhi, Solar heat gain coefficient measurement of semi-transparent photovoltaic modules with indoor calorimetric hot box and solar simulator, Energy and Building 53 (2012), pages 74-84.

[10] Hazim Moria, Radiation distribution uniformization by optimized halogen lamps arrangement for a solar simulator, Proceedings of the International Conference on Industrial Engineering and Operations Management Rabat, Morocco, 2017.

[11] Deivis L. Marinoski, Improvement of a measurement system for solar heat gain through fenestrations, Energy and Building 39 (2007), pages 478- 487.

[12] T.E. Kuhn, C. Buhler, W.J. Platzer, Evaluation of overheating protection with sun-shading systems, Solar Energy 69 (2000), pages 59-74.

[13] Leary, Gregory Patrick, Comparison of xenon lamp-based and LED-based solar simulators, Montana State University, 2016.

[14] Hsu Yung Cheng, et al., Estimating Solar Irradiance on Tilted Surface with Arbitrary Orientations and Tilt Angles, Energies, 2019, pages 14-27.

[15] G. Alvarez, A test method to evaluate the thermal performance of window glazings, Applied Thermal Engineering, Volume 20, Issue 9, June 2000, pages 803-812.

[16] Deivis L. Marinoski, et al., Development of a calorimeter for determination of the solar factor of architectural glass and fenestrations, Building and Environment Volume 47, January 2012, pages 232-242.

[17] Wright, John L., Kotey, Nathan Amon, Barnaby, Charles S., Collins, Michael R. Solar Gain through Windows with Shading Devices: Simulation Versus Measurement, ASHRAE Transactions 2009, vol. 115, part 2.

[18] Stephen J. Harrison, Michael R. Collins, Queen's university solar calorimeter-design, calibration, and operating procedure, Solar Energy Society of Canada Conference, 1999.

[19] Macias-Melo et al., Development of a solar calorimeter for the thermal evaluation of glazing samples, Journal of Building Physics, 2019, Vol. 42(6), pages 750-770.

[20] National Fenestration Rating Council, Interim standard test method for measuring the solar heat gain coefficient of fenestration systems using calorimetry hot box methods, NFRC 201-2014.

[21] Introduction to Solar Radiation, Newport Corporation, October 29, 2013.

[22] Tony R. Kuphaldt, Lessons in Electric Circuits, Volume I – DC, Fifth Edition, Chapter 16, 2006.

[23] D.L. Marinoskia, A.P. Meloa, F.S. Webera, S. Güthsb, R. Lambertsa. Measurement of solar factor of glazing and shading devices using a solar calorimeter. Building and Environment. Volume 144, 15 October 2018, pages 72-85.

[24] National Fenestration Rating Council Incorporated NFRC 200-2004 [E1A5].

[25] Glass Performance Data, National Glass, 2009. Retrieved from: https://www.nationalglass.com.au/wp-content/uploads/2019/06/Glass-Data_v4-Low-Res.pdf.

[26] Gregg D. Ander, FAIA, Windows and Glazing, Whole Building Design Guide, Southern California Edison, 2014.

[27] Product Data Sheet, Vitro Architectural Glass, 2020. Retrieved from: https://www.vitroglazings.com/media/fawluhue/vitro-vistacool-solarcool-datasheet.pdf.

[28] Dong Li, Thermal performance evaluation of glass window combining silica aerogels and phase change materials for cold climate of China, Applied Thermal Engineering Volume 165, 2020.

[29] R. Baetens, B.P. Jelle, A. Gustavsen, Phase change materials for building applications: a state-of-the-art review, Energy Build. 42 (2010).

[30] J.M. Schultz, Development of windows based on highly insulating aerogel glazings, Journal of Non-Crystalline Solids 350 (2004), pages 351–357.

[31] IEC Standard 60904, 2009, "Photovoltaic Devices - Part 9: Classification of Solar Simulator Characteristics," International Electrotechnical Commission, Geneva 20, Switzerland, 2009.

[32] ASTM Standard E927, 2010, "Standard Specification for Solar Simulation for Terrestrial Photovoltaic Testing," ASTM International, West Conshohocken, PA, 2010.

[33] U.S. Department of Energy, 2021, "Building Technologies Office (BTO) Multi-Year Program Plan," U.S. Department of Energy, Energy Efficiency & Renewable Energy, Washington D.C.

[34] NOAA Solar Calculator, Earth System Research Laboratories, Global Monitoring Laboratory, 2022, Retrieved from: https://gml.noaa.gov/grad/solcalc/.